Stability of a Liquid Thread and Stability and Nonlinear Evolution of Multi-Layer Fluid Flow

by

Julian Thompson

A thesis submitted to the University of East Anglia

for the degree of Doctor of Philosophy.

February 17, 2016

Contents

List of Figures

List of Tables

Abstract

This thesis is concerned with stability and existence of waves in interfacial and free surface problems. Considered is the curtain coating problem, with specific emphasis on trilayer and bilayer flows, and the breakup of a viscous thread with a solid core.

Experiments on curtain coating and sheet breakup are mostly conducted by industry and as such are hidden in patents or kept secret by companies trying to gain an edge in a competitive market. Experiments on curtain breakup concentrating on the effect that surfactants have upon the stability and the effect of differing fluid properties are discussed. It is shown that multiple layers of different fluid are more stable when reducing the flow rate of the lowest layer.

Single and multi-layer fluid flow down an inclined plane is studied with the emphasis on the effect of an insoluble surfactant. Bilayer and trilayer flow down an inclined plane is considered. The main point of interest here is the existence of multiple unstable modes for a single set of parameters.

A long wave model describing the multi-layer flow is discussed. Time-dependent solutions to this model system lead to the discovery of travelling wave solutions present in the dynamics.

The travelling wave solutions are further investigated through Fourier analysis leading to the discovery of branches of solutions emerging from wavenumbers for which the flow is neutrally stable.

The normal mode stability of annular Stokes flow of a viscous thread with a solid core is discussed which extends work done for negligible viscosity and small wavenumbers.

Introduction

In this thesis we discuss interfacial flow problems in open flow systems. Dynamical systems present a mathematical problem in that the position of the interface is not known explicitly but changes depending upon the fluid flow.

We first consider the curtain coating process. Curtain coating is a coating method that involves the creation of a fluid sheet falling under gravity. The object that is to be coated is then passed through the falling sheet leaving a layer of fluid on the object. Curtain coating is used in some manufacturing processes which require a layer of fluid to be applied to a solid surface (for example the manufacture of photographic film discussed by Krebs (2009)). Usually an even coating is required, so minimising disturbances is essential. Previously experiments have been done by manufacturers and consequently the results are hidden in patents. One of the aims of this thesis is to obtain new information on the curtain coating process through experiments. We performed experiments for various parameter ranges, varying viscosity, surface tension and flow rate, to deduce an acceptable parameter range for a falling liquid curtain to remain stable which are presented in section 1. A stable curtain in this thesis is defined to be a sheet of falling fluid with no holes in. Breakup of a curtain is defined to be after a hole appears in the curtain it changes to a form that is not a fluid sheet. For example multiple threads or a single thread resembling two jets coalescing. A diagram of the curtain coating setup is shown in figure 0.1.

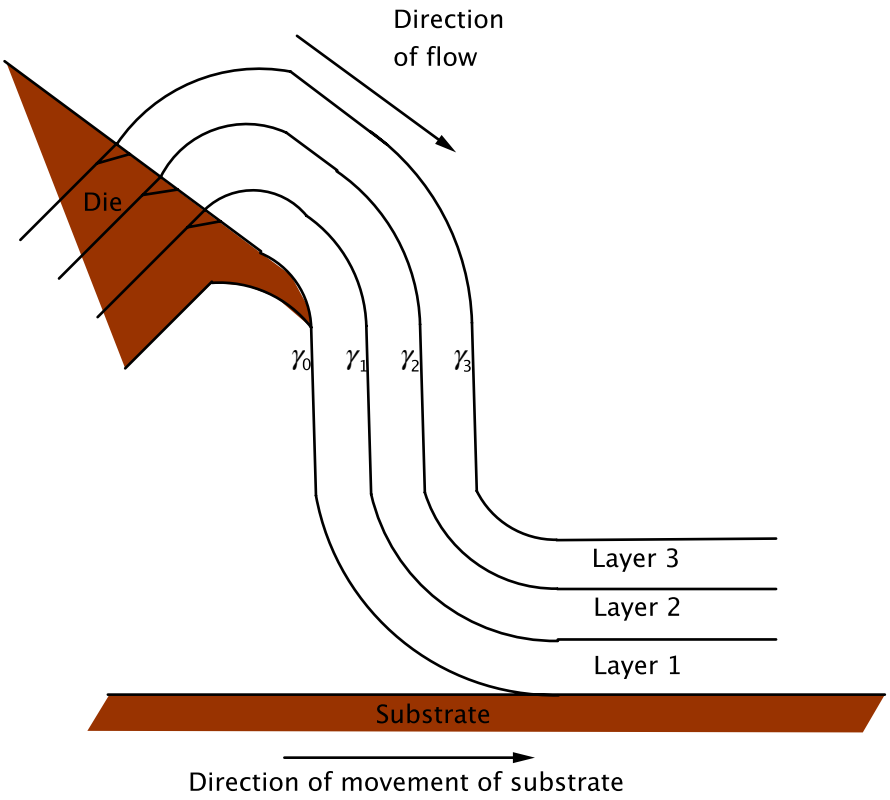

Figure 0.1: Diagram of 3 layers of fluid flowing uniformly over the die and falling onto the substrate.

Surfactants were in the fluids used in our experiments. Surfactants are a substance which reduce the surface tension of the fluid in which they are inserted. During our experiments we used insoluble surfactants which have a hydrophobic section which is attracted to free surfaces. Surfactants have the effect of lowering the surface tension. This effect has a limit called the critical micelle concentration whereby the free surface of a fluid is completely saturated with surfactant and some of the remaining surfactant in the fluid creates clumps of surfactant within the fluid. As such this means that experimentally the surface tension of a given fluid can only be reduced to a limit decided by the CMC (Critical Micelle Concentration) level. The CMC level is the surfactant concentration at which micelles start to form. Micelles are clusters of surfactant that do not migrate to the surface of the

fluid. This motivated a theoretical study of the effect of surfactants on multi-layer flow. The study of multi-layer flow is useful for understanding film coating, of which curtain coating is one example. This includes optical coating, discussed by Baumeister (2004), where it is required to produce multiple layers of thin fluid with little or no defects to coat a lens. Also for medical devices that require lubrication, such as catheters and other medical devices, a hydrophilic film coating is required to aid lubricity as discussed by LaPorte (1997). It should be noted that the experiments conducted in industry would be done on much larger apparatus. The width of the die we used in the experiments was $12cm$ whereas in industry the width of the die could be several meters. Of particular interest to industry is to minimize disturbances. In order to understand the disturbances that can occur we seek traveling wave solutions. Traveling waves are waves that occur on a free surface or interface and keep their profile and have a constant velocity.

The theoretical work, both our work and work done by others, discussed on multi-layer flow in this thesis is purely two-dimensional. This simplification was justified in an argument given by Squire (1933), for a single layer flow in a channel, where he pointed out that any disturbances found by considering a three-dimensional disturbance is governed by the same equations as for a two-dimensional disturbance in a similar flow. Hesla *et al.* (1986) extended this to two layer flow in a channel. Halpern & Frenkel (2003) extended this to include surfactants. Blyth (2008) extended Squire's work for a film flow down a plane with surfactant (and an electric field). These studies give us a good indication that a similar theorem can be reached for multi-layer film flow down an inclined plane in the presence of surfactant although no papers have been found that show this.

Single Layer Flow

For a single layer, surfactant-free flow, work has been done by Benjamin (1957) in the limit of small Reynolds number using a normal mode perturbation, expanding the equations in a power series expansion. It was found that for a long wave perturbation there is a critical Reynolds number above which the flow is unstable. This was later confirmed by Liu *et al.* (1993) experimentally. Yih (1963) also looked at a single layer of surfactant-free flow. He considered the case of small wavenumbers, for which he found that there exists a critical Reynolds number above which some disturbances are amplified. He also considered the case of small Reynolds number, for which he agrees with Benjamin (1957) and the case of large wavenumbers, for which Yih found that short amplitude waves are damped by surface tension and the rate of damping is reduced with an increase in viscosity. Work has been done by Boatto *et al.* (1993) to investigate traveling waves on a single layer of fluid on a non-inclined plane. They found that using a lubrication approximation in which the equation of motion is $h_t + (h^n h_{xxx})_x = 0$ for which h is the position of the free surface and n is a parameter which corresponds to different physical situations. The equation that they studied is in the limit of negligible inertia and is governed by viscous and capillary forces. They investigated the equation for differing values of n but never link these to any physical parameters. To our knowledge no work has been done to find traveling wave solutions for multilayer flows.

Two Layer Flow

For two layer surfactant-free flow there exists an instability even at zero Reynolds number. This was shown by Kao (1968), using a long wave approximation, for the upper layer being

more viscous than the lower layer. He also found that for a thin layer of the upper fluid the critical Reynolds number does not change with changing the viscosity of the upper layer. Loewenherz & Lawrence (1989) extended this for an arbitrary wavenumber in the limit of Stokes flow and with no surface or interfacial tension, using a normal mode analysis. They found that for a more viscous thinner upper layer there exists a stable bandwidth of finite wavenumbers. They also found that the long waves did not appear to govern the stability of the flow. Chen (1993) found that in the presence of inertia a two layer flow is always unstable if the upper layer is more viscous than the lower layer for low Reynolds numbers. This result they found using a normal mode analysis. For two layer flow with a vertically inclined plane Jiang & Lin (2005) found that it can be stabilised by oscillating the plate parallel to the plane but also this can further destabilise the flow for certain parameter ranges. Pozrikidis (1998) used the boundary integral method to compute the fully nonlinear calculations of a two layer Stokes flow and found that even a low surface tension is able to stabilise the flow. Jiang *et al.* (2004) and Gao & Lu (2008) provided an explanation of the underlying physical mechanism for the long wave inertialess instability (zero Reynolds number) of two layer film flow using an energy argument.

Effect of Surfactants

For single layer surfactant-laden flow, Whitaker & Jones (1966) and Lin (1970) extended the previous single layer analysis done by Benjamin (1957) and Yih (1963). They found that the critical Reynolds number is larger which implies that the surfactant has a stabilising effect upon the flow. Pozrikidis (2003) relaxed the long wave assumption and showed that in the inertialess zero Reynolds limit there are two modes, one that corresponds to that found by Yih (1963) and one that corresponds to the Marangoni mode. Both of

these modes are stable at zero Reynolds number. He used a boundary element method to study the nonlinear development of the instability. Blyth & Pozrikidis (2004) solved the Orr-Sommerfeld problem for a surfactant-laden film numerically and found that the Yih mode and the Marangoni mode can be unstable in the presence of inertia and one of the modes dominates dependent upon the Reynolds number. They used normal mode analysis to accomplish this.

Surfactant-laden two-layer flow was studied by Gao & Lu (2007). Normal mode analysis was conducted in the limit of Stokes flow for any wavelength. They found that there are four possible modes with surfactant only one of which can be unstable for layers of equal thickness. For the stable configuration of having a more viscous layer next to the plane they found that adding surfactant to the free surface did not destabilise the flow but adding surfactant to the interface did. For the unstable configuration of having the less viscous layer at the plane they found that adding surfactant to the free surface has a stabilising effect while adding surfactant to the interface can have a stabilising or destabilising effect dependent upon the Marangoni number of the free surface and the viscosity ratio. Samanta (2014) has recently extended this work to include the effects of inertia upon the flow. Using a normal mode analysis they found was that the interface mode cannot be completely eliminated by interface immobilisation.

Three Layer Flow

Three layer flow in the absence of surfactant has been discussed by a number of people. Work has been done on three layer flow by Wang *et al.* (1978) who found long wave instabilities due to differing viscosities in the layers but only when considering inertia.

They used a power series expansion in the wavenumber, assumed to be small, of the velocity and wave speed. Weinstein & Kurz (1991), who also worked with long wavelength perturbations, considered many parameter ranges, with differing viscosities, densities and layer thicknesses and concluded that even at zero Reynolds number a three layer flow can be unstable. In particular when the middle layer is thin and less viscous than the surrounding layers. They used a normal mode analysis expanding the wave speed and velocity in terms of the wavenumber. Finite wavelength disturbances in the absence of inertia and interfacial tension but considering surface tension was considered by Weinstein & Chen (1999) again using a normal mode analysis. They found that the instability found in Weinstein & Kurz (1991) is still present for the finite wavelength regime. When the middle layer is thin and very viscous they found a new instability for only finite wavelength perturbations. Also the magnitude of the growth rates that they found for three layers is orders of magnitude higher than those found for two layer flows by Loewenherz & Lawrence (1989). Jiang *et al.* (2005) investigated the physical mechanism behind the three layer instability. They found that Reynolds stresses in the lower layers of three layer flow are an essential part of instability unlike for two layer flow. This remains true even as the Reynolds number tends to zero.

Thesis Aims and Structure

In order to study the stability of multi-layer flows we first have to calculate the initial velocity profile in the absence of any perturbation. This is done in section 2.1. In section 2.2 we discuss the stability of two layer flows with surfactant in the absence of inertia, specifically parameter ranges not considered by Gao & Lu (2007) such as differing layer thicknesses. Also we consider the stability of three layer flows with surfactant in the ab-

sence of inertia which, to the best of our knowledge, is the first time this has been studied. Further to this in section 3.1 we derive and numerically solve a long wave approximation describing the multilayer flow. We use these same equations to study the presence of travelling wave solutions in section 3.2 concentrating on five cases which cover a range of parameters.

In section 4, we examine the dynamics of a viscous thread coating a solid core. One example of annular flow with a core in nature is spider silk. Spiders spin silk of two types, one is hard and cylindrical and is the main structure of the web (usually the outwards spokes of the web) and the other which is very elastic and is covered in sticky beads. The sticky beads are initially excreted as an annular thread over an elastic thread. These break up into uniformly spaced beads discussed by Boys (1960).

The capillary instability of an invicid liquid thread has been well studied by Rayleigh (1879), neglecting the effect of the surrounding fluid. He found that any disturbance with a wavelength greater than the circumference of the jet should cause the jet to break up into droplets. Tomotika (1935) considered the effect of the surrounding fluid using a normal mode analysis and found that there is a single wavenumber that grows more rapidly than any other wavenumber for a viscous fluid. Goren (1962) considers the instability of an annular thread of fluid surrounding a solid core but only comments on the case of negligible inertia and the case of zero viscosity. Using a normal mode Stokes analysis, he found that for a given ratio of the radii of the annular thread and the Ohnesorge number, the ratio of inertial forces to the viscous forces times the ratio of the surface tension forces to the viscous, there is a "disturbance of a certain wavelength, which grows more rapidly than any other wavelength".

We seek to extend Goren (1962) work to include the effects of viscosity and allow all wavenumbers. We conduct a normal mode analysis by assuming a small amplitude perturbation. For a given ratio of radii of the rigid core to the liquid thread and Ohnesorge number we find that there is a certain wavelength which grows more rapidly than other wavelengths of a disturbance.

In the final section we summarise the findings of the thesis and discuss future directions.

1 Curtain Coating Experiments

Many of the experimental data on the breakup of multi-layer liquid curtains are within patents and as such are inaccessible or difficult to gain insight from. Experiments were conducted at the King Abdullah University of Science and Technology using a custom built 4-layer slide die (TSE Troller AG, Switzerland). The aim of the experiments were to investigate the stability of a liquid curtain and arrive at some conclusions on the condition by which a liquid curtain maintains stability.

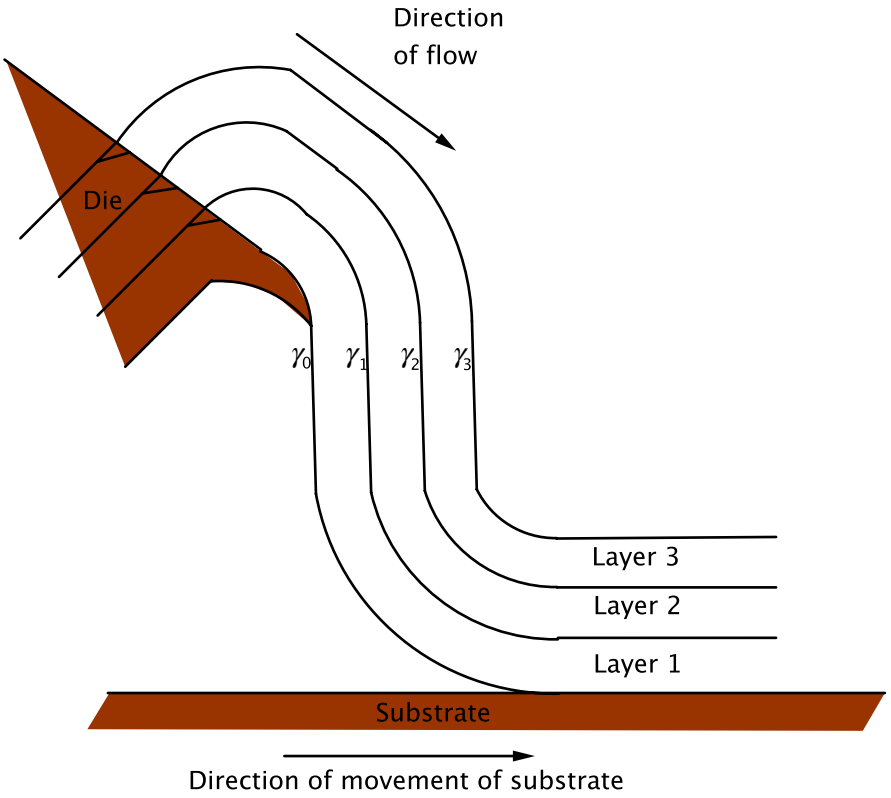

Figure 1.1: Diagram of 3 layers of fluid flowing uniformly over the die and falling onto the substrate.

Also of interest is a phenomenon know as the hysteresis window. The hysteresis window is defined as the difference between the breakup flow rate and the curtain formation flow rate. We define the breakup flow rate as the flow rate at which the curtain ceases to be

continuous and the curtain formation flow rate is the minimum flow rate that the curtain can be formed. The dies used in industry can be several meters wide but the die that we used for the experiments was $12cm$ wide.

1.1 Theoretical Background

Analytic work has been done by Taylor (1959) investigating thin fluid sheets but no stability criterion was formulated. Brown (1961) conducted experiments on liquid curtains to ascertain a stability criterion for a single layer. Lin (1981) obtained a local stability condition for a single layer of fluid falling under gravity defined by a condition on the Weber number, the ratio of the fluid inertia to the surface tension,

$$We = \frac{\rho Q v_c}{\gamma} > 2, \tag{1.1}$$

where ρ is the liquid density, Q is the local flow rate per unit width of curtain, v_c is the vertical velocity component and γ is the dynamic surface tension. This agreed with the experiments done by Brown. Dyson *et al.* (2009) extended this model for n-layers of fluid to get

$$\frac{v_c \sum_{j=1}^{n} \rho_j Q_j}{\sum_{j=0}^{n} \gamma_j} > 1, \tag{1.2}$$

where the subscripts denote the characteristics of the corresponding layers and the γ_i's denote the dynamic surface tensions where γ_0 denotes the surface tension between layer 1 and the surrounding gas, γ_1 the interfacial tension between layers 1 and 2 and so on as illustrated for three layers in figure 1.1.

1.2 Experimental Setup

No work to the authors knowledge has been done to compare the above conditions against experiments. The experiment involved four containers of fluid each with separate pumps

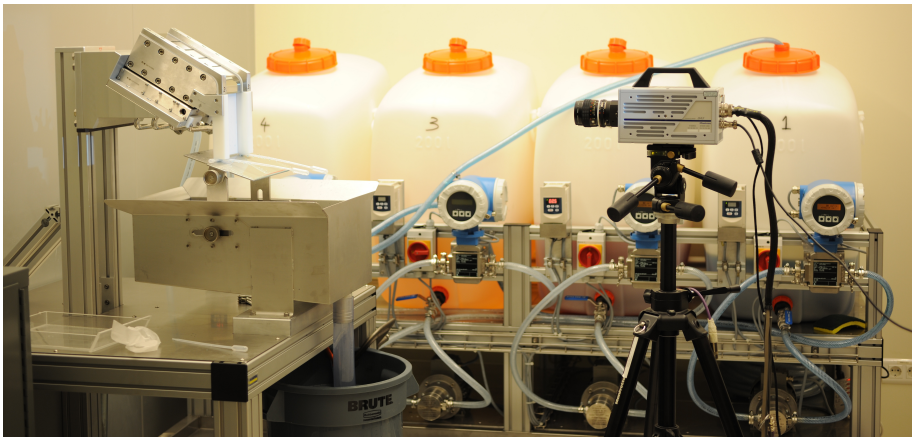

Figure 1.2: Photograph of the experimental setup.

and flow meters feeding fluid into the die and out of the four slots, three of which are shown in figure 1.1. The fluid then forms layers of flow which cascade over the lip of the die forming a curtain and landing on the target plate. For the experiments the plate was stationary.

The curtain had to be manually formed with plastic rods to pin the curtain to the edge guides, as shown at the bottom of the edge guides in figure 1.3. Pipettes were used to ensure the edges of the curtain did not de-pin before an instability broke the curtain. The fluids were sometimes reused for subsequent experiments after being given time to settle in the tanks.

Several fluids of varying viscosity and surface tension were used and the properties of the different fluids are given in table 1. The surfactant used in fluid 1 was cetyl trimethylammonium bromide (CTAB) and the other fluids had sodium dodecyl sulfate (SDS) so

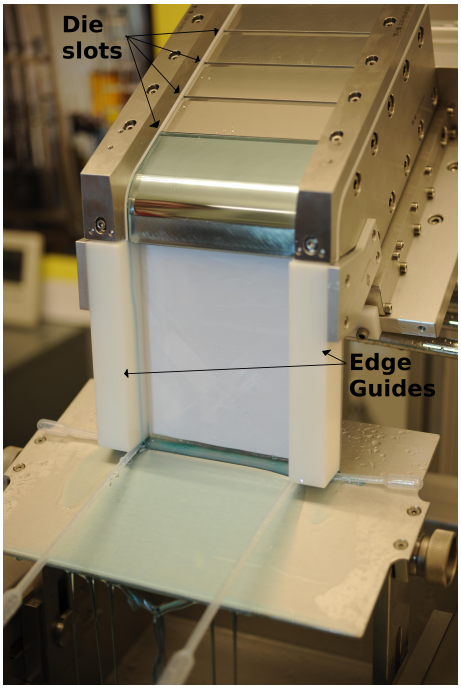

Figure 1.3: Photograph of the coating die close up with labels.

although measurements of surface tension and viscosity were taken the interactions between the different surfactants and the viscosity may be different.

Fluid	Glycerol conc. ($\%_{w/w}$)	Surfactant conc. ($\%_{w/w}$)	Viscosity ($mPa.s$)	Surface tension (mNm^{-1})	Density (kgm^{-3})
1	65.5	0.01	15.4	50.8	1171
2	74	0.21	33.4	42.21	1169
3	74	0.05	33.4	54.47	1169
4	83.5	0.21	70	47.13	1219
5	91.9	0.1	262	59.5	1241
6	91.9	0.21	262	54.8	1241
7	65.5	0.21	15.4	47.9	1171

Table 1: Table of fluid properties.

Measurements of all the flow rates are given in Appendix A. In these tables Q_{ST} denotes the flow rate measured in cm^3s^{-1} and Q_{BR} denotes the flow rate at which the curtain breaks up, also in the same units.

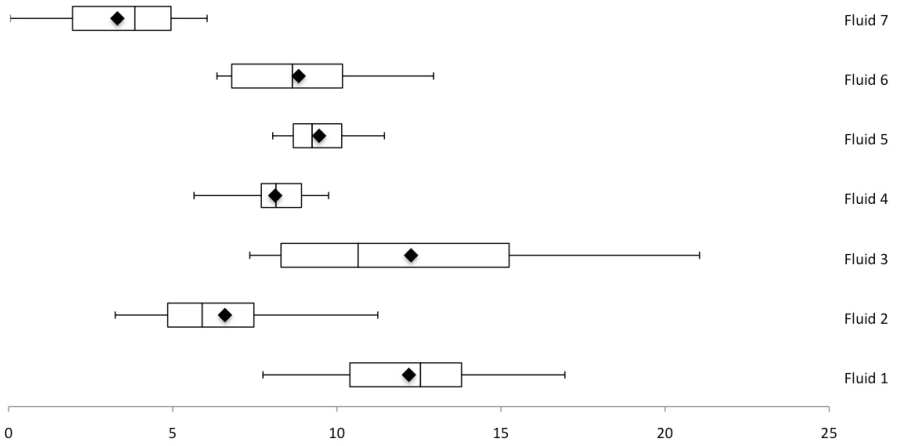

Figure 1.4: Plot of the mean, denoted W; minimum, left tick; maximum, right tick; median, middle vertical line; 1st quartile, left vertical line, and 3rd quartile, right vertical line, of the breakup flow rates (in cm^3s^{-1}) for the given fluids on the right.

In considering the stability of curtain coating flows with surfactant we will briefly talk about the migration of surfactants. When a fluid is initially ejected from the die slot the surfactants are assumed to be equally concentrated throughout the fluid but as a fluid with surfactant is exposed to a non solid interface the surfactant migrates to the newly created free surface or interface. If the surfactant laden fluid is exposed to a fluid with which there is no interfacial tension, as in the case of a fluid being exposed to a layer of the same fluid, the surfactant does not migrate to this surface. Due to this for a single layer by the time the fluid reaches the lip of the die the surfactant is mostly upon the upper free surface. This means that as the curtain is being formed at the top of the curtain the surface tension at the front of the curtain is much lower than at the back equalising as the curtain falls. If we consider the two layer case the surfactant in the upper layer is mostly

at the free surface by the time the fluid arrives at the lip of the die while it is still equally distributed in the lower layer allowing the surface tension at the back of the curtain to reduce quicker than the one layer configuration.

Further to the above paragraph there is a surfactant concentration above which micelles start being created and any more surfactant which is added wholly contributes to these micelles. We call this the CMC or Critical Micelle Concentration level and it is a characteristic of insoluble surfactant. Above the CMC level the surface tension of the surfactant laden fluid will not change significantly suggesting a surface fully laden with surfactant. A surfactant particle is made of two distinct parts, a head and tail, the head is hydrophilic or water loving and the tail is hydrophobic or water hating. This is what causes the surfactants to migrate to the surface. The surfactants that do not migrate to the surface due to the surface being saturated form micelles by grouping together with their tails centered around a point. These observations are discussed by Rosen & Kunjappu (2012) where further nuances of surfactants are discussed.

The surfactant concentrations for fluids 2, 4, 6 and 7 were chosen to be at the CMC level and therefore the lowest surface tension achievable for the fluid using an insoluble surfactant.

1.3 Single Layer

Fluid number	Average breakup flow rate	Minimum starting flow rate
1	12.15	21
2	6.54	16.9
3	12.21	22.7
4	8.08	15.7
5	9.41	12.3
6	8.79	11.1
7	4.57	14.8

Table 2: Condensed table of fluid flows for a single layer of each fluid.

Figure 1.4 shows the averages, ranges and inter-quartile ranges of the breakup flow rates for a single layer of each fluid. As we can see from figure 1.4, fluids 1 and 3 are the most unstable as the curtain formed by those fluids breaks up at a higher flow rate than the other fluids. This is due to their lower viscosity and higher surface tension. We note that fluid 5 has the highest surface tension but has a much higher viscosity which dampens out instabilities. In general a higher viscosity will dampen out any disturbances that occur but if the upper layer is more viscous than the lower layer it is well known that this causes an instability leading to waves occurring. The average breakup flow and minimum starting flow rate for a single layer of each fluid are shown in table 2.

Comparing fluids 2 and 3 in table 2 we can see that a change in the surface tension does not have an effect upon the width of the hysteresis window. This is further enforced by considering fluids 5 and 6. If we compare fluids 3 and 6 with similar surface tensions fluid

6 with a larger viscosity has a much smaller hysteresis width. Similarly when considering fluids 4 and 7 the fluid with a higher viscosity, fluid 4, has a smaller hysteresis window. Considering the needs of industry a very stable flow with a small hysteresis window is desirable.

1.4 Two Layers

We also conducted experiments on multiple layers. We conducted experiments of two layers of the same fluid to compare to a single layer of the same fluid with the same total flow rate the results of which are given for fluid 1 in table 3.

Fluid number	Breakup flow rate for single layer	Flow rate of layer 1	Average breakup flow rate of layer 2	Total average flow rate for two layers	Total minimum starting flow rate
1	12.15	8	5.7	13.7	19.5
1	12.15	7	7.9	14.9	19.8
1	12.15	6	8.1	14.1	20.2
1	12.15	5	9.1	14.1	20.1
1	12.15	4	10.1	14.1	21.0

Table 3: Condensed table of fluid flows for two layers of fluid 1.

For two layers of fluid 1 we fixed the flow rate of the lower layer and varied the flow rate of the upper layer until breakup occurred the condensed results of which are given in table 3. As we can see in table 3 the total flow rate for two layers is consistently higher implying that multiple layers of the same fluid are more unstable than a single layer. This may be

due to the effect of surfactants as described above as the surface tension of the back of the curtain will change more rapidly as it flows over the lip causing an instability. The hysteresis window for two layers of fluid 1 is not significantly different for differing layer 1 flow rates as shown in table 3. When we compare the hysteresis window of a single layer of fluid 1 to two layers of the same fluid we observe that the minimum startup flow is similar but the average breakup flow rate is higher for two layers reducing the hysteresis window for two layers.

Fluid number	Breakup flow rate for single layer	Flow rate of layer 1	Average breakup flow rate of layer 2	Total average flow rate for two layers	Minimum Starting flow rate
2	6.54	4	5.84	9.84	17.5
2	6.54	3	2.86	5.86	17.8

Table 4: Condensed table of fluid flows for two layers of fluid 2.

When considering two layers of fluid 2 as shown in table 4 we had several anomalous readings for setting the flow rate in layer 1 to $3cm^3s^{-1}$ and varying the flow rate in layer 2. One experiment gave a total breakup flow rate of $14.1cm^3s^{-1}$ which appears to be an outlier as the rest of the curtain breakup flows are in the range $3cm^3s^{-1}$ to $7.3cm^3s^{-1}$. Taking this into account gives us a revised total average flow rate of $4.68cm^3s^{-1}$. This result goes against the previous results, in that two layers of fluid 2 appear to be more stable for a lower flow rate in layer 1 which is the opposite to the results given in table 3. The hysteresis window is reduced for the higher layer 1 flow rate while it is increased for lower layer 1 flow rate.

Two layers of fluid with different surfactant concentrations with the same viscosity were

Fluid number for layer 1	Fluid number for layer 2	Flow rate of layer 1	Average breakup flow rate of layer 2	Total average flow rate for two layers	Minimum Starting flow rate
2	3	6	6.4	12.4	N/A
2	3	5	7	12	21.2
3	2	6	9.9	15.9	N/A
3	2	5	7.48	12.48	22.5

Table 5: Condensed table of fluid flows for two layers made up of fluid 2 and fluid 3.

considered. The condensed results are given in table 5. The average breakup flow rate for a single layer of fluid 3 is $12.21cm^3s^{-1}$ while for fluid 2 it is $6.54cm^3s^{-1}$. Two layers of the same fluid had the surprising effect of destabilising the flow, while for the configuration given above the total breakup flow rate is similar to that of the breakup flow rate for a single layer of the least stable fluid. The hysteresis window for fluid 2 and fluid 6 as the lower layer are similar, ignoring the higher layer 1 flow rate due to unavailable information.

Two layers of fluid with similar surface tensions and different viscosities were considered. The condensed results are given in table 6. The total flow at the time of breakup for the experiments presented in table 6 are closest to those for a single layer of fluid 4. Since the breakup flow for a single layer of fluid 3 is larger this would suggest that having a thin layer of fluid at the bottom of the curtain has a stabilising effect. There is a clear difference in the breakup flow rates between having a flow rate of $4cm^3s^{-1}$ and a flow rate of $3cm^3s^{-1}$ for the bottom layer. The results suggest the flow is more stable with a thinner

Fluid number for layer 1	Fluid number for layer 2	Flow rate of layer 1	Average breakup flow rate of layer 2	Total average flow rate for two layers	Minimum Starting flow rate
3	4	4	4.2	8.2	15.3
3	4	3	4.41	7.41	14.9
4	3	4	5.71	9.71	16.1
4	3	3	2.99	5.99	15.8

Table 6: Condensed table of fluid flows for two layers made up of fluid 3 and fluid 4.

layer on the bottom. It should be noted that although a smaller flow rate gives a thinner layer than that of a single layer of the same fluid a single layer of fluid 4 with a flow rate of $3cm^3s^{-1}$ is not necessarily thinner than a single layer of fluid 3 with a flow rate of $4cm^3s^{-1}$ since the higher viscosity of fluid 4 increases the effect of the solid boundary at the inclined plane. The hysteresis window for the first three rows of table 6 is the similar to a single layer of fluid 4 while the last row is similar to the width of the hysteresis window for fluid 3.

Two layers of fluid with different surface tensions and vastly different viscosities were considered. The condensed results are given in table 7. Comparing the single layer breakup flow rates combining two layers in the configurations given has a destabilising effect. Following on from our discussion in the previous paragraph comparing the experiments in the third and fourth rows we see the same stabilising effect shown previously but comparing the first and second rows reducing the flow rate for the lower layer, being fluid 2, has the effect of destabilising the flow. This is possibly due to the low surface tension coupled

Fluid number for layer 1	Fluid number for layer 2	Flow rate of layer 1	Average breakup flow rate of layer 2	Total average flow rate for two layers	Minimum Starting flow rate
6	2	4	4.25	9.25	14.0
6	2	3	6.3	10.3	13.7
2	6	4	4.76	9.76	12.2
2	6	3	3.31	7.31	11.2

Table 7: Condensed table of fluid flows for two layers made up of fluid 2 and fluid 6.

with the concentration of surfactant causing a steep surface tension gradient near the die lip at the back of the curtain. The width of the hysteresis window is similar to that of a single layer of fluid 6.

Fluid number for layer 1	Fluid number for layer 2	Flow rate of layer 1	Average breakup flow rate of layer 2	Total average flow rate for two layers
7	2	5	6.65	16.65
7	2	4	6.32	14.32
7	2	3	6.8	12.8

Table 8: Condensed table of fluid flows for two layers made up of fluid 2 and fluid 7.

Two layers of fluid with similar surface tensions and different viscosities were considered. The condensed results are given in table 8. Here we can further see the stabilising effect of

reducing the flow rate of the lower layer although the total breakup flow rates are greater than those for a single layer of fluid 2 or fluid 7.

Fluid number for layers	Flow rate of layer 1 at breakup	Flow rate of layer 2 at breakup	Flow rate of layer 3 at breakup	Total average flow rate for three layers	Minimum Starting flow rate
1	4	4	6.95	14.95	20.3
1	4	3	8.48	15.48	20.5
1	3	4	8.65	15.65	20.5
1	4	9.18	4	17.18	22.0
1	4	9.1	3	16.1	21.1
1	3	7.75	4	14.75	21.1

Table 9: Condensed table of fluid flows for three layers made up of fluid 1.

Three layers of the same fluid were considered. The condensed results are given in table 9. We considered three layers of fluid 1, as this fluid has a higher breakup flow rate than most of the other fluids considered. We were able to form a three layer curtain while still being able to observe breakup. There does not appear to be much difference in the total breakup flow rates between the first three rows in table 9. This suggests that the change in the flow rates considered in these rows are not significant enough to show any pattern. In considering the fourth through sixth rows of table 9 we see the stabilising effect of reducing the flow rate of either layer 3 or layer 1 but the total breakup flow rate is not reduced enough to be significantly more stable than that of the total breakup flow rates given in the first to third rows. The hysteresis window for three layers of fluid 1 is

smaller than a single layer of the same fluid. This is due to the three layer flow being more unstable but the startup flow rate is similar to that of a single layer.

1.5 Summary

In this section we have given an overview of the experiments we performed on curtain coating stability. We have shown that in general for multiple layers of fluid reducing the flow rate in layer 1 has the effect of reducing the total breakup flow rate and stabilising the curtain.

We were unable to compare directly against the Dyson formula for stability due to not knowing the thickness of the curtain as it falls. Also the measurements of surface tension we have are for a static fluid, as the surface tension changes with fluid flow due to the use of insoluble surfactants, so the dynamic surface tension of the falling film are not known.

We have looked at varyious fluids and their effects upon the hysteresis window. We found that multiple layers of the same fluid have a similar minimum startup flow while the breakup flow is mostly larger causing a smaller hysteresis window.

2 Stability of Multi-layer Flow Down an Inclined Plane

In order to understand the instabilities present in the curtain coating flows presented in section 1 we consider the flow over the face of the die before it arrives at the lip. Specifically the stability of the flow and the existence of any waves that we would expect to observe which could lead to instabilities in the curtain. To calculate the linear stability of the flow we must first start with a base state which we take to be a unidirectional flow parallel to the inclined plane. To this we apply a small perturbation which has a wavenumber and growth rate. Using appropriate boundary conditions we arrive at an equation relating the wavenumber to the growth rate with parameters based upon the fluid properties.

2.1 Unidirectional Flow

In figure 2.1 we give the arrangement of our layers whereby we denote the first layer to be the layer closest to the inclined plane increasing until we arrive at the layer n which has a free surface. We denote the thickness of the ith layer to be h_i and the angle between the horizontal and the inclined plane to be α. We take the x-axis to be parallel to the inclined plane and the y-axis to be perpendicular as shown in figure 2.1. To calculate the unidirectional flow we consider laminar flow over an inclined plane with multiple layers of fluid as shown in figure 2.1.

To find the velocity field and the thicknesses of the layers of the fluids we consider the Navier-Stokes equations,

$$\rho_i \left(\frac{\partial \mathbf{u}^{(i)}}{\partial t} + \mathbf{u}^{(i)} \cdot \nabla \mathbf{u}^{(i)} \right) = -\nabla p^{(i)} + \mu_i \nabla^2 \mathbf{u}^{(i)} + \rho_i \mathbf{g}, \tag{2.1}$$

where $\mathbf{u}^{(i)}$ denotes the velocity field, ρ_i denotes the density, $p^{(i)}$ denotes the pressure, μ_i

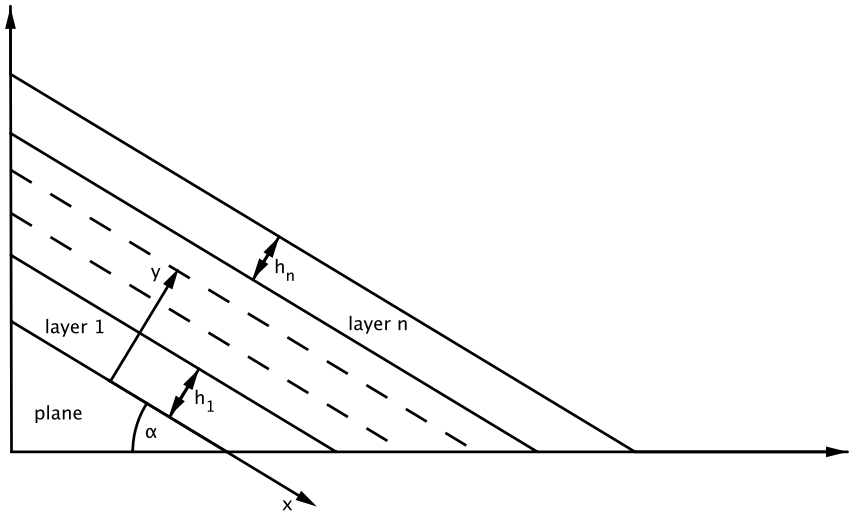

Figure 2.1: Illustration of multiple layers of fluid flowing down an inclined plane.

denotes the viscosity, **g** denotes the acceleration due to gravity exerted upon the fluid and the superscripts, (i) denote the fluid layer. For a steady flow with the velocity components only depending upon y we are left with

$$0 = -p_x^{(i)} + \mu_i u_{yy}^{(i)} + g\rho_i \sin(\alpha), \tag{2.2a}$$

$$0 = -p_y^{(i)} + g\rho_i \cos(\alpha), \tag{2.2b}$$

where $u^{(i)}$ is the velocity in the x-direction and α is the angle between the horizontal and the plane. Solving (2.2b) for p_i gives us

$$p^{(i)} = \kappa_i(x) + g\rho_i y \cos(\alpha), \tag{2.3}$$

where $\kappa_i(x)$ is the constant (with respect to y) of intergration. The no slip boundary condition at the plane is

$$u^{(i)} = 0, \qquad \text{at} \quad y = 0, \tag{2.4}$$

and the continuity of velocity, continuity of pressure and dynamic conditions at the interface are

$$u^{(i)} = u^{(i+1)}, \qquad \text{at} \quad y = \sum_{j=1}^{i} h_j, \tag{2.5a}$$

$$\mu_i u_y^{(i)} = \mu_{i+1} u_y^{(i+1)}, \qquad \text{at} \quad y = \sum_{j=1}^{i} h_j, \tag{2.5b}$$

$$p^{(i)} = p^{(i+1)}, \qquad \text{at} \quad y = \sum_{j=1}^{i} h_j, \tag{2.5c}$$

for i from 1 to $n-1$ and the continuity of pressure and dynamic conditions at the surface are

$$u_y^{(n)} = 0, \qquad \text{at} \quad y = \sum_{j=1}^{n} h_j, \tag{2.6a}$$

$$p^{(n)} = p^{(a)}, \qquad \text{at} \quad y = \sum_{j=1}^{n} h_j. \tag{2.6b}$$

We can prove by mathematical induction that the $p^{(i)}$'s are only dependent upon y by first calculating the pressure at the interface of fluid n and the ambient fluid which gives us

$$\kappa_n(x) = p^{(a)} - g\rho_n \cos(\alpha) \sum_{j=1}^{n} h_j. \tag{2.7}$$

Then we calculate the pressure at the interface of the i^{th} and $(i+1)^{st}$ fluid which gives us

$$\kappa_i(x) = \kappa_{i+1} + g\cos(\alpha) \left(\rho_{i+1} \sum_{j=1}^{i+1} h_j - \rho_i \sum_{j=1}^{i} h_j \right). \tag{2.8}$$

So by mathematical induction κ is independent of x and hence the $p^{(i)}$'s are only dependent upon y. Substituting (2.3) into (2.2a) and setting κ to be a constant and solving for u gives

$$u^{(i)}(y) = -g\frac{\rho_i}{2\mu_i} \sin(\alpha) y^2 + b_i y + c_i. \tag{2.9}$$

2.1.1 Single Layer

For 1 layer we have the velocity profile

$$u^{(1)}(y) = \frac{g\rho_1 \sin\alpha}{\mu_1} \left(h_1 y - \frac{y^2}{2} \right), \tag{2.10}$$

which we derive from (2.9), (2.4), (2.5) and (2.6). Now we want to find the height of the fluid given a flow rate, s_1, so we want to solve

$$s_1 = \int_0^{h_1} u^{(1)}(y)\mathrm{d}y, \tag{2.11}$$

for h_1, which implies

$$\hat{s}_1 = h_1^3/3, \tag{2.12}$$

where $\hat{s}_1 = \mu_1 s_1/(g\rho_1 \sin\alpha)$, which has one real solution,

$$h_1 = \left(\frac{3\mu_1 s_1}{g\rho_1 \sin\alpha}\right)^{1/3}, \tag{2.13}$$

given by solving (2.12). We can verify this is consistent with experiments by substituting in the values for one layer of fluid 2, with parameters given in table 1, with a flow rate of $s_1 = 0.002/0.12m^2s^{-1}$ giving $h_1 = 0.00124m$ to three significant figures. So for the given flow rate the thickness of the layer is about $1.24mm$ which is consistent with our experimental observations comparing visually the height of the fluid at the edge of the flow against the known height of the edge guides.

2.1.2 Two Layers

For 2 layers we have the velocity profiles

$$u^{(1)}(y) = -\frac{g\rho_1 \sin(\alpha)\, y^2}{2\mu_1} + \frac{g\sin(\alpha)\,(\rho_2 h_2 + \rho_1 h_1)\, y}{\mu_1}, \tag{2.14a}$$

$$\begin{aligned} u^{(2)}(y) = &-\frac{g\rho_2 \sin(\alpha)\, y^2}{2\mu_2} + \frac{g\rho_2 \sin(\alpha)\,(h_1 + h_2)\, y}{\mu_2} \\ &+\frac{g\sin(\alpha)\, h_1\,(\rho_1 h_1 \mu_2 + 2\,\mu_2\rho_2 h_2 - \rho_2 h_1 \mu_1 - 2\,\rho_2\mu_1 h_2)}{2\mu_1\mu_2}. \end{aligned} \tag{2.14b}$$

Now we want to find the height of the fluids given a flow rates s_1 and s_2 so we want to solve

$$s_1 = \int_0^{h_1} u^{(1)}(y)\mathrm{d}y, \tag{2.15a}$$

$$s_2 = \int_{h_1}^{(h_1+h_2)} u^{(2)}(y)\mathrm{d}y, \tag{2.15b}$$

for h_1 and h_2. Substituting equations (2.14a) and (2.14b) into (2.15a) and (2.15b) and integrating out gives two coupled cubics in h_1 and h_2 given by

$$s_1 = \frac{g\sin(\alpha)\,{h_1}^2\,(2\,\rho_1 h_1 + 3\,\rho_2 h_2)}{6\mu_1}, \tag{2.16a}$$

$$s_2 = \frac{g\sin(\alpha)\,h_2\left(2\,\rho_2\mu_1{h_2}^2 + 3\,\rho_1{h_1}^2\mu_2 + 6\,h_1\mu_2\rho_2 h_2\right)}{6\mu_1\mu_2}. \tag{2.16b}$$

We can solve (2.16a) for h_2 and substitute into (2.16b) to give a cubic in $z = h_1^3$ given by

$$f(h_1^3; s_1, s_2) = az^3 + bz^2 + cz + d = 0, \tag{2.17}$$

where

$$a = \frac{g{\rho_1}^2\sin(\alpha)\,(9\,\mu_2\rho_2 - 8\,\rho_1\mu_1)}{81{\rho_2}^2\mu_1\mu_2}, \tag{2.18a}$$

$$b = \frac{8\,{\rho_1}^2 s_1\mu_1 - 15\,\rho_1\mu_2\rho_2 s_1 - 9\,s_2{\rho_2}^2\mu_2}{9{\rho_2}^2\mu_2}, \tag{2.18b}$$

$$c = \frac{4\mu_1{s_1}^2\,(3\,\mu_2\rho_2 - 2\,\rho_1\mu_1)}{3{\rho_2}^2 g\mu_2\sin(\alpha)}, \tag{2.18c}$$

$$d = \frac{8{s_1}^3{\mu_1}^3}{3{\rho_2}^2 g^2\left(\sin(\alpha)\right)^2\mu_2}. \tag{2.18d}$$

In solving (2.16a) for h_2 we have implicitly placed a restriction on h_1. Since $h_2 > 0$ from (2.16a) we arrive after some manipulation to the condition

$$h_1 < \left(\frac{3s_1\mu_1}{g\rho_1\sin\alpha}\right)^{1/3} \equiv \hat{z}^{1/3}. \tag{2.19}$$

In general, equation (2.17) has three solutions which are dependent upon the coefficients (2.18). It is not immediately obvious whether there is one unique realistic solution. By considering the sign of the coefficients of (2.18) and the turning points of $f(z)$, we are able to determine that there is only one realistic solution to (2.17), the proof of which we give below.

We note that the parameters μ_1, μ_2 and s_1 are all positive. So $d > 0$ for all values of the parameters, which gives that $f(0) > 0$. Also we note that $f(\hat{z}) < 0$. So by the intermediate value theorem there exists at least one root in the interval $z = 0$ to $z = \hat{z}$.

Case 1

We consider what happens when $a > 0$. Since $a > 0$ this gives after some manipulation that $b < 0$ and $c < 0$. Since $a > 0$ two of the roots are at a position less than zero and greater than $\hat{z}$ respectively as shown in figure 2.2. Giving us the one root in our interval as required.

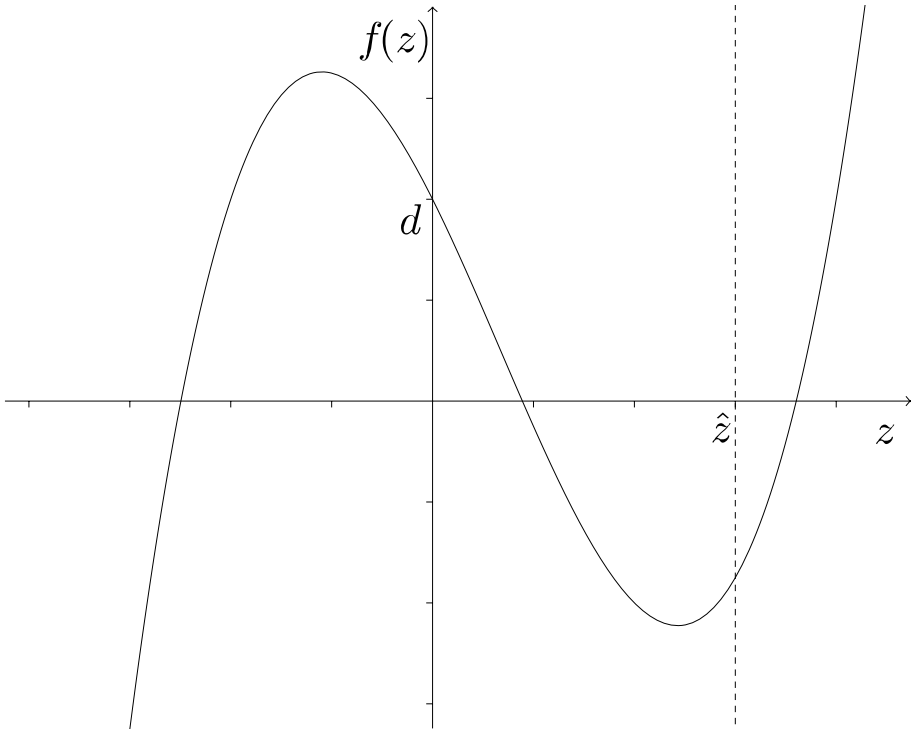

Figure 2.2: Sketch of a possible $f(z)$ for the restrictions given in case 1.

Case 2a

For $a < 0$ we cannot determine more information so we consider $c > 0$ which gives after

some manipulation $b < 0$. Considering the stationary points given by the solution of

$$\frac{df(z)}{dz} = 3az^2 + 2bz + c = 0, \tag{2.20}$$

the solutions of (2.20) are given by

$$z = \frac{-b \pm \sqrt{b^2 - 3ac}}{3a}, \tag{2.21}$$

which has one positive and one negative solution so the only configuration is one root in the interval $z = 0$ to $z = \hat{z}$ as shown in figure 2.3.

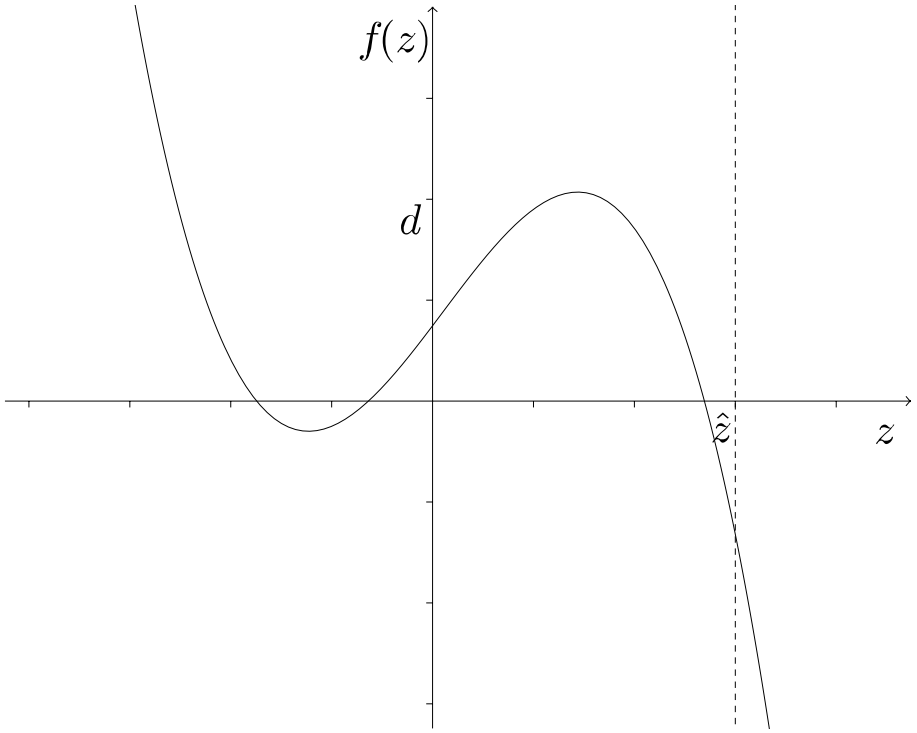

Figure 2.3: Sketch of a possible $f(z)$ for the restrictions given in case 2a or 2b(i).

Case 2b(i)

Next we consider $c < 0$. This does not determine the sign of b so first we consider $b < 0$. Considering the midpoint of the two turning points given by

$$z'' = -\frac{b}{3a} < 0. \tag{2.22}$$

This leads to a configuration as shown in figure 2.3. But if the discriminant of (2.20) is negative then there are no turning points and figure 2.4 shows a case of this.

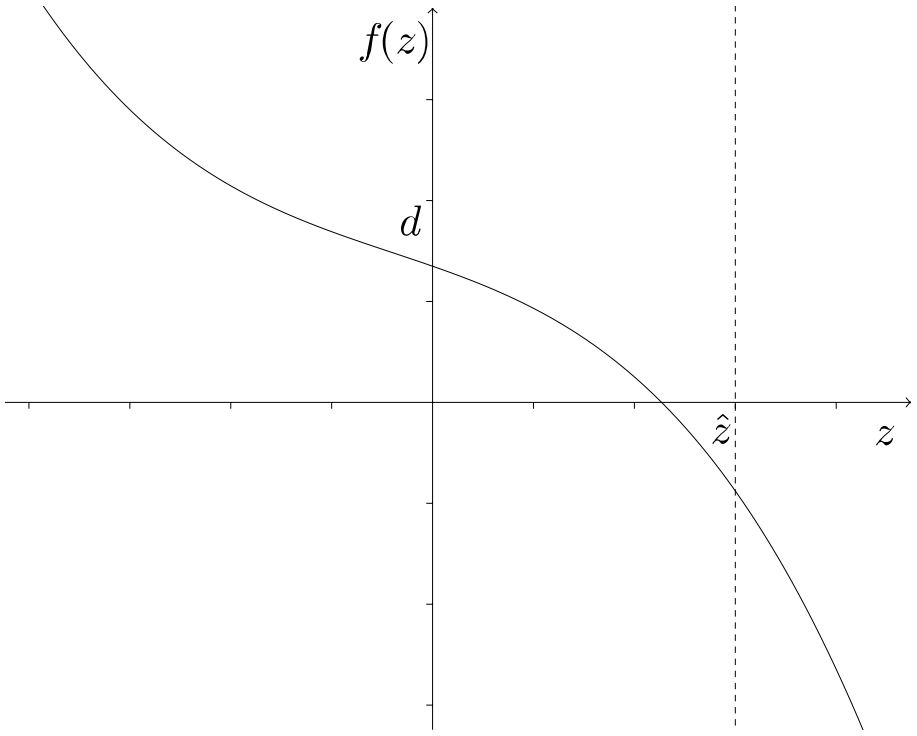

Figure 2.4: Sketch of a possible $f(z)$ for the restrictions given in case 2b(i) or 2b(ii).

Case2b(ii)

For the final case we consider $c < 0$ and $b > 0$. If $b > 0$ then the discriminant of (2.20), $b^2 - 3ac$, is negative then $f(z)$ has no turning points and figure 2.4 is what our $f(z)$ should look like.

We have considered all possible signs of the coefficients of (2.17) and proved that there is only one root of (2.17) in the range $z = 0$ to $z = \hat{z}$.

To illustrate a typical velocity profile for two layers we have computed the velocity profiles, plotting (2.14a) and (2.14b), for a two layer flow given by the first row of table 5, at breakup, shown in figure 2.5.

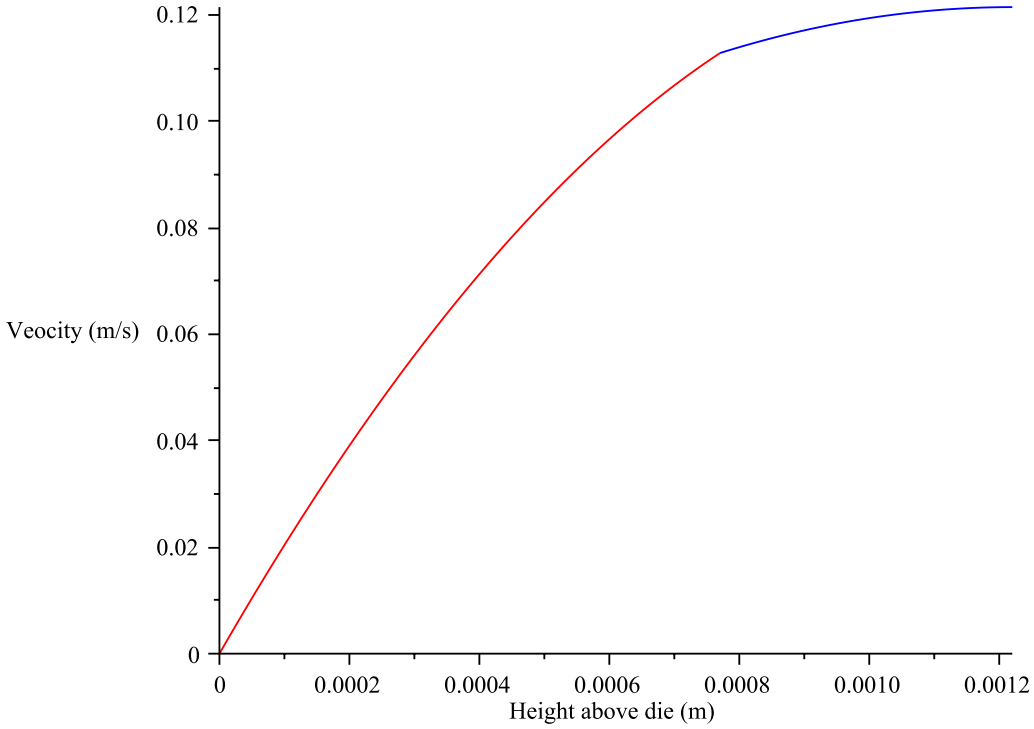

Figure 2.5: Plot of (2.14a) and (2.14b) for the two layer flow given by row 1 of table 5.

2.1.3 Three Layers

For three layers we have the velocity profiles

$$u^{(1)}(y) = -\frac{g\rho_1 \sin(\alpha)\, y^2}{2\mu_1} + \frac{g \sin(\alpha)\,(\rho_2 h_2 + \rho_1 h_1)\, y}{\mu_1}, \tag{2.23a}$$

$$\begin{aligned} u^{(2)}(y) = &-\frac{g\rho_2 \sin(\alpha)\, y^2}{2\mu_2} + \frac{g\rho_2 \sin(\alpha)\,(h_1 + h_2)\, y}{\mu_2} \\ &-\frac{g \sin(\alpha)\, h_1\,(-\rho_1 h_1 \mu_2 - 2\,\mu_2 \rho_2 h_2 + \rho_2 h_1 \mu_1 + 2\,\rho_2 \mu_1 h_2)}{2\mu_1\mu_2}, \end{aligned} \tag{2.23b}$$

$$\begin{aligned} u^{(3)}(y) = &-\frac{g\rho_3 \sin(\alpha)\, y^2}{2\mu_3} + \frac{g \sin(\alpha)\,(-\rho_2 h_3 + \rho_3 h_1 + \rho_3 h_2 + \rho_3 h_3)\, y}{\mu_3} \\ &+\frac{1}{2\mu_1} g \sin(\alpha)\, h_1\,(\rho_1 h_1 + 2\,\rho_2 h_2) + \frac{1}{2\mu_2} g \sin(\alpha)\,\rho_2\left({h_2}^2 - {h_3}^2\right) \\ &-\frac{1}{2\mu_3} g \sin(\alpha)\left(\rho_3 {h_1}^2 + 2\,\rho_3 h_1 h_2 + 2\,\rho_3 h_1 h_3 + \rho_3 {h_2}^2 + 2\,\rho_3 h_2 h_3\right. \\ &\left. +\rho_3 {h_3}^2 - 2\,\rho_2 h_3 h_1 - 2\,\rho_2 h_3 h_2 - 2\,\rho_2 {h_3}^2\right), \end{aligned} \tag{2.23c}$$

and the pressures

$$p^{(1)}(y) = p^{(a)} + g\cos(\alpha)\,(\rho_1 y - h_1\rho_1 - h_2\rho_2 - h_3\rho_3), \tag{2.24a}$$

$$p^{(2)}(y) = p^{(a)} + g\cos(\alpha)\left(\rho_2 y - h_1\rho_2 - h_2\rho_2 - h_3\rho_3\right), \tag{2.24b}$$

$$p^{(3)}(y) = p^{(a)} + g\cos(\alpha)\left(\rho_3 y - h_1\rho_3 - h_2\rho_3 - h_3\rho_3\right), \tag{2.24c}$$

which were computed using equations (2.4), (2.5), (2.6) and (2.9) using a maple script. We do not pursue the analysis here, but we expect that these equations to have precisely one solution as for the three layer unidirectional flow on the grounds that only one solution has been observed experimentally.

2.2 Stability of Three Layer Flow Down an Inclined Plane

We consider an inclined plane with three layers of fluid, numbered 1, 2 and 3 with 1 being the layer closest to the plane and 3 being the layer with a free surface as shown in figure 2.6. We take the x-axis pointing down along the plane and the y-axis perpendicular pointing away from the plane. We start by considering the solution for unidirectional flow down an inclined plane, given in the previous section. To this unidirectional solution we add a small perturbation of the velocity and pressure.

As we are considering small perturbations of the velocity and pressure we can take the Navier-Stokes equations and ignore nonlinear terms (since we are considering small perturbations of a steady state) and ignore external forces, excepting gravity, we arrive at the Stokes equations

$$-\frac{\partial p_j}{\partial x} + \mu_j\left(\frac{\partial^2 u_j}{\partial x^2} + \frac{\partial^2 u_j}{\partial y^2}\right) + \rho_j g\sin(\theta) = 0, \tag{2.25a}$$

$$-\frac{\partial p_j}{\partial y} + \mu_j\left(\frac{\partial^2 v_j}{\partial x^2} + \frac{\partial^2 v_j}{\partial y^2}\right) - \rho_j g\cos(\theta) = 0, \tag{2.25b}$$

$$\frac{\partial u_j}{\partial x} + \frac{\partial v_j}{\partial y} = 0 \tag{2.25c}$$

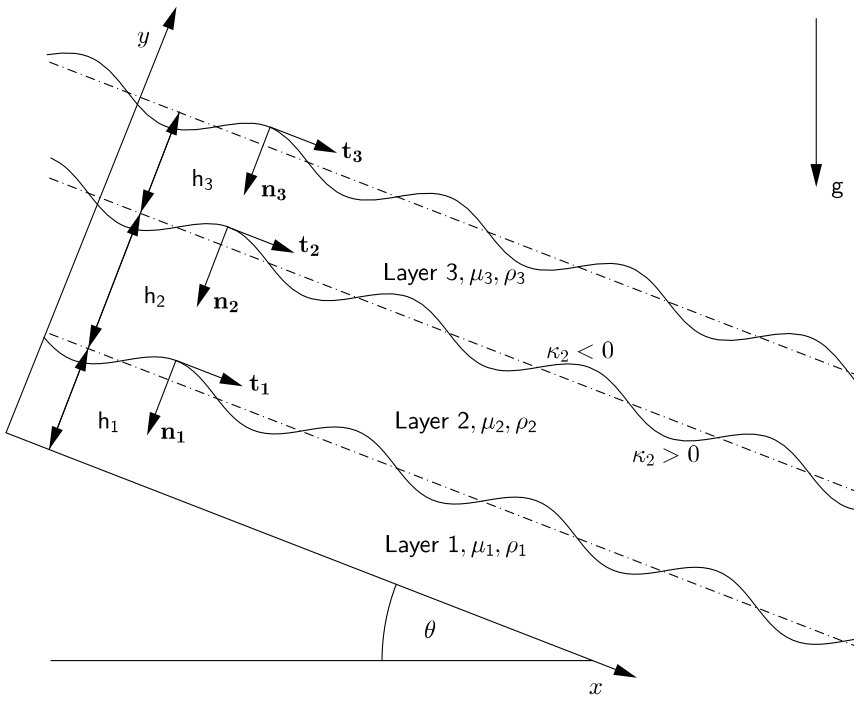

Figure 2.6: Illustration of a three layer flow down an inclined plane.

where the μ_j's are the dynamic viscosities, the ρ_j's are the densities of the fluids, the u_j's are the velocities in the x direction, the v_j's the velocities in the y direction, g is gravity, θ is the angle between the horizontal and the incline plane and the p_j's are the pressures. The subscripts $j = 1$ to 3 denote the lower, middle and upper fluid respectively. We non-dimensionalise by scaling the velocity by $\hat{U} = \rho_1 g h_1^2 \sin(\theta)/\mu_1$, time by $h_1/\hat{U}$, pressure by $\mu_1 \hat{U}/h_1$ and having a length scale of h_1. We introduce the streamfunctions ψ_j such that

$$u_j = U_j(y) + \frac{\partial \psi_j}{\partial y}, \tag{2.26a}$$

$$v_j = -\frac{\partial \psi_j}{\partial x}, \tag{2.26b}$$

where $U_j(y)$ is the unidirectional steady state velocity solution derived in the previous section, in which case (2.25c) is automatically satisfied. Taking the partial derivative of (2.25a) with respect to y, the partial derivative of (2.25b) with respect to x and taking

the difference of these two equations eliminates the pressure and leaves

$$\frac{\partial}{\partial y}\left(\frac{\partial^2 u_j}{\partial x^2}+\frac{\partial^2 u_j}{\partial y^2}\right)-\frac{\partial}{\partial x}\left(\frac{\partial^2 v_j}{\partial x^2}+\frac{\partial^2 v_j}{\partial y^2}\right)=0. \tag{2.27}$$

We assume that the perturbations have a normal mode from of $\exp(ik(x-ct))$. So taking a small perturbation parameter $0<\epsilon\ll 1$ we assume

$$\psi_j(x,y,t)=\epsilon\phi_j(y)\exp(ik(x-ct)), \tag{2.28a}$$

$$p_j(x,y,t)=P_j(y)+\epsilon q_j(y)\exp(ik(x-ct)), \tag{2.28b}$$

$$\gamma_j(x,t)=1+\epsilon\zeta_j\exp(ik(x-ct)), \tag{2.28c}$$

$$\Gamma_j(x,t)=1+\epsilon\xi_j\exp(ik(x-ct)), \tag{2.28d}$$

$$h_j(x,t)=de_j+\epsilon\eta_j\exp(ik(x-ct)), \tag{2.28e}$$

where $P_i(y)$ is the unidirectional steady state pressure derived in the previous section, k is the wavenumber of the perturbation, c is the complex growth rate of the perturbation, $de_1=0$, $de_2=h_2$ and $de_3=h_2+h_3$ as shown in Gao & Lu (2007). Substituting (2.26a) and (2.26b) into (2.27) gives

$$\frac{\partial}{\partial y}\left(\frac{\partial^2}{\partial x^2}\frac{\partial\psi_j}{\partial y}+\frac{\partial^2}{\partial y^2}\frac{\partial\psi_j}{\partial y}\right)+\frac{\partial}{\partial x}\left(\frac{\partial^2}{\partial x^2}\frac{\partial\psi_j}{\partial x}+\frac{\partial^2}{\partial y^2}\frac{\partial\psi_j}{\partial x}\right)=0, \tag{2.29}$$

which, substituting (2.28a) in, simplifies to the Orr-Sommerfeld equations in the limit of Stokes flow Gao & Lu (2007)

$$(\mathrm{D}^2-k^2)^2\phi_j=0, \tag{2.30}$$

where D= $\frac{d}{dy}$. We take the unidirectional flow (2.23a)-(2.24c) which for three layers in dimensionless constants and variables is

$$U_1(Y)=-\frac{1}{2}Y^2+YR_3\delta_3+YR_2\delta_2+Y, \tag{2.31a}$$

$$U_2(Y) = -\frac{1}{2}\frac{R_2 Y^2}{m_2} + \frac{Y R_3 \delta_3}{m_2} + \frac{Y R_2}{m_2} + \frac{Y R_2 \delta_2}{m_2} + R_3\delta_3 + R_2\delta_2 - \frac{R_3\delta_3}{m_2} - \frac{1}{2}\frac{R_2}{m_2} - \frac{R_2\delta_2}{m_2} + \frac{1}{2}, \tag{2.31b}$$

$$U_3(Y) = -\frac{1}{2}\frac{R_3 Y^2}{m_3} + \frac{Y R_3}{m_3} + \frac{Y R_3 \delta_2}{m_3} + \frac{Y R_3 \delta_3}{m_3} + \frac{1}{2}\frac{R_2 {\delta_2}^2}{m_2} - \frac{R_3\delta_2}{m_3} - \frac{1}{2}\frac{R_3 {\delta_2}^2}{m_3} + R_3\delta_3 + R_2\delta_2 + \frac{1}{2} - \frac{1}{2}\frac{R_3}{m_3} - \frac{R_3\delta_3}{m_3} - \frac{R_3\delta_2\delta_3}{m_3} + \frac{R_3\delta_2\delta_3}{m_2}, \tag{2.31c}$$

$$P_1(Y) = -\cot(\alpha) - R_2\cot(\alpha)\,\delta_2 + Pa - R_3\cot(\alpha)\,\delta_3 + Y\cot(\alpha), \tag{2.31d}$$

$$P_2(Y) = -R_2\cot(\alpha) - R_2\cot(\alpha)\,\delta_2 + Pa - R_3\cot(\alpha)\,\delta_3 + Y R_2\cot(\alpha), \tag{2.31e}$$

$$P_3(Y) = Pa - R_3\cot(\alpha) - R_3\cot(\alpha)\,\delta_2 - R_3\cot(\alpha)\,\delta_3 + Y R_3\cot(\alpha), \tag{2.31f}$$

where $Y = y/h_1$, $m_2 = \mu_2/\mu_1$, $m_3 = \mu_3/\mu_1$, $\delta_1 = h_2/h_1$, $\delta_2 = (h_2 + h_3)/h_1$, $R_2 = \rho_2/\rho_1$ and $R_3 = \rho_3/\rho_1$ are respectively the non-dimensional length and the ratios of viscosities, fluid thicknesses and densities. We introduce the non-dimensional constants the capillary number $Ca_j = \mu_j\hat{U}/\gamma_{j0}$ which is the ratio of the inertia to the surface tension and the Marangoni number$Ma_j = E_j\Gamma_{j0}/\gamma_{j0}$ where γ_{j0} is the uniform surface tension, E_j is the surface elasticity and Γ_{j0} is the basic value of the surfactant concentration which gives the sensitivity of the surface tension to the surfactant concentration. The non-dimensional force balance across the free surface is

$$\boldsymbol{\sigma}_3\cdot\mathbf{n}_3 + Ca_3^{-1}(\gamma_1\nabla\cdot\mathbf{n}_3)\mathbf{n}_3 - Ca_3^{-1}\frac{1}{H_3}\frac{\partial\gamma_3}{\partial x}\mathbf{t}_3 = 0, \tag{2.32}$$

where $\boldsymbol{\sigma}_3$ is the stress tensor, $H_3 = \sqrt{1 + (\partial h_3/\partial x)^2}$, $\mathbf{n}_3$ is the normal vector pointing in the direction of increasing y and $\mathbf{t}_3$ is the tangential vector pointing in the direction of increasing x. The dynamic condition at the interfaces are

$$(\boldsymbol{\sigma}_3 - \boldsymbol{\sigma}_2)\cdot\mathbf{n}_2 + Ca_2^{-1}(\gamma_2\nabla\cdot\mathbf{n}_2)\mathbf{n}_2 - Ca_2^{-1}\frac{1}{H_2}\frac{\partial\gamma_2}{\partial x}\mathbf{t}_2 = 0, \tag{2.33a}$$

$$(\boldsymbol{\sigma}_2 - \boldsymbol{\sigma}_1)\cdot\mathbf{n}_1 + Ca_1^{-1}(\gamma_1\nabla\cdot\mathbf{n}_1)\mathbf{n}_1 - Ca_1^{-1}\frac{1}{H_1}\frac{\partial\gamma_1}{\partial x}\mathbf{t}_1 = 0, \tag{2.33b}$$

where $H_j = \sqrt{1 + (\partial h_j/\partial x)^2}$ for $j = 1, 2$. The stress tensor is defined as

$$\boldsymbol{\sigma}_j = \begin{pmatrix} 2m_j \frac{\partial u}{\partial x} - p_j & \frac{\partial v}{\partial x} + \frac{\partial u}{\partial y} \\ \frac{\partial v}{\partial x} + \frac{\partial u}{\partial y} & 2m_j \frac{\partial v}{\partial y} - p_j \end{pmatrix}. \tag{2.34}$$

Also we apply the kinematic condition

$$\frac{\partial h_j}{\partial t} + u_j \frac{\partial h_j}{\partial x} = v_j, \tag{2.35}$$

at the free surface and interfaces.

A convection-diffusion equation governs the concentrations of insoluble surfactants which can be written as Halpern & Frenkel (2003)

$$\frac{\partial H_j \Gamma_j}{\partial t} + \frac{\partial H_j \Gamma_j u_j}{\partial x} = D_{sj} \frac{\partial}{\partial x} \left(\frac{1}{H_j} \frac{\partial \Gamma_j}{\partial x} \right), \tag{2.36}$$

in the one dimensional case where D_{sj} is the surfactant diffusivity. For our problem we assume $D_{sj} = 0$ and in practice the surface diffusivity is negligible Gao & Lu (2007). A linear approximation of the relationship between the surfactant concentration and surface tension is

$$\gamma_j - 1 = Ma_j(\Gamma_j - 1). \tag{2.37}$$

The no slip boundary conditions at the wall gives

$$\phi_1 = 0, \, \mathrm{D}\phi_1 = 0 \text{ at } y = -1. \tag{2.38}$$

The continuity of velocity and dynamic conditions across the interface closest to the wall gives

$$\eta_1 \mathrm{D}U_1 + \mathrm{D}\phi_1 = \eta_1 \mathrm{D}U_2 + \mathrm{D}\phi_2, \tag{2.39a}$$

$$\phi_1 = \phi_2, \tag{2.39b}$$

$$m_2(\mathrm{D}^2 - 3k^2)\mathrm{D}\phi_2 = (\mathrm{D}^2 - 3k^2)\mathrm{D}\phi_1 - Ca_1^{-1} i k^3 \eta_1, \tag{2.39c}$$

$$(\mathrm{D}^2 + k^2)\phi_2 - (\mathrm{D}^2 + k^2)\phi_1 = -Ma_1 Ca_1^{-1} ik\xi_1, \tag{2.39d}$$

at $y = 0$. The continuity of velocity and dynamic conditions across the second interface gives

$$\eta_2 \mathrm{D}U_3 + \mathrm{D}\phi_3 = \eta_2 \mathrm{D}U_2 + \mathrm{D}\phi_2, \tag{2.40a}$$

$$\phi_2 = \phi_3, \tag{2.40b}$$

$$m_3(\mathrm{D}^2 - 3k^2)\mathrm{D}\phi_3 = m_2(\mathrm{D}^2 - 3k^2)\mathrm{D}\phi_2 - Ca_2^{-1} ik^3\eta_2, \tag{2.40c}$$

$$(\mathrm{D}^2 + k^2)\phi_3 - (\mathrm{D}^2 + k^2)\phi_2 = -Ma_2 Ca_2^{-1} ik\xi_2, \tag{2.40d}$$

at $y = \delta_1$. The dynamic conditions at the free surface are

$$ik\eta_3 \mathrm{D}P_3 + m_3(\mathrm{D}^2 - 3k^2)\mathrm{D}\phi_3 = -Ca_3^{-1} ik^3\eta_3, \tag{2.41a}$$

$$\eta_3 \mathrm{D}^2 U_3 + (\mathrm{D}^2 + k^2)\mathrm{D}\phi_3 = -Ma_3 Ca_3^{-1} ik\xi^3, \tag{2.41b}$$

at $y = \delta_2$. The kinematic conditions and transport equations are

$$\eta_1(U_1 - c) + \phi_1 = 0, \quad \text{at } y = 0, \tag{2.42a}$$

$$\eta_2(U_2 - c) + \phi_2 = 0, \quad \text{at } y = \delta_1, \tag{2.42b}$$

$$\eta_3(U_3 - c) + \phi_3 = 0, \quad \text{at } y = \delta_2, \tag{2.42c}$$

$$\xi_1(U_1 - c) + \eta_1 \mathrm{D}U_1 + \mathrm{D}\phi_1 = 0, \quad \text{at } y = 0, \tag{2.42d}$$

$$\xi_2(U_2 - c) + \eta_2 \mathrm{D}U_2 + \mathrm{D}\phi_2 = 0, \quad \text{at } y = \delta_1, \tag{2.42e}$$

$$\xi_3(U_3 - c) + \mathrm{D}\phi_3 = 0, \quad \text{at } y = \delta_2. \tag{2.42f}$$

Where we have resolved the pressure terms by rearranging the stokes equations in the x-direction.

The general solution to (2.30) is

$$\phi_j(y) = A_j \cosh(ky) + b_j \sinh(ky) + C_j y \cosh(ky) + h_j y \sinh(ky), \tag{2.43}$$

where the coefficients A, B, C and D are to be found. We substitute (2.43) into (2.38) - (2.42f) and arrive at a homogeneous linear set of equations which can be expressed as a matrix as so

$$\mathbf{M} \cdot w = 0, \tag{2.44}$$

where $w = [A_1, B_1, C_1, h_1, A_2, B_2, C_2, h_2, A_3, B_3, C_3, h_3, \eta_1, \eta_2, \eta_3, \xi_1\xi_2\xi_3]^T$ is the vector of unknowns and the matrix $\mathbf{M}$ is an 18 by 18 matrix with c appearing only linearly on the diagonal. This allows us to formulate it as a generalized eigenvalue problem of the form

$$\mathbf{M}' \cdot w = c\,\mathbf{c}' \cdot w, \tag{2.45}$$

where $\mathbf{M}'$ is the matrix $\mathbf{M}$ with c set to zero and $\mathbf{c}'$ is a diagonal matrix of the coefficients of c. It can be noted that one can also set $det(\mathbf{M}) = 0$, ignoring the trivial case of $w = 0$, to get a polynomial of degree six but finding the roots is not a trivial task. The parameters that remain after solving (2.45) are the wave speed c and wavenumber k, the thickness ratios δ_1 and δ_2, the viscosity ratios m_2 and m_3, the density ratios R_2 and R_3, the Marangoni numbers Ma_1, Ma_2 and Ma_3, the capillary numbers Ca_1, Ca_2 and Ca_3 and the angle of inclination of the plane θ. For simplicity we will assume that the densities are equal, the capillary numbers are all equal to unity and set the angle of inclination of the plane to be $\theta = 0.2$.

2.3 Plots of Linear Stability Analysis

We now consider the solutions of (2.45) considering the varying wavenumber to the corresponding growth rate. We present our results as a comparison between the growth rate and wavenumber kc and the wavenumber k.

Briefly we consider two layers of fluid. We label them as in figure 2.1 ignoring layer 3.

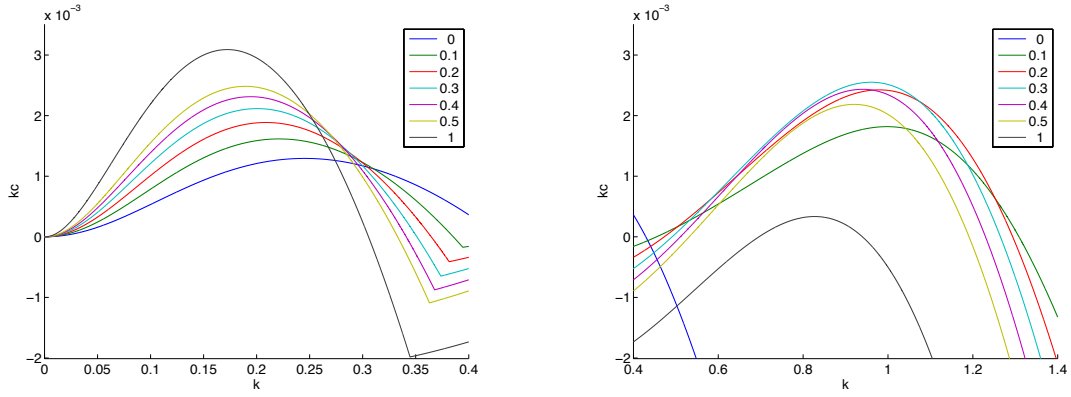

(a) Small wavenumber

(b) Large wavenumber

Figure 2.7: Effect of surfactant on the stability of a two layer flow for $\delta = 0.5$, $m = 2.5$, $Ca_1 = Ca_2 = 1$, $Ma_2 = 0$, $\theta = 0.2$ and varying Ma_1 at the interface.

We introduce the non-dimensional variables $\delta = h_2/h_1$, $m = \mu_2/\mu_1$, Ca_1, Ca_2, Ma_1 and Ma_2, where the Ma's and Ca's are defined as above. Considering two layers of fluid we can see by figures 2.7a and 2.7b that choosing $\delta = 1/2$ can lead to multimode solutions and stable bandwidths. It should be noted that Gao & Lu (2007) only presented results where $\delta = 1$.

First we consider the effect of adding an additional layer to Gao & Lu (2007) figure 2a, where the free surface has surfactant laden on it and the interface is clean. We consider an additional layer placed above the two layers of Gao & Lu (2007) with the same viscosity and thickness as our layer 2 and having a clean free surface. This is equivalent to letting $\delta_1 = \delta_2 = 1$, $m_1 = m_2 = 2.5$, $Ca_1 = Ca_2 = Ca_3 = 1$, $\theta = 0.2$ and $Ma_1 = Ma_3 = 0$ and varying Ma_2 as shown in figure 2.8. Similar to Gao & Lu (2007) no instability occurs when $m_1 < 1$ and $m_2 < 1$. Since the upper layers are more viscous than the lower layer we expect an instability without surfactant as verified in figure 2.8. As in Gao & Lu (2007) the presence of surfactant both decreases the maximum growth rate and reduces the bandwidth of the unstable wavenumbers monotonically. The instability

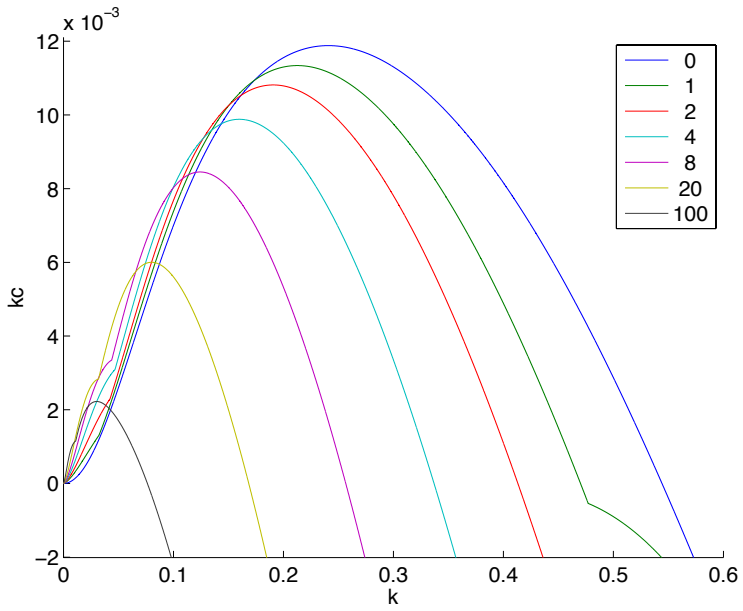

Figure 2.8: Effect of surfactant on the stability for $\delta_1 = \delta_2 = 1$, $m_1 = m_2 = 2.5$, $Ca_1 = Ca_2 = Ca_3 = 1$, $Ma_1 = Ma_3 = 0$, $\theta = 0.2$ and varying Ma_2.

arising from the more viscous upper layers cannot be completely eliminated by introducing surfactant to the second interface but is reduced greatly, as there is always a sufficiently small wavenumber which is unstable for $0 < Ma_2 < \infty$.

Unlike in Gao & Lu (2007) figure 2a we observe kinks in the maximum unstable wavenumber, near $k = 0$ in figure 2.8, these are where two different modes overlap as shown in figure 2.9. Unlike for two layer flow with surfactant we can observe multiple unstable modes which lead to interesting interactions with a change in parameters, as we will further investigate. This phenomenon is believed to be a new observation for stability of multilayer film flows.

Next we consider three layers of fluid where the total initial thickness of the upper two layers is equal to the lower layer, so $\delta_1 = \delta_2 = 1/2$, and we have surfactant only on the second interface, so $Ma_1 = Ma_3 = 0$. The other parameters are as follows, $m_1 = m_2 = 2.5$,

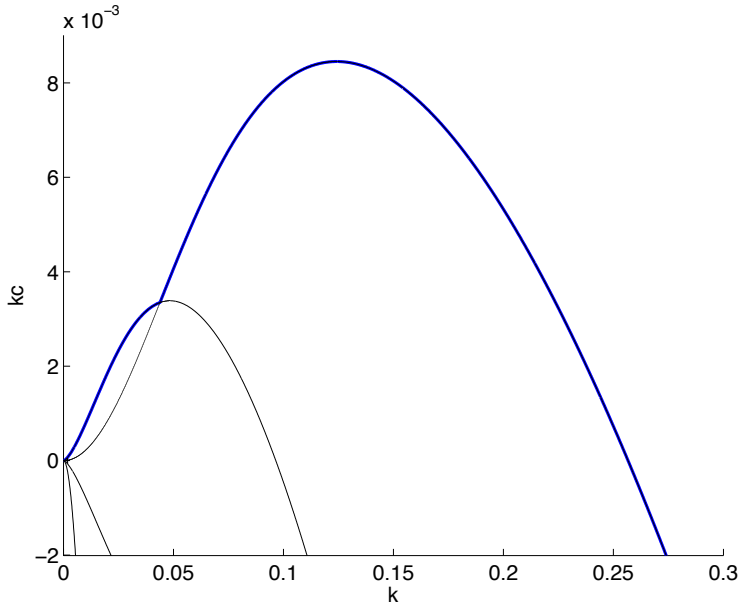

Figure 2.9: Multiple modes of stability for $\delta_1 = \delta_2 = 1$, $m_1 = m_2 = 2.5$, $Ca_1 = Ca_2 = Ca_3 = 1$, $Ma_1 = Ma_3 = 0$, $\theta = 0.2$ and $Ma_2 = 8$.

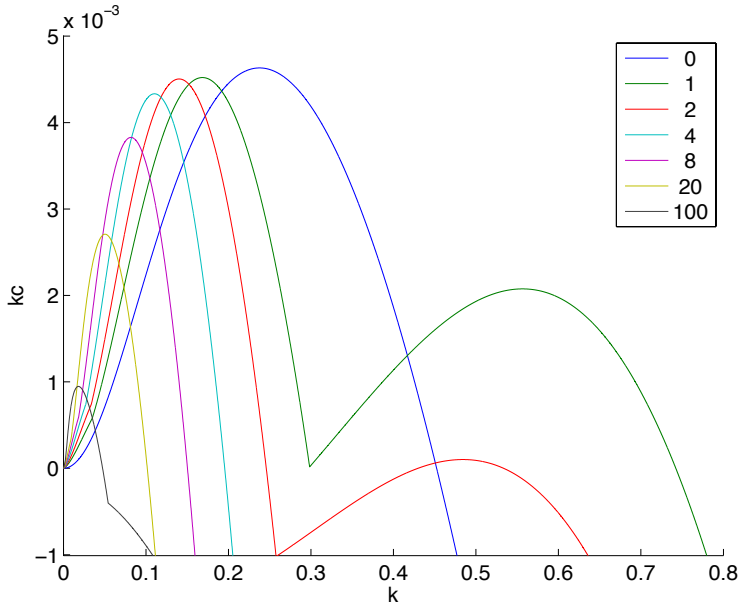

Figure 2.10: Effect of surfactant on the stability for $\delta_1 = \delta_2 = 0.5$, $m_1 = m_2 = 2.5$, $Ca_1 = Ca_2 = Ca_3 = 1$, $Ma_1 = Ma_3 = 0$, $\theta = 0.2$ and varying Ma_2.

$Ca_1 = Ca_2 = Ca_3 = 1$ and $\theta = 0.2$ shown in figure 2.10. This leads to a situation whereby we can observe a stable bandwidth of wavenumbers sandwiched between two unstable

bandwidths of wavenumbers. We note also that both modes behave monotonically when we increase the surfactant concentration of the second interface.

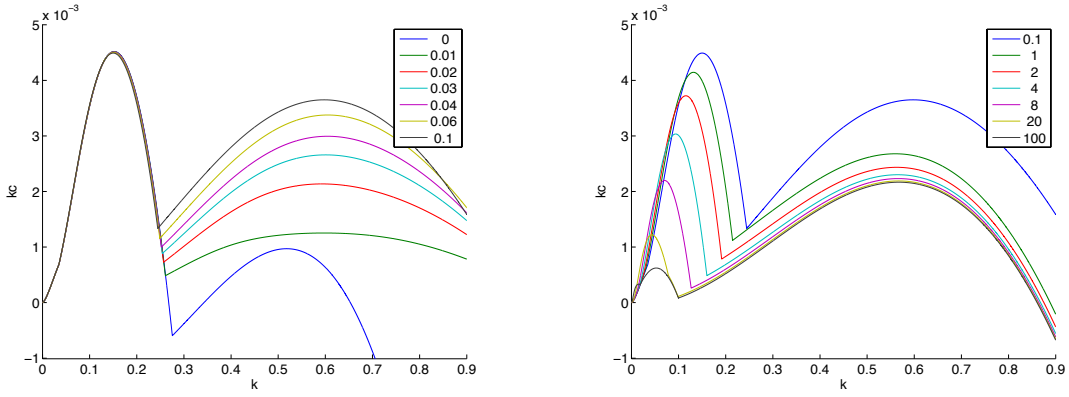

(a) Small Ma_3 (b) Large Ma_3

Figure 2.11: Effect of surfactant on the stability for $\delta_1 = \delta_2 = 0.5$, $m_1 = m_2 = 2.5$, $Ca_1 = Ca_2 = Ca_3 = 1$, $Ma_1 = 0$, $Ma_2 = 1.5$, $\theta = 0.2$ and varying Ma_3.

Taking the case of having a stable bandwidth sandwich from figure 2.10 by letting $Ma_2 = 1.5$ we introduce surfactant to the free surface as shown in figures 2.11a and 2.11b. In figure 2.11a we can see that increasing Ma_3 form 0 to 0.1 causes the second mode to grow while having little effect upon the first mode. While in figure 2.11b increasing Ma_3 from 0.1 to 100 dampens both modes, but notably the first mode much more than the second. This is also showing adding surfactant is causing the first mode to monotonically decrease whilst the second mode is exhibiting non-monotonic behavior. When $Ma_3 \approx 7.756$ we can see that there is not one but two most rapidly growing wavenumbers. As $Ma_3 \to \infty$ the growth rates do not tend to zero but to a curve close to $Ma_3 = 100$, that is a growth rate which is comparable in magnitude to having little or no surfactant upon the surface. This implies that surface immobility does not ensure a stable system.

Again looking at the case in figure 2.10 where a stable bandwidth sandwich is present we

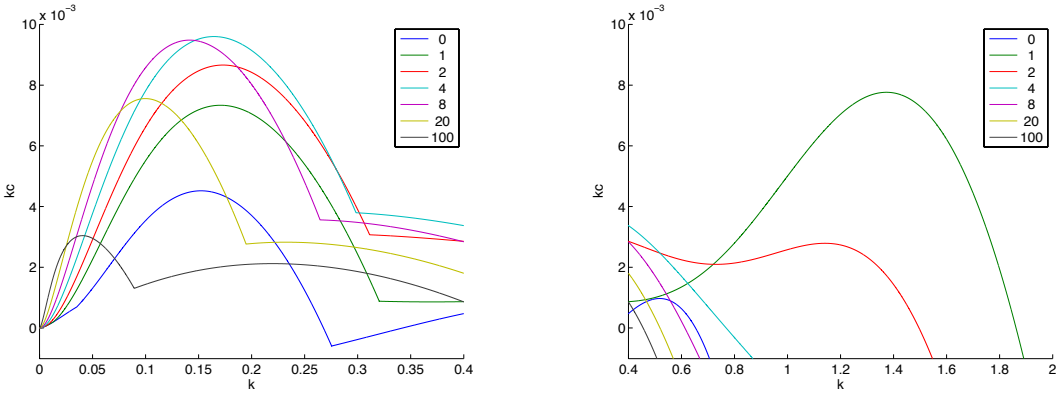

(a) Small wavenumber

(b) Large wavenumber

Figure 2.12: Effect of surfactant on the stability for $\delta_1 = \delta_2 = 0.5$, $m_1 = m_2 = 2.5$, $Ca_1 = Ca_2 = Ca_3 = 1$, $Ma_2 = 1.5$, $Ma_3 = 0$, $\theta = 0.2$ and varying Ma_1.

now consider adding surfactant to the first interface as shown in figures 2.12a and 2.12b. For the purposes of visualization we have split the plot into two figures with different k-scales. Both modes are exhibiting non-monotonic behavior over differing Ma_1 scales. The first modes maximum peaks when $Ma_1 \approx 6$ while the second modes maximum peaks at $Ma_1 \approx 1$. While in figures 2.11a and 2.11b the maximum growth rates of the two modes are decreasing slowly whereas in figures 2.12a and 2.12b the maximum growth rates of the two modes are decreasing more rapidly.

To further illustrate more clearly what is happening in figures 2.12a and 2.12b we look more closely at the range of $Ma_1 = 0.05$ to 4, shown in figures 2.13a and 2.13b. In this range the first mode monotonically increases whilst the second mode increases to a peak near $Ma_1 \approx 0.5$ whereupon it decreases.

Adding surfactant to the free surface, of a stable configuration with $\delta_1, \delta_2 < 1$, has a destabilising effect upon the flow as shown in figure 2.14. Here we have a stable configuration for $Ma_3 < 0.45$ which becomes unstable as we increase Ma_3 reaching a maximum

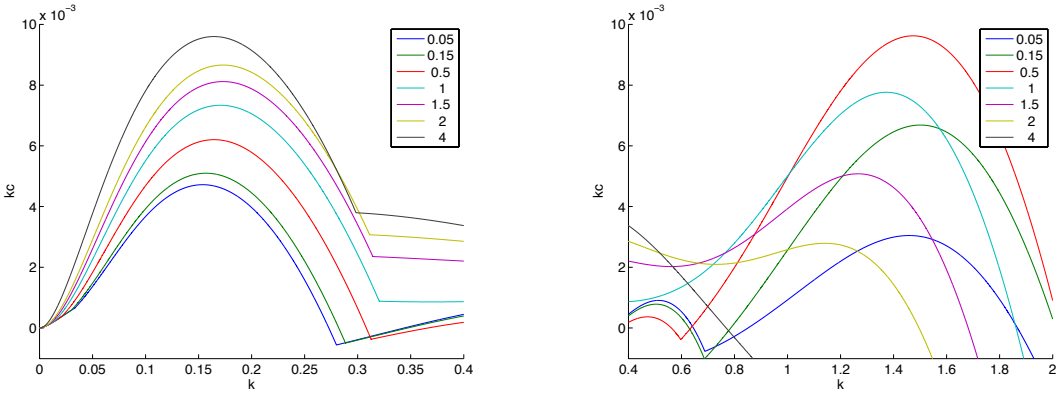

(a) Small wavenumber

(b) Large wavenumber

Figure 2.13: Effect of surfactant on the stability for $\delta_1 = \delta_2 = 0.5$, $m_1 = m_2 = 2.5$, $Ca_1 = Ca_2 = Ca_3 = 1$, $Ma_2 = 1.5$, $Ma_3 = 0$, $\theta = 0.2$ and varying Ma_1.

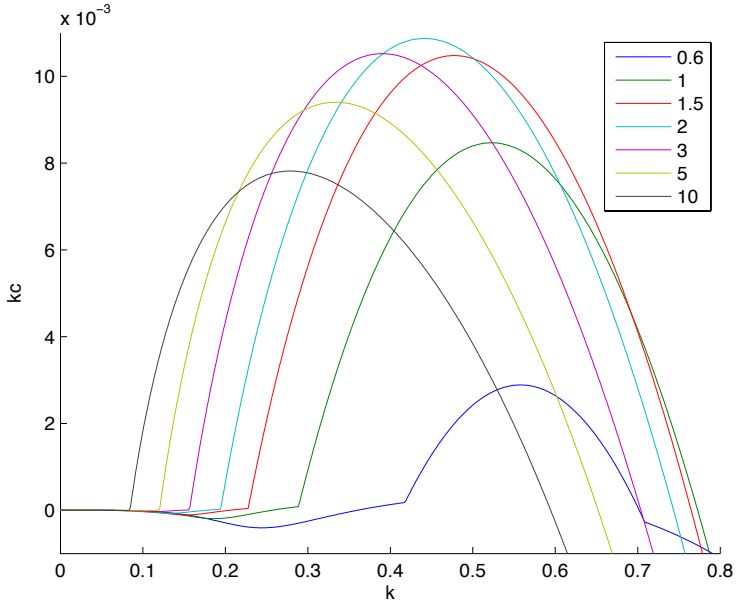

Figure 2.14: Effect of surfactant on the stability for $\delta_1 = \delta_2 = 0.25$, $m_1 = m_2 = 0.5$, $Ca_1 = Ca_2 = Ca_3 = 1$, $Ma_1 = Ma_2 = 0$, $\theta = 0.2$ and varying Ma_3.

at $Ma_3 \approx 2$ after which increasing Ma_3 has a stabilising effect. Unlike earlier examples the band of unstable wavenumbers starts at a non zero k implying that large wavelength perturbations are stable. Increasing Ma_3 from $Ma_3 = 0.6$ increases the upper limit of the unstable band until $Ma_3 = 1$ where increasing Ma_3 from here decreases the upper limit.

The lower limit of the unstable band decreases as Ma_3 increases from $Ma_3 = 0.6$. This case is interesting in particular due to having a stable bandwidth between zero and the k position of the smallest unstable wavenumber.

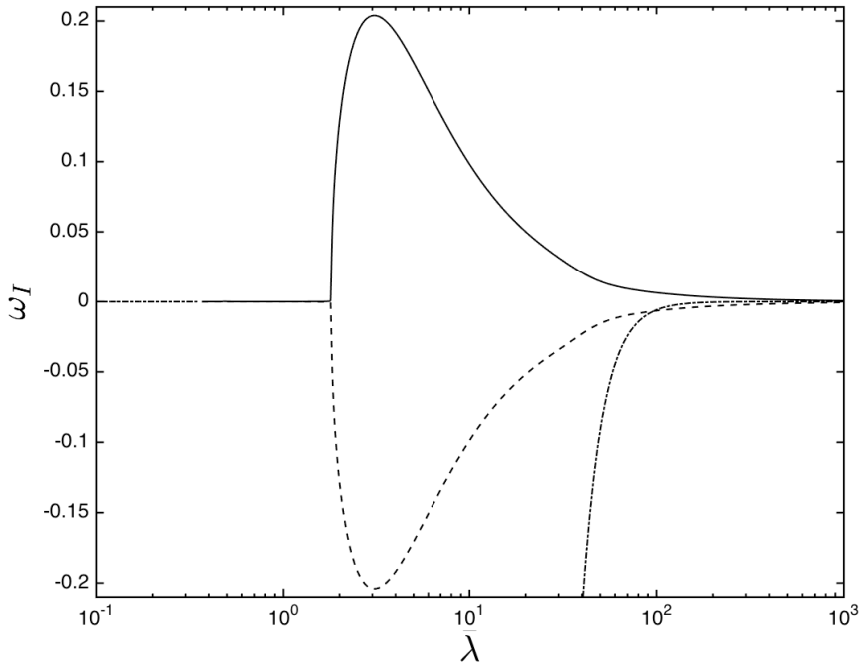

Figure 2.15: Plot of growth rate ω_I against wavelength $\bar{\lambda}$ for the parameters given in Weinstein and Chen's figure 3, where we have taken $\beta = \pi/2$.

To give more confidence that our equations are correct we compared our results with those of Weinstein & Chen (1999). In particular we computed their figure 3 using our equations which led to figure 2.15. It should be noted that we took $Ca = 1/1000$ rather than $Ca = 1000$ as in Weinstein & Chen (1999) as taking a large capillary number does not lead to the plot shown suggesting a typo. With these changes and keeping the other parameters as quoted in the figure caption we arrive at figure 2.15. As we can see our figure is almost identical to that found in Weinstein & Chen (1999) figure 3. This agreement supports our equations, especially the cases with no surfactant. To relate the wavelength and growth rate to our variables we assigned $\bar{\lambda} = \frac{2\pi}{k}$ and $\omega_I = \mathbb{I}\mathrm{m}(kc)$.

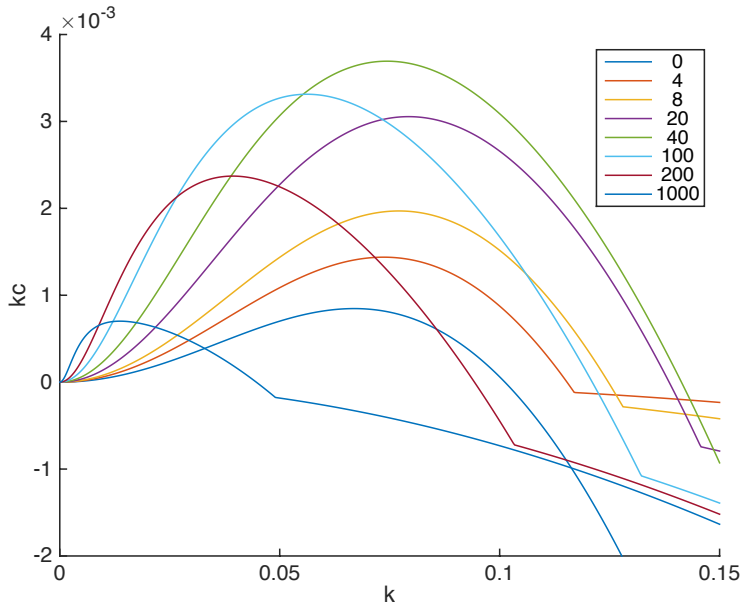

Figure 2.16: Plot of growth rate kc against wavenumber k for the parameters given in Gao & Lu (2007) figure 2b.

In comparing our results to those of Gao & Lu (2007) we must note that we found small differences between our equations and theirs', namely the m in both equations (2.18) and (2.20) are not present in our calculations of these equations, thus we expect our results to be slightly different. After careful analysis of our equations and comparing them to Weinstein & Chen (1999) we conclude that the equations are correct as we present them. This is shown in figures 2.16 and 2.17 where we have computed Gao & Lu (2007) figure 2b and 5 respectively. For figure 2.16 we have plotted the mode with the largest growth rate for each k rather than the unstable mode. It should be noted that although the most unstable configuration occurs when the Marangoni number related to the free surface equals 40 whereas Gao & Lu (2007) found the most unstable configuration to have a Marangoni number of 20 the figures are qualitatively the same. So there is a non-monotonic relationship between the maximum growth rate and the Marangoni number as shown by Gao & Lu (2007).

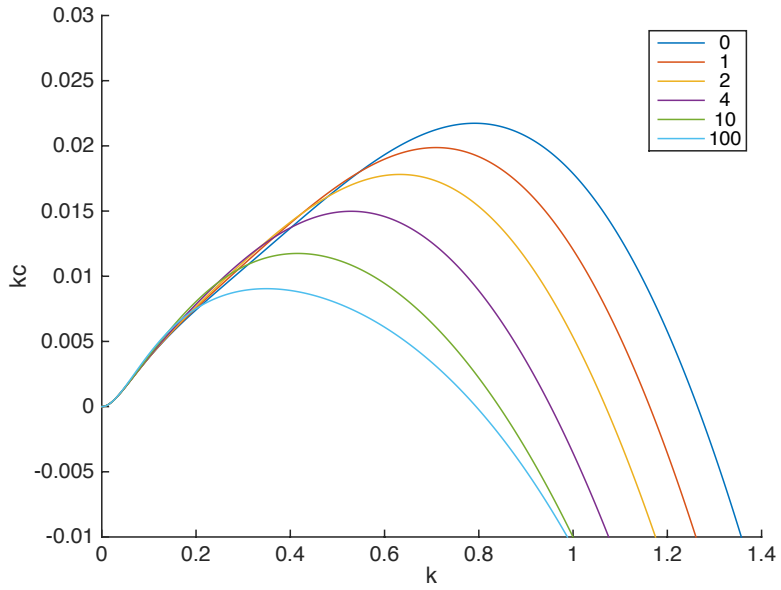

Figure 2.17: Plot of growth rate kc against wavenumber k for the parameters given in Gao & Lu (2007) figure 5.

In figure 2.17 again we find small differences between our calculation and Gao & Lu (2007). The maximum of each case in figure 2.17 are slightly lower than in Gao & Lu (2007) figure 5 and the values of the growth rate curves at $c = 0$ are larger but again qualitatively both figures show the same results whereby adding surfactant to the free surface where there is already surfactant on the interface has a stabilising effect.

All of the plots in Gao & Lu (2007) were recalculated using our equations and similar results were found as above where a general agreement was found with small but noticeable differences in the exact values being found. Apart from the discrepancy with the presence of viscosity ratios in some equations the results are in general agreement for all the parameter sets given in Gao & Lu (2007) paper.

3 Nonlinear Investigations of Three Layer Flow Down an Inclined Plane

In order to better understand the evolution of the unstable flows we derive nonlinear equations which we solve numerically in section 3.1. These equations lead us to travelling wave solutions which we find by considering the travelling wave form of the equations found for the nonlinear evolution. These we solve by a similar numerical method giving rise to travelling wave branches discussed in detail in section 3.2.

3.1 Nonlinear Evolution of Three Layer Flow Down an Inclined Plane

To further understand the effects of surfactants upon the dynamics of multi layer flow we consider the nonlinear evolution of the flow by taking a long wave approximation of the flow similar to that considered in Tseluiko *et al.* (2008).

We consider an inclined plane with three layers of fluid, numbered 1, 2 and 3 with 1 being the layer closest to the inclined plane and 3 being the uppermost layer with a free surface. We take the x-axis pointing parallel with the inclined plane in the direction of positive gravitational force and the y-axis perpendicular to and pointing away from the inclined plane.

We take the Navier-Stokes equations

$$\rho_j \left(\frac{\partial \mathbf{u}_j}{\partial t} + \mathbf{u}_j \cdot \nabla \mathbf{u}_j \right) = -\nabla p_j + \mu_j \nabla^2 \mathbf{u}_j + \rho_j \mathbf{g}, \tag{3.1a}$$

$$\nabla \cdot \mathbf{u}_j = 0 \tag{3.1b}$$

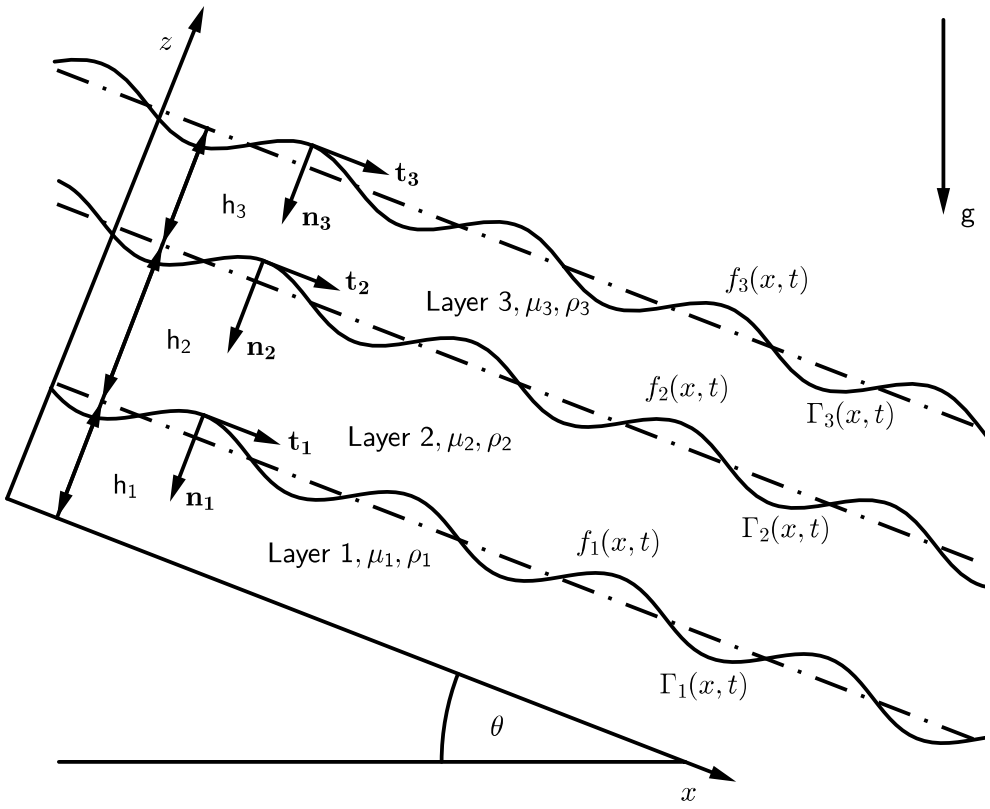

Figure 3.1: Illustration of a three layer flow down an inclined plane.

where the μ_j's are the dynamic viscosities, the ρ_j's are the densities of the fluids, the $\mathbf{u}_j = (u_j, v_j)$ are the velocities in the x and z direction respectively and the p_j's are the pressures. The subscripts $j = 1$ to 3 denote the lower, middle and upper fluid respectively. The no-slip condition and the impermeability of the boundary require that

$$\mathbf{u}_1 = 0 \tag{3.2}$$

at the plane, $z = 0$. At the first and second interfaces, $z = f_j(x,t)$, we have the kinematic condition,

$$v_j = \frac{\partial f_j}{\partial t} + u_j \frac{\partial f_j}{\partial x}, \tag{3.3}$$

continuity of velocity,

$$v_j = v_{j+1}, \tag{3.4a}$$

$$u_j = u_{j+1}, \tag{3.4b}$$

and the dynamic balance of stress,

$$(\boldsymbol{\sigma}_{j+1} - \boldsymbol{\sigma}_j) \cdot \mathbf{n}_j - (\gamma_j \nabla \cdot \mathbf{n}_j)\, \mathbf{n}_j + \frac{1}{H_j} \frac{\partial \gamma_j}{\partial x} \mathbf{t}_j = 0, \tag{3.5}$$

where $H_j = \sqrt{1 + (\partial h_j / \partial x)^2}$, for $j = 1, 2$. At the free surface, $z = f_3(x, t)$, we have the kinematic condition,

$$v_3 = \frac{\partial f_3}{\partial t} + u_3 \frac{\partial f_3}{\partial x}, \tag{3.6}$$

and the dynamic balance of stress,

$$-\boldsymbol{\sigma}_3 \cdot \mathbf{n}_3 - (\gamma_3 \nabla \cdot \mathbf{n}_3 + p_a)\, \mathbf{n}_3 + \frac{1}{H_3} \frac{\partial \gamma_3}{\partial x} \mathbf{t}_3 = 0, \tag{3.7}$$

where $H_3 = \sqrt{1 + (\partial h_3 / \partial x)^2}$, the $\boldsymbol{\sigma}_j$'s are the stress tensors, the γ_j's are the surface tensions, p_a is the atmospheric pressure, $\mathbf{t}_j$'s are the unit tangents to the interfaces and free surface respectively and the $\mathbf{n}_j$'s are the unit normals to the interfaces and free surface respectively. The normal and tangential stress balances at the interfaces are

$$\mathbf{n}_j \cdot (\boldsymbol{\sigma}_{j+1} - \boldsymbol{\sigma}_j) \cdot \mathbf{n}_j = \gamma_j \nabla \cdot \mathbf{n}_j, \qquad \mathbf{t}_j \cdot (\boldsymbol{\sigma}_{j+1} - \boldsymbol{\sigma}_j) \cdot \mathbf{n}_j + \frac{1}{H_j} \frac{\partial \gamma_j}{\partial x} = 0, \tag{3.8}$$

for $j = 1, 2$ and

$$-\mathbf{n}_3 \cdot \boldsymbol{\sigma}_3 \cdot \mathbf{n}_3 = \gamma_3 \nabla \cdot \mathbf{n}_3 + p_a, \qquad -\mathbf{t}_3 \cdot \boldsymbol{\sigma}_3 \cdot \mathbf{n}_3 + \frac{1}{H_3} \frac{\partial \gamma_3}{\partial x} = 0, \tag{3.9}$$

at the free surface.

The surfactant concentrations, Γ_j, are governed by a convection-diffusion equation Halpern & Frenkel (2003), which in one dimensions can be written as

$$\frac{\partial H_j \Gamma_j}{\partial t} + \frac{\partial H_j \Gamma_j u_j}{\partial x} = D_{sj} \frac{\partial}{\partial x} \left(\frac{1}{H_j} \frac{\partial \Gamma_j}{\partial x} \right), \tag{3.10}$$

for $j = 1, 2, 3$ where D_{sj} is the surfactant diffusivity Gao & Lu (2007). The surfactant diffusivity can be considered negligible, so we take $D_{sj} = 0$.

The relationship between the surfactant concentration and surface or interfacial tension is

$$\gamma_j - \gamma_{j0} = -E_j \left(\Gamma_j - \Gamma_{j0} \right), \tag{3.11}$$

where E_j are the surfactant elasticities, for $j = 1, 2, 3$. We introduce the shifted pressure, $\tilde{p}_j$, to simplify presentation as so

$$p_j = \tilde{p}_j + p_a + \rho_j g x \sin\theta - \rho_j g z \cos\theta, \tag{3.12}$$

where θ is the angle between the inclined plane and the horizontal. We non-dimensionalize variables by writing

$$\left.\begin{aligned} x^* = \frac{1}{h_1}x, \qquad z^* = \frac{1}{h_1}z, \qquad t^* = \frac{U_0}{h_1}t, \qquad u_j^* = \frac{1}{U_0}u_j, \qquad v_j^* = \frac{1}{U_0}v_j, \\ p_j^* = \frac{h_1}{\mu_1 U_0}\tilde{p}_j, \qquad \gamma_j^* = \frac{1}{\gamma_{j0}}\gamma_j, \qquad \Gamma_j^* = \frac{1}{\Gamma_{j0}}\Gamma_j, \qquad f_j^* = \frac{1}{h_1}f_j, \end{aligned}\right\} \tag{3.13}$$

as in Tseluiko *et al.* (2008), for $j = 1, 2, 3$ where the asterisk denotes a dimensionless quantity and $U_0 = \rho_1 g h_1^2 \sin\theta/\mu_1$ is the Nusselt surface speed of a flat film flowing down an inclined plane. We also introduce the Reynolds number, Re_j, the capillary number, Ca_j, and the Marangoni number, Ma_j,

$$\begin{gathered} Re_j = \frac{\rho_j U_0 h_1}{\mu_j} = \frac{Ro_j \rho_1^2 g h_1^3 \sin\theta}{2 m_j \mu_1^2}, \qquad Ca_j = \frac{\mu_j U_0}{\gamma_{j0}} = \frac{m_j \rho_1 g h_1^2 \sin\theta}{\gamma_{j0}}, \\ Ma_j = \frac{E_j \Gamma_{j0}}{\gamma_{j0}}, \end{gathered} \tag{3.14}$$

where $Ro_j = \rho_j/\rho_1$ and $m_j = \mu_j/\mu_1$ noting that $m_j = Ro_1 = 1$. Substituting (3.13) into (3.1), dropping the asterisks, we obtain

$$Re_j \left(\frac{\partial u_j}{\partial t} + u_j \frac{\partial u_j}{\partial x} + v_j \frac{\partial u_j}{\partial z} \right) = -\frac{\partial p_j}{\partial x} + m_j \left(\frac{\partial^2 u_j}{\partial x^2} + \frac{\partial^2 u_j}{\partial z^2} \right), \tag{3.15a}$$

$$Re_j \left(\frac{\partial v_j}{\partial t} + u_j \frac{\partial v_j}{\partial x} + v_j \frac{\partial v_j}{\partial z} \right) = -\frac{\partial p_j}{\partial z} + m_j \left(\frac{\partial^2 v_j}{\partial x^2} + \frac{\partial^2 v_j}{\partial z^2} \right), \tag{3.15b}$$

$$\frac{\partial u_j}{\partial x} + \frac{\partial v_j}{\partial z} = 0. \tag{3.15c}$$

The conditions at the wall are $u_1 = 0$ and $v_1 = 0$ at $z = 0$. At the interfaces and free surface $z = f_j(x,t)$ the kinematic condition becomes

$$v_j = \frac{\partial f_j}{\partial t} + u_j \frac{\partial f_j}{\partial x}, \tag{3.16}$$

for $j = 1, 2, 3$. The tangential stress balances are given by

$$\begin{aligned} 2f_{1x}\left(m_2 v_{2z} - v_{1z}\right) - \left(f_{1x}^2 - 1\right)\left(m_2\left(u_{2z} + v_{2x}\right) - \left(u_{1z} + v_{1x}\right)\right) \\ = -\frac{1}{Ca_1}\left(1 + f_{1x}^2\right)^{1/2}\gamma_{1x}, \end{aligned} \tag{3.17a}$$

$$\begin{aligned} 2f_{2x}\left(\frac{m_3}{m_2}v_{3z} - v_{2z}\right) - \left(f_{2x}^2 - 1\right)\left(\frac{m_3}{m_2}\left(u_{3z} + v_{3x}\right) - \left(u_{2z} + v_{2x}\right)\right) \\ = -\frac{1}{Ca_2}\left(1 + f_{2x}^2\right)^{1/2}\gamma_{2x}, \end{aligned} \tag{3.17b}$$

$$2f_{3x}v_{3z} + \left(1 - f_{3x}^2\right)\left(u_{3z} + v_{3x}\right) = \frac{1}{Ca_3}\left(1 + f_{2x}^2\right)\gamma_{3x}. \tag{3.17c}$$

and the normal stress balances are given by

$$\begin{aligned} \frac{\left(f_{1x}^2 + 1\right)}{\left(f_{1x}^2 - 1\right)}\left(m_2 v_{2z} + v_{1z}\right) + \left(p_1 - p_2 + \left(x - z\cot\left(\theta\right)\right)\left(1 - Ro_2\right)\right) \\ = \frac{1}{Ca_1}\left(\gamma_1\kappa_1 + \frac{f_{1x}\gamma_{1x}}{\left(f_{1x}^2 + 1\right)^{1/2}\left(f_{1x}^2 - 1\right)}\right), \end{aligned} \tag{3.18a}$$

$$\begin{aligned} \frac{\left(f_{2x}^2 + 1\right)}{\left(f_{2x}^2 - 1\right)}\left(\frac{m_3}{m_2}v_{3z} + v_{2z}\right) + \frac{1}{m_2}\left(p_2 - p_3 + \left(x - z\cot\left(\theta\right)\right)\left(Ro_2 - Ro_3\right)\right) \\ = \frac{1}{Ca_2}\left(\gamma_2\kappa_2 + \frac{f_{2x}\gamma_{2x}}{\left(f_{2x}^2 + 1\right)^{1/2}\left(f_{2x}^2 - 1\right)}\right), \end{aligned} \tag{3.18b}$$

$$\begin{aligned} \frac{\left(1 + f_{3x}^2\right)}{\left(1 - f_{3x}^2\right)}v_{3x} - \frac{1}{m_3}\left(p_3 + Ro_3 x - Ro_3 z\cot\left(\theta\right)\right) \\ = -\frac{1}{Ca_3}\left(\gamma_3\kappa_3 + \frac{f_{3x}\gamma_{3x}}{\left(f_{3x}^2 + 1\right)^{1/2}\left(f_{3x}^2 - 1\right)}\right). \end{aligned} \tag{3.18c}$$

The surfactant relation is given by

$$\gamma_j = 1 - Ma_j(\Gamma_j - 1), \tag{3.19}$$

and the convection-diffusion equation remains unchanged after non-dimensionalizing.

We introduce a long wave scaling by introducing the parameter $0 < \upsilon \ll 1$ and writing

$$\begin{aligned} x = \frac{\xi}{\upsilon}, \qquad z = z, \qquad t = \frac{\tau}{\upsilon}, \qquad v = \upsilon w, \qquad u_j = U_j + \mathcal{O}(\upsilon), \\ w_j = W_j + \mathcal{O}(\upsilon), \qquad p_j = \upsilon^{-1} P_j + \mathcal{O}(1), \qquad f_j = F_j + \mathcal{O}(\upsilon), \end{aligned} \tag{3.20}$$

as in Tseluiko *et al.* (2008). To retain Maringoni traction and surface tension effects, we assume that

$$Ca_j = \upsilon^3 C'_j, \qquad Ma_j = \upsilon^2 M'_j, \tag{3.21}$$

where $C'_j = \mathcal{O}(1)$ and $M'_j = \mathcal{O}(1)$. Also we take $\gamma_j = \mathcal{O}(1)$ and $\Gamma_j = \mathcal{O}(1)$. We also neglect the gravitational component in the z-direction which is the same as letting $\cot(\theta) \ll \upsilon^{-1}$. We can ignore the nonlinear components of the Navier-Stokes equation by letting $Re_j \ll \upsilon^{-1}$ for all j. Expanding the equations at leading order gives

$$P_{j\xi} = m_j U_{jzz}, \tag{3.22a}$$

$$P_{jz} = 0, \tag{3.22b}$$

$$U_{j\xi} = -W_{jz}, \tag{3.22c}$$

$$U_1 = 0, \qquad z = 0, \tag{3.22d}$$

$$W_1 = 0, \qquad z = 0, \tag{3.22e}$$

$$W_j = F_{j\tau} + U_j F_{j\xi}, \qquad z = F_j, \tag{3.22f}$$

$$m_2 U_{2z} - U_{1z} = \frac{M'_1 \Gamma_{1\xi}}{C'_1}, \qquad z = F_1, \tag{3.22g}$$

$$\frac{m_3}{m_2} U_{3z} - U_{2z} = \frac{M'_2 \Gamma_{2\xi}}{C'_2}, \qquad z = F_2, \tag{3.22h}$$

$$U_{3z} = -\frac{M'_3 \Gamma_{3\xi}}{C'_3}, \qquad z = F_3, \tag{3.22i}$$

$$P_1 - P_2 + \xi\,(1 - Ro_2) = -\frac{F_{1\xi\xi}}{C_1'}, \quad z = F_1, \tag{3.23a}$$

$$P_2 - P_3 + \xi\,(Ro_2 - Ro_3) = -m_2\frac{F_{2\xi\xi}}{C_2'}, z = F_2, \tag{3.23b}$$

$$P_3 + \xi Ro_3 = -m_3\frac{F_{3\xi\xi}}{C_3'}, z = F_3, \tag{3.23c}$$

$$W_1 = W_2, \qquad z = F_1, \tag{3.23d}$$

$$W_2 = W_3, \qquad z = F_2, \tag{3.23e}$$

$$U_1 = U_2, \qquad z = F_1, \tag{3.23f}$$

$$U_2 = U_3, \qquad z = F_2, \tag{3.23g}$$

$$\Gamma_{j\tau} + (\Gamma_j U_j)_\xi = 0, \qquad z = F_j, \tag{3.23h}$$

where $j = 1, 2, 3$.

Substituting (3.22f) into (3.22c) and using (3.22e), (3.23d) and (3.23e) gives us a set of linked partial differential equations describing the interface and free surface positions given by

$$F_{1\tau} = -\left(q_1\right)_\xi, \tag{3.24a}$$

$$F_{2\tau} = -\left(q_1 + q_2\right)_\xi, \tag{3.24b}$$

$$F_{3\tau} = -\left(q_1 + q_2 + q_3\right)_\xi, \tag{3.24c}$$

where the fluxes q_1, q_2 and q_3 are given by

$$q_1 = \int_0^{F_1} U_1 dz, \tag{3.25a}$$

$$q_2 = \int_{F_1}^{F_2} U_2 dz, \tag{3.25b}$$

$$q_3 = \int_{F_2}^{F_3} U_3 dz. \tag{3.25c}$$

Equations (3.24) describe the relationship between the interfaces and free surface positions and the local velocities of the fluids below. The rate of change with respect to time of

the interfaces and free surface is equal to the negative of the rate of change of the fluxes, given by (3.25), of the fluids below the particular interface or free surface with respect to distance parallel to the inclined plane. We find the U_i's by solving (3.22a) for U_i using (3.22b) giving

$$U_1 = \frac{z^2}{2}P_{1\xi} + A_1 z, \tag{3.26a}$$

$$U_2 = \frac{z^2}{2m_2}P_{2\xi} + A_2 z + B_2, \tag{3.26b}$$

$$U_3 = \frac{z^2}{2m_3}P_{3\xi} + A_3 z + B_3, \tag{3.26c}$$

where we find the P_i's by solving (3.23a), (3.23b) and (3.23c) giving

$$P_1 = -\frac{F_{1\xi\xi}}{C_1'} - m_2\frac{F_{2\xi\xi}}{C_2'} - m_3\frac{F_{3\xi\xi}}{C_3'} - \xi, \tag{3.27a}$$

$$P_2 = -m_2\frac{F_{2\xi\xi}}{C_2'} - m_3\frac{F_{3\xi\xi}}{C_3'} - \xi Ro_2, \tag{3.27b}$$

$$P_3 = -m_3\frac{F_{3\xi\xi}}{C_3'} - \xi Ro_3, \tag{3.27c}$$

where the A_i's are found using (3.22g), (3.22h) and (3.22i) and the B_i's are found using (3.23f) and (3.23g)

$$A_1 = -\frac{M_1'\Gamma_{1\xi}}{C_1'} - F_1 P_{1\xi} + F_1 P_{2\xi} + m_2 A_2, \tag{3.28a}$$

$$A_2 = -\frac{M_2'\Gamma_{2\xi}}{C_2'} - \frac{F_2 P_{2\xi}}{m_2} + \frac{F_2 P_{3\xi}}{m_2} + \frac{m_3 A_3}{m_2}, \tag{3.28b}$$

$$A_3 = -\frac{M_3'\Gamma_{3\xi}}{C_3'} - \frac{F_3 P_{3\xi}}{m_3}, \tag{3.28c}$$

$$B_2 = \frac{F_1^2}{2}\left(P_{1\xi} - \frac{P_{2\xi}}{m_2}\right) + F_1\left(A_1 - A_2\right), \tag{3.28d}$$

$$B_3 = \frac{F_2^2}{2}\left(\frac{P_{2\xi}}{m_2} - \frac{P_{3\xi}}{m_3}\right) + F_2\left(A_2 - A_3\right) + B_2. \tag{3.28e}$$

These equations have no clear analytic solution so we resort to numerical analysis of the

equations. We use an implicit first order time step given by

$$\left(\frac{F^{(j),n+1}-F^{(j),n}}{d\tau}\right)+\frac{1}{2}q_{\xi}^{(j),n+1}+\frac{1}{2}q_{\xi}^{(j),n}=0, \tag{3.29a}$$

$$\left(\frac{G^{(j),n+1}-G^{(j),n}}{d\tau}\right)+\frac{1}{2}Q_{\xi}^{(j),n+1}+\frac{1}{2}Q_{\xi}^{(j),n}=0, \tag{3.29b}$$

where $F^{(j),n}$ is the position of the j interface at the n time step, $G^{(j),n}$ is the surfactant concentration of the j interface at the n time step, $q^{(j),n}$ is the quantity within the ξ derivative on the right hand side of (3.24), $Q^{(j),n}$ is the quantity within the ξ derivative of (3.23h), (j) denotes the different fluids, n is the time step and $d\tau$ is the time step size for $j=1,2,3$. We define $d\xi=2L/(N+1)$ where L is half the wavelength and N determines the number of points in space. We then approximate $F^{(j),n+1}=f^{(j)}$ and $G^{(j),n+1}=g^{(j)}$, say, spectrally by writing them as a discrete Fourier transform

$$f^{(j)}(z)=\sum_{n=-N}^{N}\hat{f}^{(j),n}\exp\left(ikz\right), \tag{3.30a}$$

$$g^{(j)}(z)=\sum_{n=-N}^{N}\hat{g}^{(j),n}\exp\left(ikz\right), \tag{3.30b}$$

where $j=1,2,3$, $i=\sqrt{-1}$ and the hat denotes the Fourier coefficients. This makes numerically computing the derivatives simpler and faster. Let $H_i^{(j),n+1}$ and $K_i^{(j),n+1}$ be the left hand sides of (3.29) defined by

$$H_i^{(j),n+1}=\frac{f_i^{(j)}-F^{(j),n}}{d\tau}+\frac{1}{2}\hat{q}_{\xi,i}^{(j),n+1}+\frac{1}{2}\hat{q}_{\xi,i}^{(j),n}, \tag{3.31a}$$

$$K_i^{(j),n+1}=\frac{g_i^{(j)}-G^{(j),n}}{d\tau}+\frac{1}{2}\hat{Q}_{\xi,i}^{(j),n+1}+\frac{1}{2}\hat{Q}_{\xi,i}^{(j),n}, \tag{3.31b}$$

where $j=1,2,3$ and the hat denotes the q's and Q's evaluated with the approximation of the discrete Fourier transform as given by (3.30). We seek to make the $H_i^{(j),n+1}$'s and $K_i^{(j),n+1}$'s zero by using Newtons method as described below. Let

$$\begin{aligned}\mathbf{x}=\Big(&\hat{f}^{(1),-N},...,\hat{f}^{(1),N},\hat{g}^{(1),-N},...,\hat{g}^{(1),N},\hat{f}^{(2),-N},...,\hat{f}^{(2),N},\hat{g}^{(2),-N},...,\hat{g}^{(2),N},\\&\hat{f}^{(3),-N},...,\hat{f}^{(3),N},\hat{g}^{(3),-N},...,\hat{g}^{(3),N}\Big),\end{aligned} \tag{3.32}$$

be the vector of discrete Fourier transform coefficients which we are using Newton's method to calculate and

$$\begin{aligned}\mathbf{H} = \Big(&H_1^{(1),n+1}, ..., H_{2N+1}^{(1),n+1}, K_1^{(1),n+1}, ..., K_{2N+1}^{(1),n+1}, H_1^{(2),n+1}, ..., H_{2N+1}^{(2),n+1}, \\ &K_1^{(2),n+1}, ..., K_{2N+1}^{(2),n+1}, H_1^{(3),n+1}, ..., H_{2N+1}^{(3),n+1}, K_1^{(3),n+1}, ..., K_{2N+1}^{(3),n+1}\Big),\end{aligned} \tag{3.33}$$

be the vector of the equations we are solving for. Given an initial guess $\mathbf{x} = \mathbf{X}$ say there is an improved guess given by $\mathbf{X}+\mathbf{h}$ such that $\mathbf{H}(\mathbf{X}+\mathbf{h}) \approx \mathbf{0}$. Expanding this as a Taylor series gives

$$\mathbf{H}(\mathbf{X}+\mathbf{h}) = \mathbf{H}(\mathbf{X}) + \mathbf{h}\cdot\mathbf{J}(\mathbf{X}) + \mathcal{O}(\mathbf{h}^2), \tag{3.34}$$

where $j = 1, 2, 3$ and $J_{i,n} = \partial\mathbf{H}_i/\partial\mathbf{x}_n$. Rearranging (3.34), ignoring $\mathcal{O}(\mathbf{h}^2)$ and using the assumption that $\mathbf{H}(\mathbf{X}+\mathbf{h}) \approx 0$, gives

$$\mathbf{h} = -\mathbf{J}^{-1}\cdot\mathbf{H}(\mathbf{X}), \tag{3.35}$$

where $j = 1, 2, 3$. So the new corrected guess is $\mathbf{x} = \mathbf{X} - \mathbf{J}^{-1}\cdot\mathbf{H}(\mathbf{X})$. We iterate this until the 2-norm drops below a specified tolerance, say 10^{-5}. This gives us the wave profile at the new time step which we can march forward to a specified end time.

Shown in figure 3.2 is the comparison of the maximum growth rate given by a linear stability analysis of equations (3.24) above compared to the nonlinear evolution calculation above. As we can see in figure 3.2 the change in the maximum from the nonlinear evolution calculation agrees with the linear growth rate for a short time period which we expect as after this the nonlinear dynamics start to take over.

3.2 Travelling Wave Solutions of Multi Layer Flows

Numerical calculations of the nonlinear evolution equations for large τ suggest that there exists travelling wave solutions. For two layers of fluid taking $\delta = 1.5$ $m = Ro = Ca_2 =$

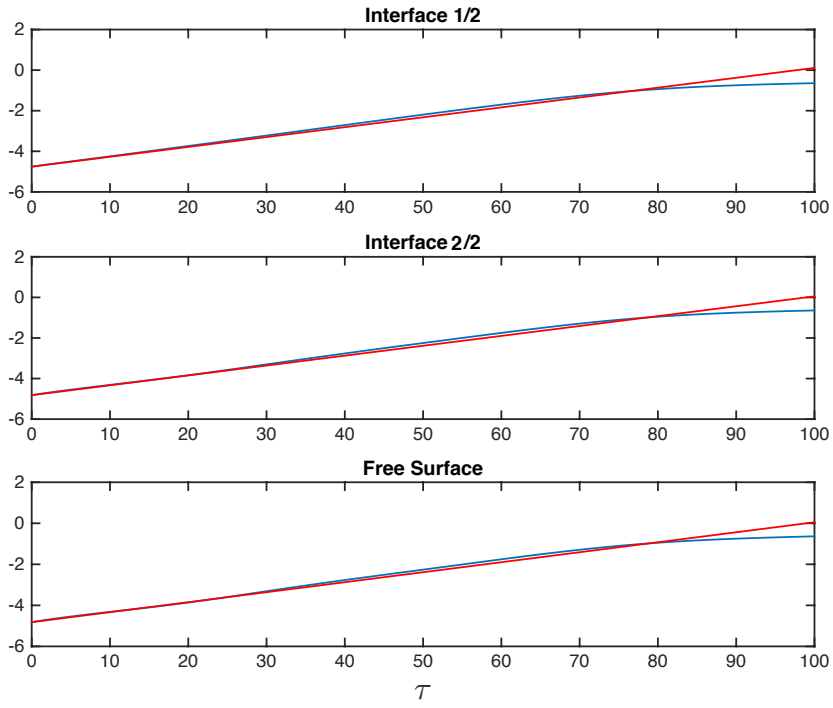

Figure 3.2: Plot of the logarithm of the maximum of the amplitude over time τ in blue and the a straight line with slope given by the growth rate determined by normal mode linear stability analysis of (3.24) in red.

$Ma_1 = Ma_2 = 1$, $Ca_1 = 1.1$ and $k = 0.7$, calculating the initial condition based on the wave profile of the unstable mode at this k and marching foreword in time to $\tau = 800$ gives figure 3.3 and figure 3.4. As we can see from figure 3.3 and figure 3.4, after $\tau \approx 100$ the amplitude of the free surface and interface position and surfactant concentration does not change suggesting we have arrived at a stable solution which could be a travelling wave solution. We also show the waveforms at $\tau = 800$ in figure 3.5. We investigate this travelling wave further in case study 2 section 3.2.2.

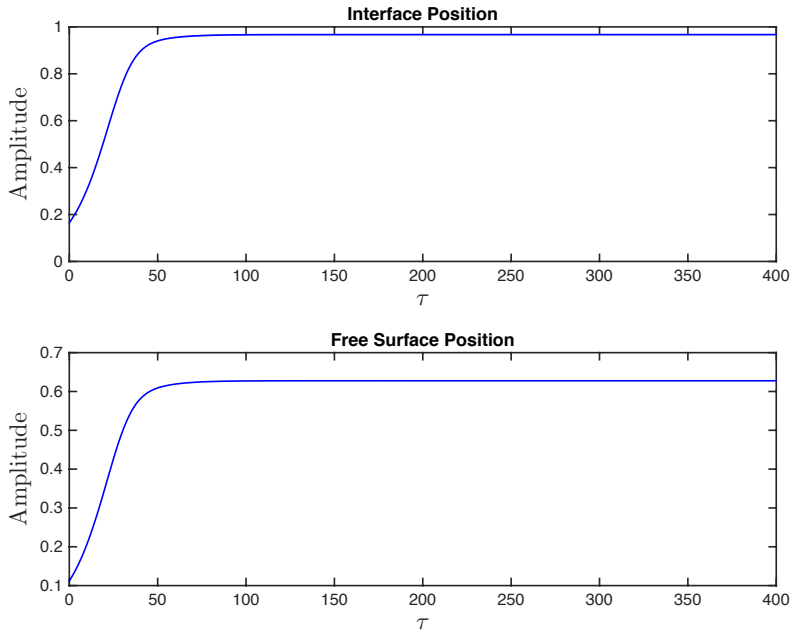

Figure 3.3: Amplitude of free surface and interface position over τ for $\delta = 1.5$, $m = Ro = Ca_2 = Ma_1 = Ma_2 = 1$, $Ca_1 = 1.1$ and $k = 0.7$.

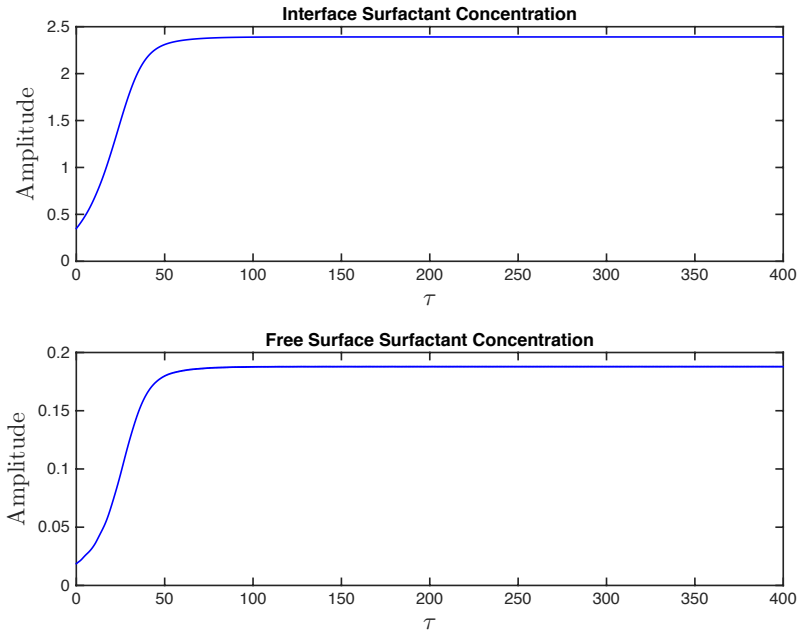

Figure 3.4: Amplitude of free surface and interface surfactant concentration over τ for $\delta = 1.5$, $m = Ro = Ca_2 = Ma_1 = Ma_2 = 1$, $Ca_1 = 1.1$ and $k = 0.7$.

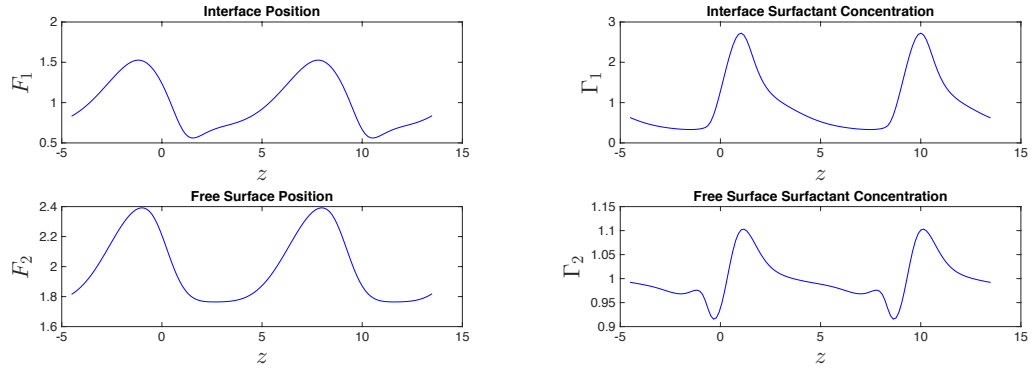

Figure 3.5: Plot of two periods of interface and free surface, position and surfactant concentration for travelling wave solution at $k = 0.7$ with $\delta = 1.5$, $m = Ro = Ca_2 = Ma_1 = Ma_2 = 1$ and $Ca_1 = 1.1$.

We seek steady state travelling wave solutions of (3.24) by writing (3.24) and (3.23h) as

$$F_\tau^{(j)} + q_\xi^{(j)} = 0, \tag{3.36a}$$

$$G_\tau^{(j)} + Q_\xi^{(j)} = 0, \tag{3.36b}$$

where $j = 1, 2, 3$ and $q_\xi^{(j)}$ corresponds to the integrals on the right hand side of (3.24) and $Q^{(j)} = G_j U_j$, where U_j is defined in (3.26). Introducing a travelling wave coordinate $z = \xi - c\tau$, where c is a wave speed to be found, seeking solutions $F^{(j)}(z)$, $G^{(j)}(z)$, $q^{(j)}(z)$ and $Q^{(j)}(z)$ and using the chain rule gives

$$-cF_z^{(j)} + q_z^{(j)} = 0, \tag{3.37a}$$

$$-cG_z^{(j)} + Q_z^{(j)} = 0, \tag{3.37b}$$

where $j = 1, 2, 3$ and the $F^{(j)}$'s, $G^{(j)}$'s $q^{(j)}$'s and $Q^{(j)}$'s are dependent upon z only. This means we now have six coupled ordinary differential equations which can be integrated to

give

$$-cF^{(j)} + q^{(j)} = d^{(j)}, \tag{3.38a}$$

$$-cG^{(j)} + Q^{(j)} = d^{(j+3)}, \tag{3.38b}$$

where $j = 1, 2, 3$ and d_j, for $j = 1, 2, ..., 6$, are constants to be determined. To calculate the $d^{(j)}$ we consider the conservation of volume for the three profile equations, (3.38a), and conservation of total concentration for the three surfactant equations, (3.38b). Taking (3.36) and integrating with respect to ξ over a period gives

$$\frac{\partial}{\partial \tau} \int_{\xi=0}^{L} F^{(j)} d\xi + \left[q^{(j)}\right]_{\xi=0}^{L} = 0, \tag{3.39a}$$

$$\frac{\partial}{\partial \tau} \int_{\xi=0}^{L} G^{(j)} d\xi + \left[Q^{(j)}\right]_{\xi=0}^{L} = 0, \tag{3.39b}$$

where $j = 1, 2, 3$, $L = 2\pi/k$ the wavelength and k is the wavenumber. Since $q^{(j)}$ and $Q^{(j)}$ are periodic (3.39) reduces to

$$\int_{\xi=0}^{L} F^{(j)} d\xi = \text{const.}, \qquad \int_{\xi=0}^{L} G^{(j)} d\xi = \text{const.}. \tag{3.40}$$

Since $\int_{\xi=0}^{L} F^{(j)} d\xi = Lh^{(j0)}$ and $\int_{\xi=0}^{L} G^{(j)} d\xi = Lg^{(j0)}$ for the unidirectional case, where the $h^{(j0)}$'s are the unperturbed film thicknesses and the $g^{(j0)}$'s are the unperturbed surfactant concentrations, and we are considering evolutions of the flow from this initial position and since there is no time dependence for the travelling wave solution (3.40) becomes

$$\frac{1}{L} \int_{\xi=0}^{L} F^{(j)} d\xi = h^{(j0)}, \qquad \frac{1}{L} \int_{\xi=0}^{L} G^{(j)} d\xi = g^{(j0)}, \tag{3.41}$$

where $j = 1, 2, 3$. Given an initial profile these equations do not lead to a unique solution as the phase of a travelling wave solution is not set due to the translational invariance of the flow. This can be uniquely defined by imposing

$$\int_{\xi=0}^{L} \xi F^{(1)} d\xi = 0. \tag{3.42}$$

It can be shown that this fixes a wave with translational invariance by considering the function $F^{(1)}(\xi) = \sin(\xi + \phi)$, where ξ is in the range 0 to 2π and ϕ is left unset. We apply (3.42) to our function to give $\phi = \pi/2 + 2\pi n$ but since $\sin(x) = \sin(x + 2\pi)$ the only solution is $\phi = \pi/2$, since sin is periodic, so $F^{(1)}(\xi) = \sin(\xi + \pi/2) = \cos(\xi)$.

In considering where to start looking for travelling wave solutions we consider the linear stability analysis in section 2.2. Travelling wave solutions exist at least where the growth rate, given by the linear stability analysis, of a particular set of parameters is zero. So in considering figure 2.9 at $k \approx 0.25$ and $k \approx 0.1$ we expect a travelling wave branch starting here since the growth rates vanish. We cannot seek a travelling wave exactly where the growth rate is zero as this corresponds to a zero amplitude wave. To calculate the initial wave profiles we perform stability analysis on (3.24) and (3.23h) by letting

$$F^{(j)} = h^{(j0)} + \epsilon F^{(j0)} \exp(ikz), \qquad G^{(j)} = g^{(j0)} + \epsilon G^{(j0)} \exp(ikz), \tag{3.43}$$

where $j = 1, 2, 3$, $F^{(j0)}$ and $G^{(j0)}$ define the waveform which we calculate below, and $\epsilon > 0$ a small parameter. Substituting (3.43) into (3.24) and (3.23h) gives a system of linear equations given by the generalized eigenvalue problem for c

$$\mathbf{MF} = c\mathbf{I}(6)\mathbf{F} \tag{3.44}$$

where $\mathbf{I}(6)$ is the six by six identity matrix, $\mathbf{F} = \left(F^{(10)}, F^{(20)}, F^{(30)}, G^{(10)}, G^{(20)}, G^{(30)}\right)$ and $\mathbf{M}$ is a six by six matrix with the parameters Ma_1, Ma_2, Ma_3, Ca_1, Ca_2, Ca_3, Ro_2, Ro_3, δ_2, δ_3, m_2 and m_3. The eigenvalues of the generalized eigenvalue problem (3.44) give us the values of c the imaginary part of which are the growth rates of the stability problem. If we substitute a c corresponding to a particular growth rate into (3.44) we can solve the new generalized eigenvalue problem (3.44) to give the eigenvectors. We choose the eigenvector whose corresponding eigenvalue is zero, since this is where the travelling wave

branch is expected to start. This eigenvalue is precisely the $\mathbf{F}$ that we require for the initial wave profile which we set to be

$$F^{(j)} = h^{(j0)} + 2\epsilon \mathbb{R}\mathrm{e}(F^{(j0)} \exp(ik\xi)), \tag{3.45a}$$

$$G^{(j)} = g^{(j0)} + 2\epsilon \mathbb{R}\mathrm{e}(G^{(j0)} \exp(ik\xi)), \tag{3.45b}$$

where $j = 1, 2, 3$. Now we have an initial wave profile which we expect to be close to the travelling wave solution for a wavenumber close to the zero growth rate. We introduce a grid to discretize the spatial dimension by letting Nx be the number of spatial points. To evolve our initial wave profile towards the travelling wave solution for this wavenumber we iterate Newton's method in order to solve (3.38), (3.41) and (3.42) by approximating the wave profile spectrally by sampling the wave profile given by (3.45) at each grid point over the wavelength, L. We then approximate $F^{(j)} = f^{(j)}$ and $G^{(j)} = g^{(j)}$, spectrally by writing them as a discrete Fourier transform

$$f^{(j)}(z) = \sum_{n=-N}^{N} \hat{f}^{(j),n} \exp(ikz), \qquad g^{(j)}(z) = \sum_{n=-N}^{N} \hat{g}^{(j),n} \exp(ikz), \tag{3.46}$$

where $j = 1, 2, 3$, $i = \sqrt{-1}$ and the hat denotes the Fourier coefficients. We substitute the discrete Fourier transform estimate into the equations we want to solve, (3.38), (3.41) and (3.42). In order to arrive at a satisfactory estimate for the Fourier coefficients we define the quantities,

$$H_i^{(j)} = -cf^{(j)} + \hat{q}^{(j)} - d^j, \tag{3.47a}$$

$$K_i^{(j)} = -cg_j + \hat{Q}^{(j)} - d_{j+3}, \tag{3.47b}$$

$$L_j = \frac{1}{L}\int_{\xi=0}^{L} f_j d\xi - h_{j0}, \tag{3.47c}$$

$$L_{j+3} = \frac{1}{L}\int_{\xi=0}^{L} g_j d\xi - g_{j0}, \tag{3.47d}$$

$$L_7 = \int_{\xi=0}^{L} \xi f_1 d\xi, \tag{3.47e}$$

where $j = 1, 2, 3$ and the hat denotes the q_j's and Q_j's evaluated with the approximation of the discrete Fourier transform as given by (3.46). We require the equations (3.47) to be zero in order to satisfy (3.38), (3.41) and (3.42). In order to achieve this we let

$$\begin{aligned}\mathbf{x} = \Big(&\hat{f}^{(1),-N}, ..., \hat{f}^{(1),N}, \hat{g}^{(1),-N}, ..., \hat{g}^{(1),N}, \hat{f}^{(2),-N}, ..., \hat{f}^{(2),N}, \hat{g}^{(2),-N}, ..., \hat{g}^{(2),N}, \\ &\hat{f}^{(3),-N}, ..., \hat{f}^{(3),N}, \hat{g}^{(3),-N}, ..., \hat{g}^{(3),N}\Big),\end{aligned} \tag{3.48}$$

be the vector of discrete Fourier transform coefficients which we are using Newton's method to calculate and

$$\begin{aligned}\mathbf{H} = \Big(&H_1^{(1),n+1}, ..., H_{2N+1}^{(1),n+1}, K_1^{(1),n+1}, ..., K_{2N+1}^{(1),n+1}, H_1^{(2),n+1}, ..., H_{2N+1}^{(2),n+1}, \\ &K_1^{(2),n+1}, ..., K_{2N+1}^{(2),n+1}, H_1^{(3),n+1}, ..., H_{2N+1}^{(3),n+1}, K_1^{(3),n+1}, ..., K_{2N+1}^{(3),n+1}, L_1, ..., L_7\Big),\end{aligned} \tag{3.49}$$

be the vector of the equations we are solving for. We use the same method given as (3.34) and (3.35) in the previous section to calculate an improved guess. This gives us the wave profile at the new k which we can step by a small enough step size to progress the travelling wave branch.

After much experimenting with various parameter ranges several points become apparent. Selecting a k too close to the bifurcation point sometimes leads to the zero amplitude solution, which equates to the flat profile constant surfactant concentration solution. The direction of the travelling wave branch, either k increasing from the bifurcation point or k decreasing, does not appear to be easy to predict apart from noting that at least one branch decreases from the bifurcation point. If the amplitude of initial guess is too high the method will not converge but the amplitude of the wave close to the bifurcation point is difficult to predict. If an amplitude too small is chosen the method tends to converge to the flat profile. Interestingly when trying to find a particularly difficult traveling wave branches sometimes, counterintuitively, less spatial grid points are needed to obtain the first traveling wave solution. In the cases shown below in order to find the traveling wave

we chose a k within 10^{-2} of the bifurcation point, an N of around 40 except for the case discussed above where an N of 20 was required to find the traveling wave solution and an amplitude of around 0.1 to 0.01.

In order to test the convergence of Newtons method for our setup we plot our initial profile of the wave given by (3.45) over plots of the first three iterations of Newtons method as shown in figure 3.6 for $k = 0.97$ with $Ca_1 = 1.1$ and $Ca_2 = Ro = Ma_1 = Ma_2 = m = \delta = 1$. After three iterations of Newtons method the profiles do not change enough to show on the plots in figure 3.6 but it takes five iterations of Newtons method to converge for a tolerance of 10^{-4}. As we can see from figure 3.6 the method allows for an initial guess of the profiles to be quite different from the solution while converging quickly to the solution.

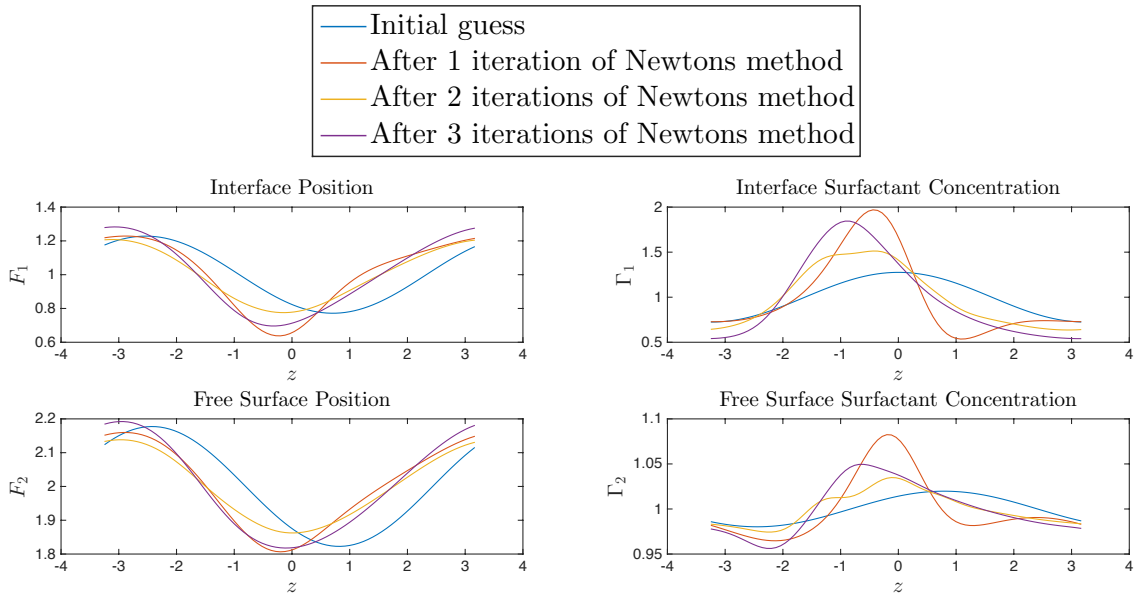

Figure 3.6: Plot of convergence of Newtons method from an initial guess for $k = 0.97$ with $Ca_1 = 1.1$ and $Ca_2 = Ro = Ma_1 = Ma_2 = m = \delta = 1$.

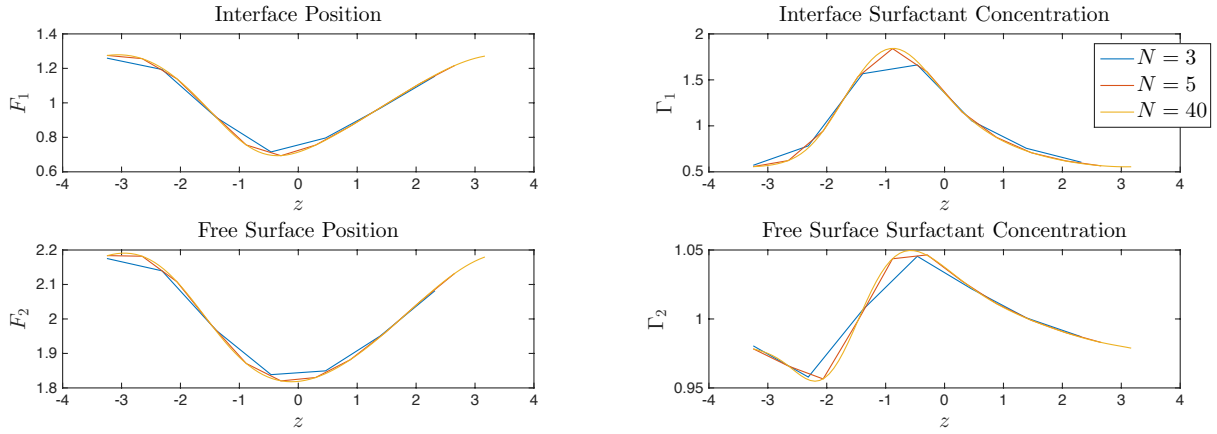

Figure 3.7: Plot of convergence of Newtons method increasing the number of Fourier coefficients for $k = 0.97$ with $Ca_1 = 1.1$ and $Ca_2 = Ro = Ma_1 = Ma_2 = m = \delta = 1$.

Figure 3.7 illustrates what happens when we increase the number of spatial points from a small amount. Doing so shows that as we increase the number of spatial grid points we tend towards a unique profile that is not determined by the number of spatial grid points. A greater number of grid points is desirable as it increases the accuracy of the profiles but with an increase in grid points comes an increase in the time taken for each iteration of Newtons method. Taking $N = 40$ seems to be a reasonable compromise whereby a good accuracy is achieved and each iteration of Newtons method takes less than a second on a basic computer system.

Considering the number of Fourier coefficients as given then the other constant we need to consider for the numerical method is the step size for k. A smaller step size means less iterations of Newtons method but since one has to perform at least one iteration per step there is a limit to how much a small step size can speed up the method. The step size used varied greatly between the cases considered. Sometimes a step size for k of 0.1 while at others a much smaller step size for k of 10^{-4} was required due to a rapid change in the profiles.

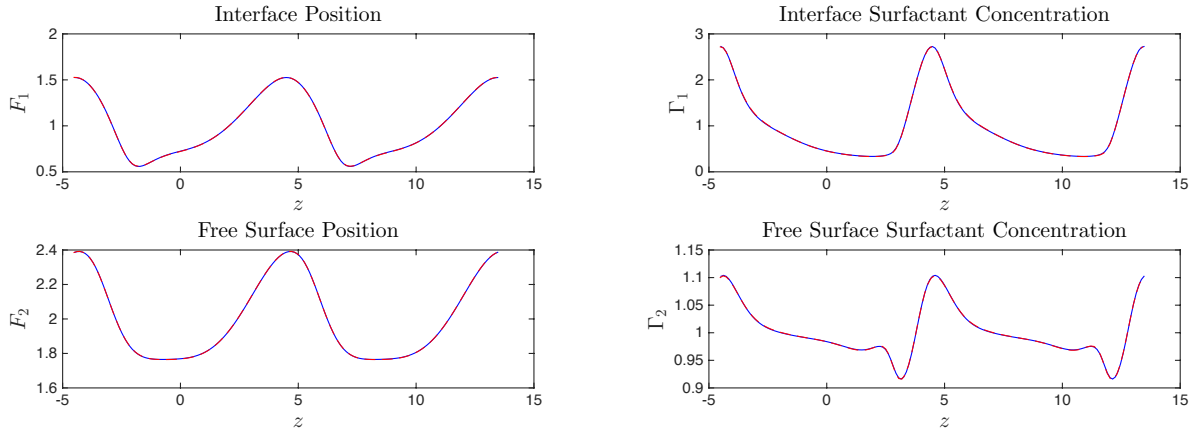

Figure 3.8: Plot of comparison of a run of the nonlinear code as in figure 3.5 and calculating the travelling wave solution using the method described above for $k = 0.7$ with $Ca_1 = 1.1$ and $Ca_2 = Ro = Ma_1 = Ma_2 = m = \delta = 1$.

In figure 3.8 we compare the profiles from running the nonlinear equations using the method described above, in red dashes, and the profiles generated by calculating the traveling wave profile using the method described above, shown in a blue solid line. The two profiles show excellent agreement suggesting that at least some long runs of the nonlinear evolution equations tend to traveling wave forms.

We concentrate on two layer flows for our travelling wave investigation. We compare the growth rate based on the linear stability analysis of the nonlinear equations (3.24) to the amplitude, defined as the absolute value of the difference between the maximum and minimum, of the interface position.

3.2.1 Case Study 1 - $Ca_1 = Ca_2 = Ro = 1$, $m = 5$, $\delta = 1.5$ and $Ma_1 = Ma_2 = 0$

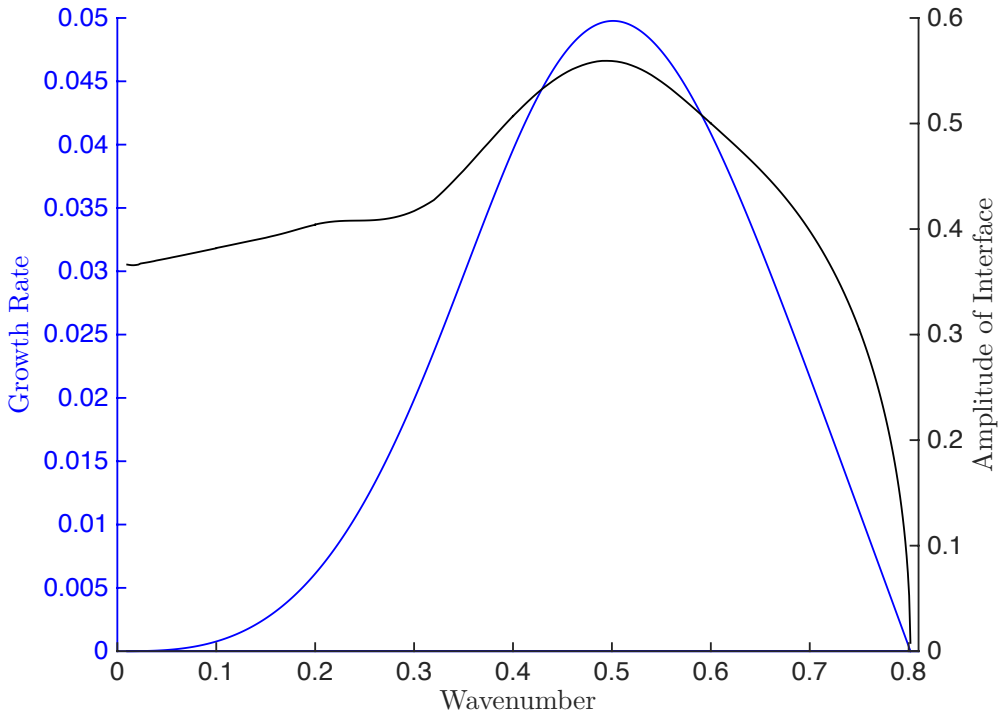

Figure 3.9: Comparison of the linear growth rate to the amplitude of the travelling wave solution by wavenumber, k, for $Ca_1 = Ca_2 = Ro = 1$, $\delta = 1.5$, $m = 5$ and no surfactant, $Ma_1 = Ma_2 = 0$.

We have found a travelling wave branch for a surfactant-free two layer flow where $m = 5$, $\delta = 1.5$ and $Ca_1 = Ca_2 = Ro = 1$ as shown in figure 3.9. This shows, as we expect, that travelling wave solutions exist without the presence of surfactant. The travelling wave branch bifurcates from $k \approx 0.8018$ which is where the growth rate is zero, as shown in figure 3.9, and is defined for decreasing k. As we follow the branch closer to $k = 0$ the branch becomes harder to resolve requiring a very small step in k due to the increasing wavelength. As k approaches zero the amplitude of both the free surface and interface

tend to different non-zero values. This suggests that there may exist an infinitely large wavelength, non-zero amplitude, travelling wave solution, suggesting that there may exist a non-periodic single wave solution in the limit of $k \to 0$. The maximum amplitude of the interface occurs at a similar wavenumber, $k \approx 0.5$, as the maximum growth rate.

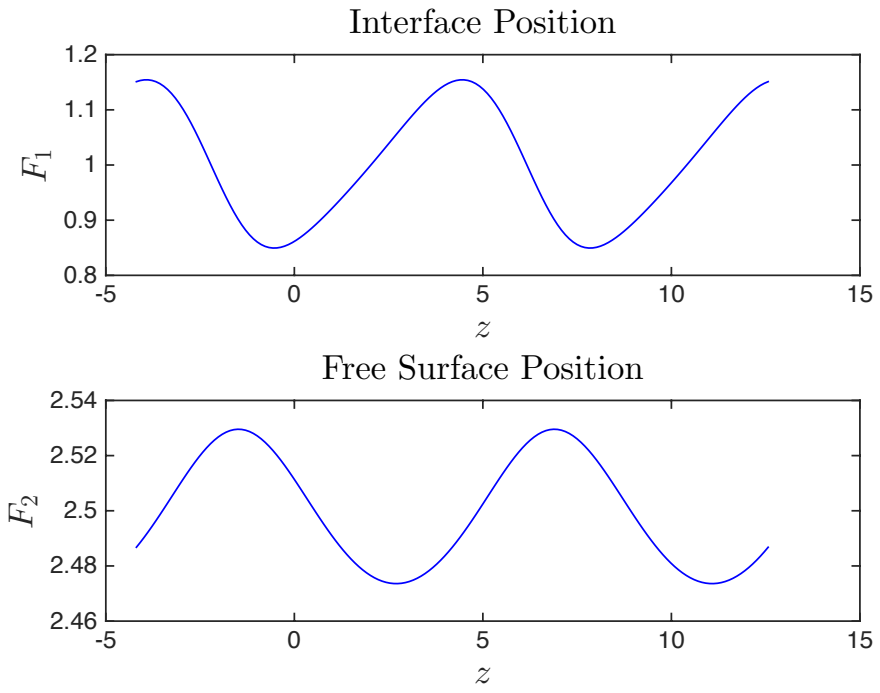

Figure 3.10: Plot of two periods of interface and free surface position for travelling wave solution at $k = 0.75$ with $Ca_1 = Ca_2 = Ro = 1$, $\delta = 1.5$, $m = 5$ and $Ma_1 = Ma_2 = 0$.

The profiles close to the bifurcation point, shown in figure 3.10, are close to sine waves with a relative phase shift close to π. This is what we would expect as we are close to the bifurcation point where zero growth rate occurs and so the wave profile should be close to the wave given from the linear stability analysis which is a sine wave.

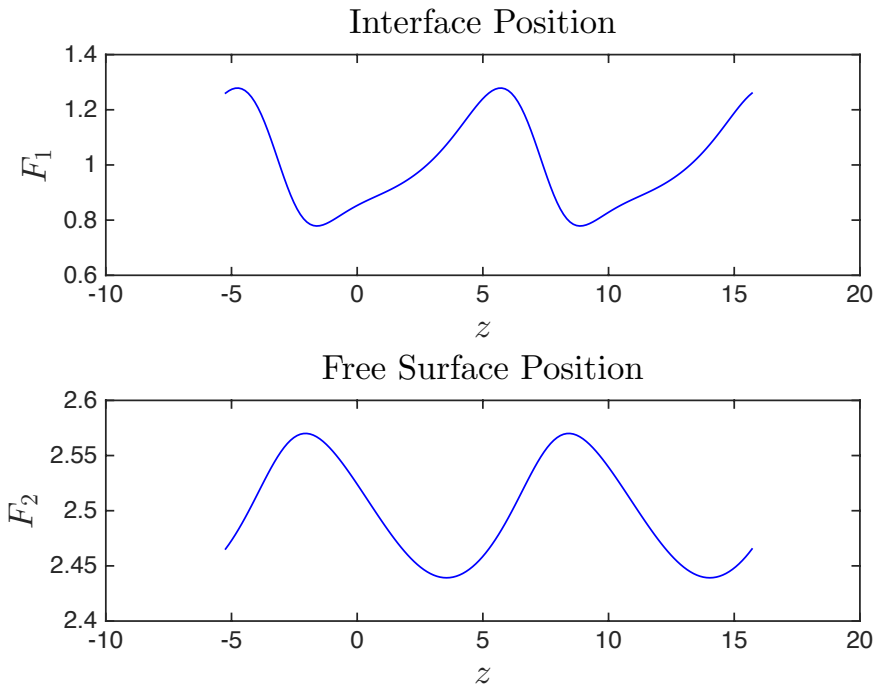

Figure 3.11: Plot of two periods of interface and free surface position for travelling wave solution at $k = 0.6$ with $Ca_1 = Ca_2 = Ro = 1$, $\delta = 1.5$, $m = 5$ and $Ma_1 = Ma_2 = 0$.

In figure 3.11 we can see a small deformation appearing to the right of the minimum on the interface and the free surface profile is starting to resemble an inverse sawtooth waveform.

In figure 3.12 the deformation near $z = 0$ on the interface has become more pronounced while the free surface has become more rounded near at its maximum and more pointed near its minimum.

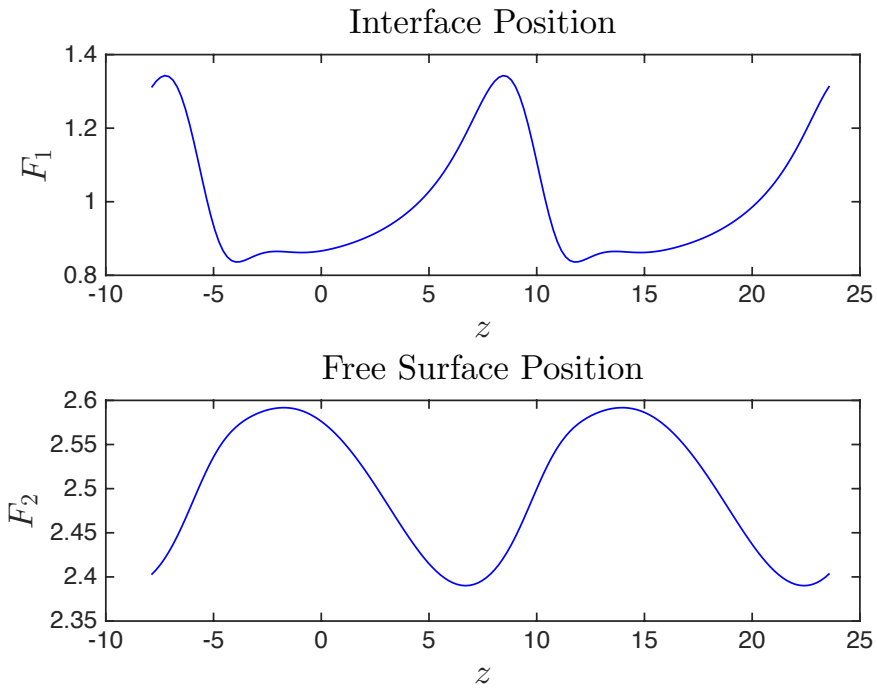

Figure 3.12: Plot of two periods of interface and free surface position for travelling wave solution at $k = 0.4$ with $Ca_1 = Ca_2 = Ro = 1$, $\delta = 1.5$, $m = 5$ and $Ma_1 = Ma_2 = 0$.

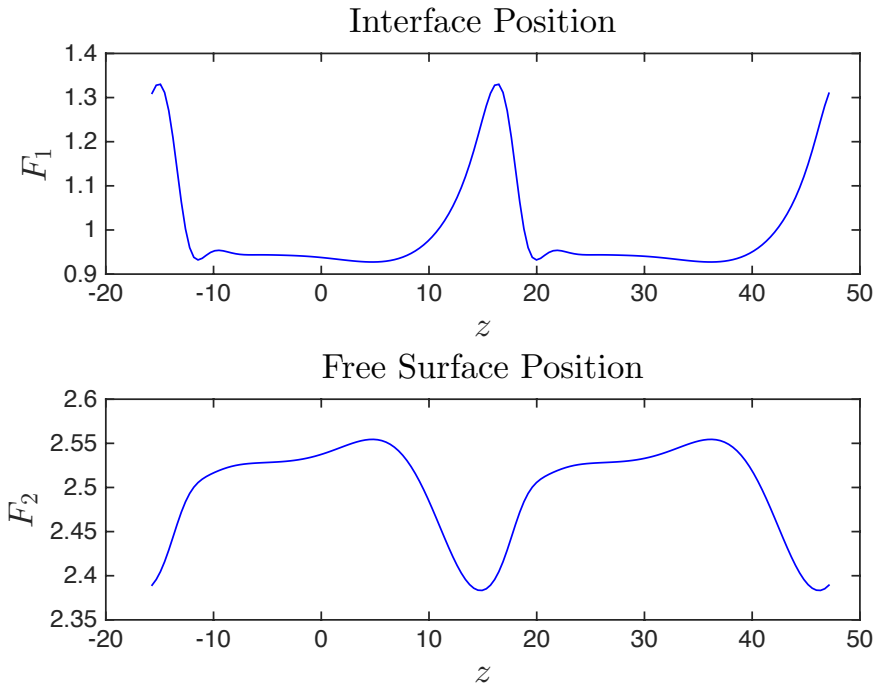

Figure 3.13: Plot of two periods of interface and free surface position for travelling wave solution at $k = 0.2$ with $Ca_1 = Ca_2 = Ro = 1$, $\delta = 1.5$, $m = 5$ and $Ma_1 = Ma_2 = 0$.

In figure 3.13 we can see a pulse starting to form around the transition between periods as the interface and free surface position between the pulses is tending to a flat state.

In figure 3.14 we can see the interface and free surface position between the pulses has become nearly flat while the pulses have become more defined.

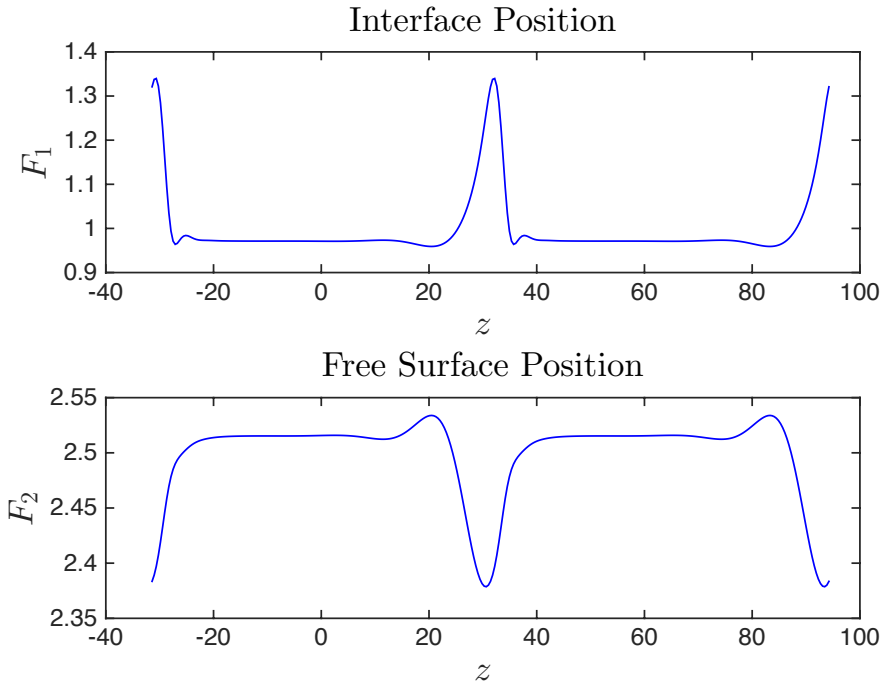

Figure 3.14: Plot of two periods of interface and free surface position for travelling wave solution at $k = 0.1$ with $Ca_1 = Ca_2 = Ro = 1$, $\delta = 1.5$, $m = 5$ and $Ma_1 = Ma_2 = 0$.

As we get close to $k = 0$, as seen in figure 3.15, we see the pulse solution over the transition between periods where the rest of the profile is flat. The pulses occur at the same position in the period and mirror each other in their maximum deviation from the flat profile.

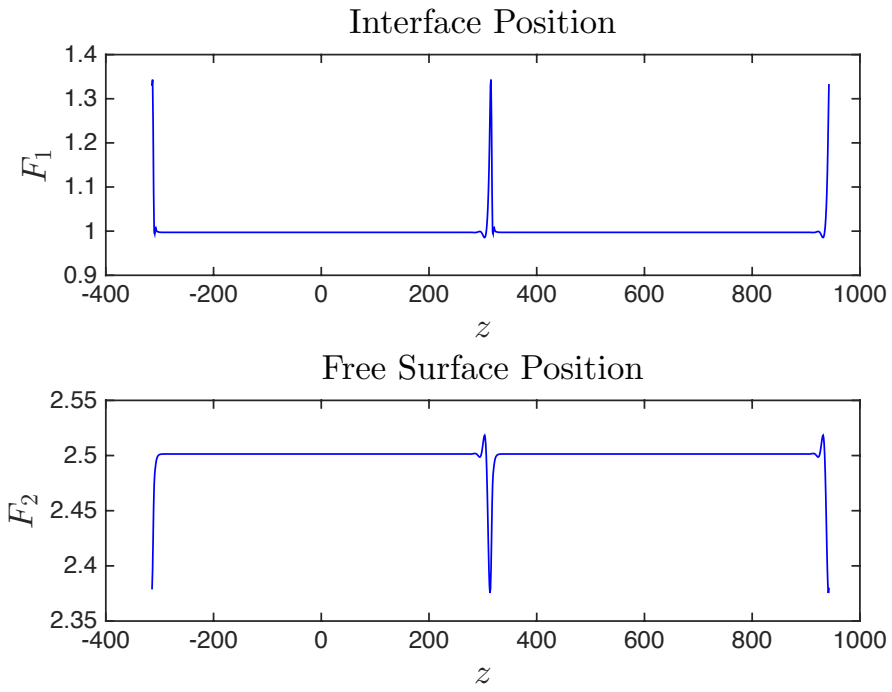

Figure 3.15: Plot of two periods of interface and free surface position for travelling wave solution at $k = 0.01$ with $Ca_1 = Ca_2 = Ro = 1$, $\delta = 1.5$, $m = 5$ and $Ma_1 = Ma_2 = 0$.

3.2.2 Case Study 2 - $Ca_1 = 1.1$ and $Ca_2 = Ro = m = Ma_1 = Ma_2 = \delta = 1$

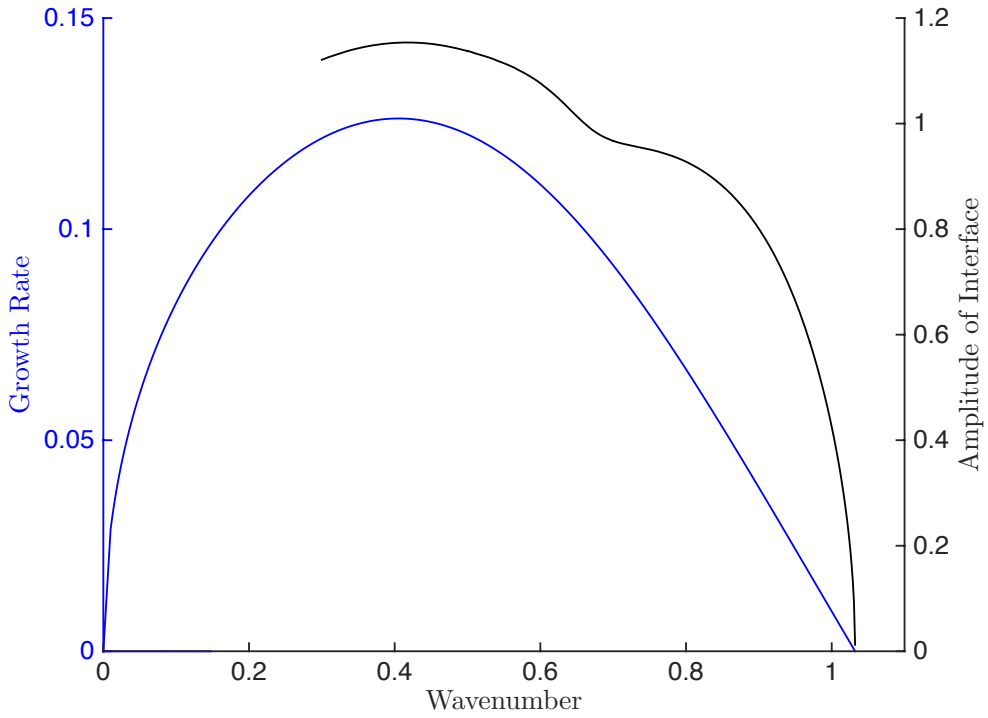

Figure 3.16: Comparison of the growth rate based on the linear stability to the amplitude of the travelling wave solution by wavenumber for $Ca_1 = 1.1$ and $Ca_2 = Ro = m = Ma_1 = Ma_2 = \delta = 1$.

We have found a travelling wave branch for a two layer flow where $Ca_1 = 1.1$ and $Ca_2 = Ro = m = Ma_1 = Ma_2 = \delta = 1$ as shown in figure 3.16. The travelling wave branch bifurcates from $k \approx 1.0321$ where it tends towards $k = 0$. As we get closer to $k = 0$ the brach becomes harder to resolve as the surfactant on the interface tends to zero for part of a period which causes numerical problems near the transition between zero and non-zero surfactant concentration. Also a discontinuity in the first derivative of the free surface surfactant concentration develops at the z position where the interface surfactant concentration sharply changes from a zero to a non-zero value. The maximum of the amplitude of the interface is roughly at the same wavenumber, $k \approx 0.4$, as the maximum

of the growth rate.

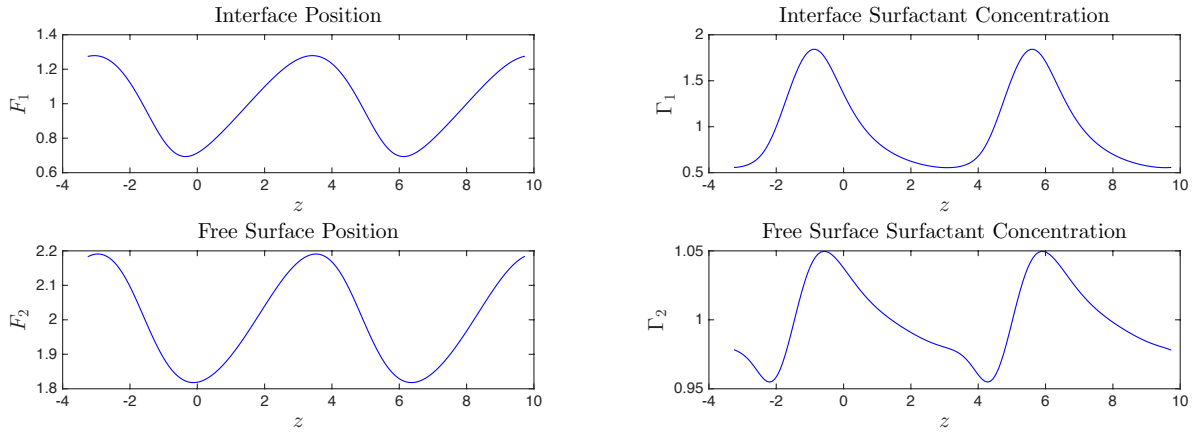

Figure 3.17: Plot of two periods of interface and free surface, position and surfactant concentration for travelling wave solution at $k = 0.97$ with $Ca_1 = 1.1$ and $Ca_2 = Ro = m = Ma_1 = Ma_2 = \delta = 1$.

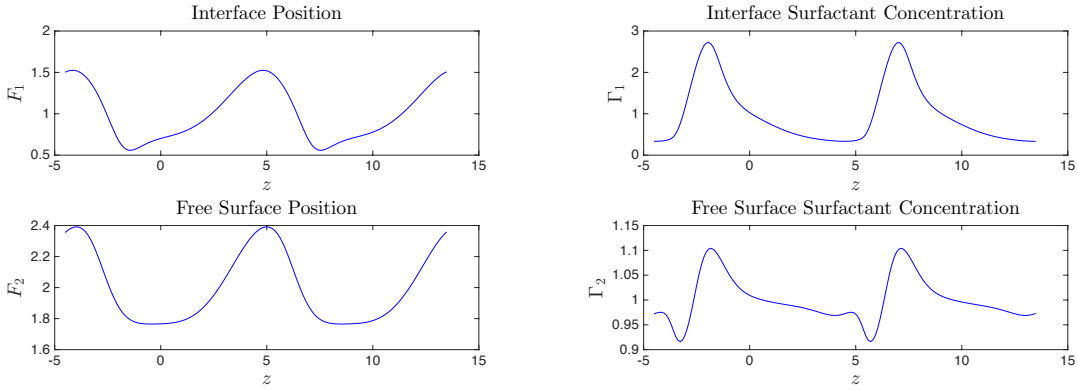

Figure 3.18: Plot of two periods of interface and free surface, position and surfactant concentration for travelling wave solution at $k = 0.7$ with $Ca_1 = 1.1$ and $Ca_2 = Ro = m = Ma_1 = Ma_2 = \delta = 1$.

In figure 3.17 the positions are similar to sine waves similar to figure 3.11 but with the same relative phase. Whereas the surfactant on the interface is already approaching a bell

curve shape while the surfactant on the free surface is starting to look like a pulse.

In figure 3.18 a small deformation has appeared to the right of the minima on the interface position. The free surface is tending towards a bell curve shape. We note the maxima of the interface and free surface positions are in the same z position. The amplitude of surfactant concentration on the interface is increasing while the concentration near the transition between periods tends to zero as k decreases. The surfactant concentration on the free surface has now become a pulse.

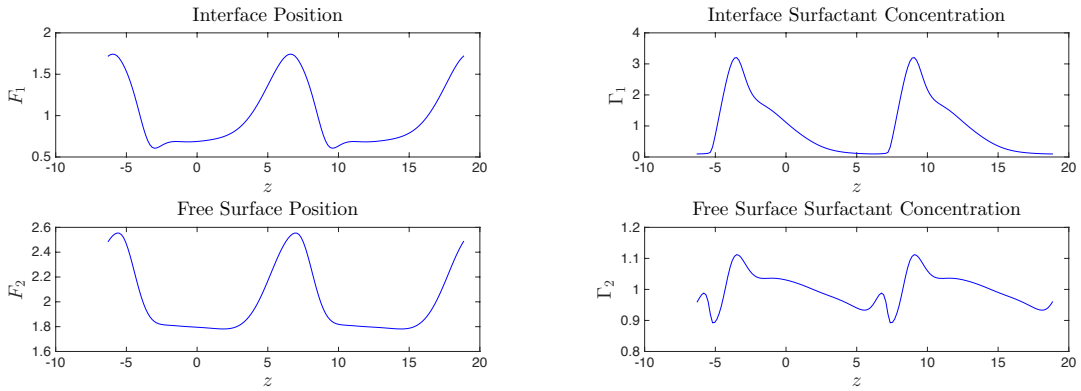

Figure 3.19: Plot of two periods of interface and free surface, position and surfactant concentration for travelling wave solution at $k = 0.5$ with $Ca_1 = 1.1$ and $Ca_2 = Ro = m = Ma_1 = Ma_2 = \delta = 1$.

In figure 3.19 we see that both the interface and free surface positions are tending to a bell curve shape with a capillary ripple on the right hand side of the interface position. The minima on the free surface position occurs to the right of the bell curve shape while it occurs to the left on the free surface position. The surfactant concentration on the interface has nearly reduced to zero for part of the period. This suggests that the surfactant is migrating into the small deformation where the minima is on the interface. The free

surface surfactant concentration has developed a small deformation to the right of the maxima and the local maxima to the left of the minima has increased.

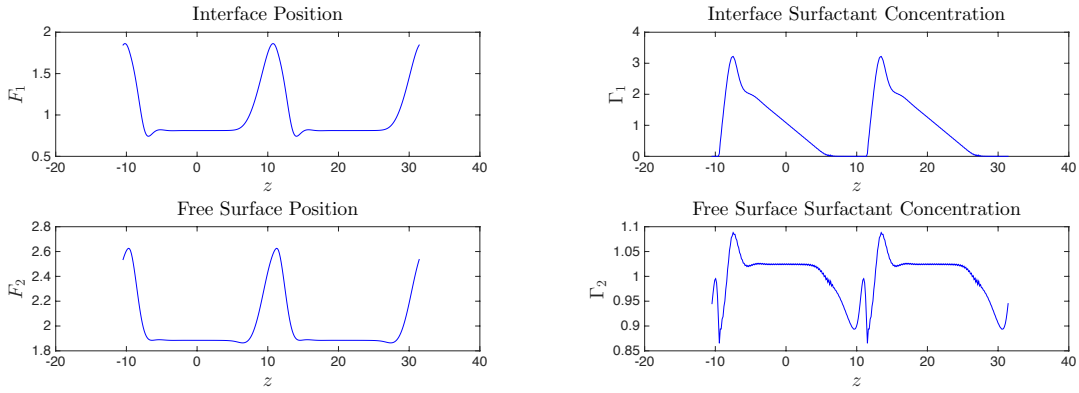

Figure 3.20: Plot of two periods of interface and free surface, position and surfactant concentration for travelling wave solution at $k = 0.3$ with $Ca_1 = 1.1$ and $Ca_2 = Ro = m = Ma_1 = Ma_2 = \delta = 1$.

In figure 3.20 we can see the positions have developed into a more localized deformation with the same general profiles as before. The surfactant concentrations have developed in the same manner. There is a discontinuity in the first derivative at $z \approx -9$ ($\pm$ wavelength) which may contribute to the numerical calculation breaking down at this wavenumber.

3.2.3 Case Study 3 - $Ca_1 = Ca_2 = Ro = 1$, $m = 2$, $\delta = 0.1$, $Ma_1 = 0.1$ and $Ma_2 = 10.391$

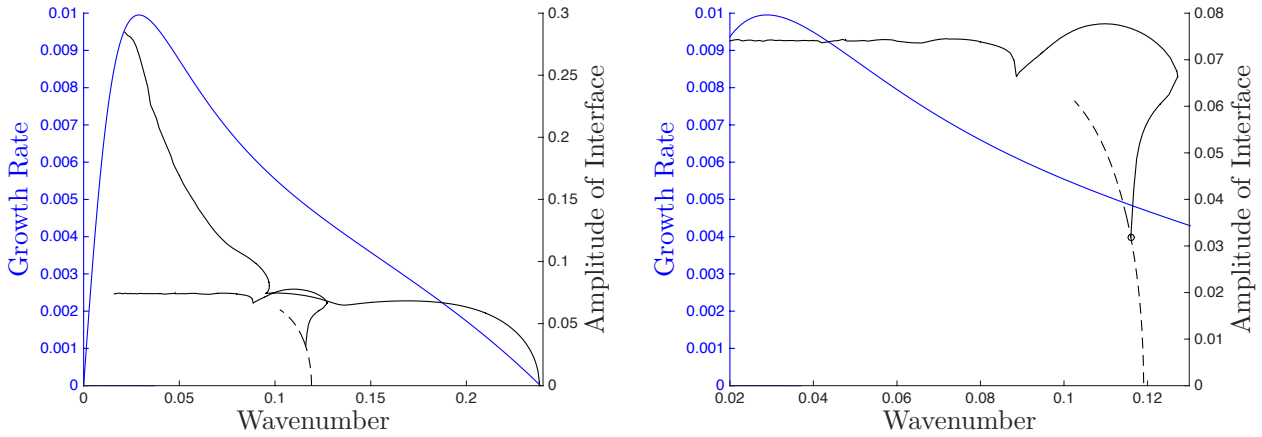

Figure 3.21: Comparison of the growth rate based on the linear stability to the amplitude of the travelling wave solution by wavenumber for $Ca_1 = Ca_2 = Ro = 1$, $Ma_1 = 0.1$, $Ma_2 = 10.391$, $m = 2$ and $\delta = 0.1$.

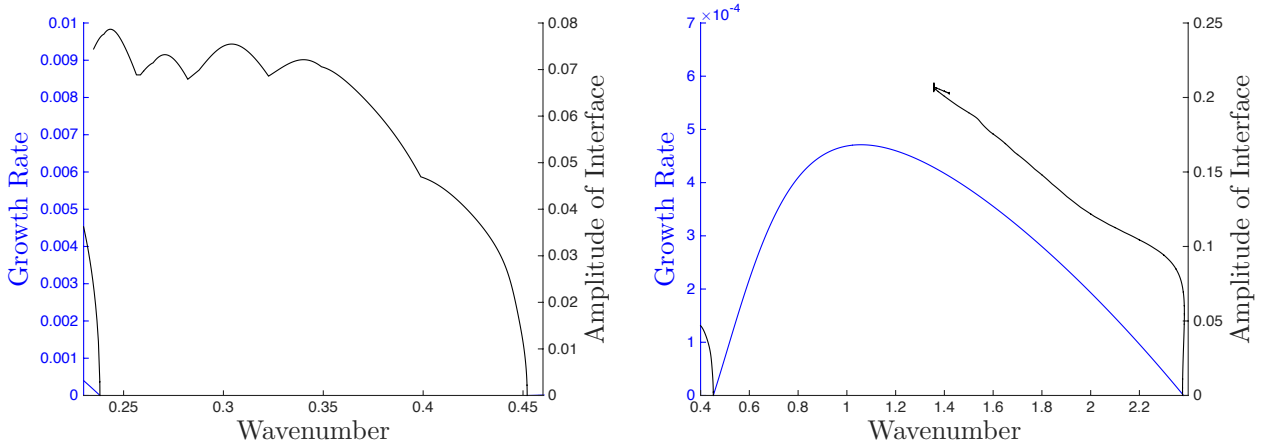

Figure 3.22: Comparison of the growth rate based on the linear stability to the amplitude of the travelling wave solution by wavenumber for $Ca_1 = Ca_2 = Ro = 1$, $Ma_1 = 0.1$, $Ma_2 = 10.391$, $m = 2$ and $\delta = 0.1$.

We have found four travelling wave branches for the two layer flow where $Ca_1 = Ca_2 = Ro = 1$, $Ma_1 = 0.1$, $Ma_2 = 10.391$, $m = 2$ and $\delta = 0.1$ as shown on the left of figure 3.21

and both plots in figure 3.22. For the growth rate we have two unstable modes with a stable bandwidth separating them. The first travelling wave branch bifurcates from $k \approx 0.2381$ where the branch tends towards $k = 0$, the second branch bifurcates from $k \approx 0.4521$ where it also tends towards $k = 0$, the third branch bifurcates from $k \approx 2.3768$ where the branch initially tends towards $k = 2.4$ before turning around and tending towards $k \approx 1.3565$ before turning around a second time and the fourth branch was discovered when following the first branch where it turns around at $k \approx 0.1$. As the first branch gets close to $k = 0.02$ the branch becomes harder to resolve, possibly due to the shock-like structure developing on the interface and free surface positions. As the second branch approaches $k = 0.237$ the branch becomes difficult to resolve further, possibly due to the increase in the number of oscillations on the interface position. The third branch becomes difficult to resolve when it approaches $k = 1.42$ after turning around at $k \approx 1.3565$.

A fourth branch was found after calculating the first branches second turning point the method found a different branch which does not emerge from a point of zero growth rate. Given a typical wave profile as given in figure 3.24 we can find a solution at half the wavenumber, $\hat{k} = k/2$, which is the same profiles repeated such that they fit twice the wavelength, a so called harmonic of the branch with wavenumber k. From this we can construct a branch which has the same wave profiles and concentrations repeated as those at twice the wavenumber. We shall refer to this as a pseudo-branch. The fourth branch is different to the other branches in that it branches off from a pseudo-branch as opposed to a point of zero growth rate as the other branches do.

Branch 1

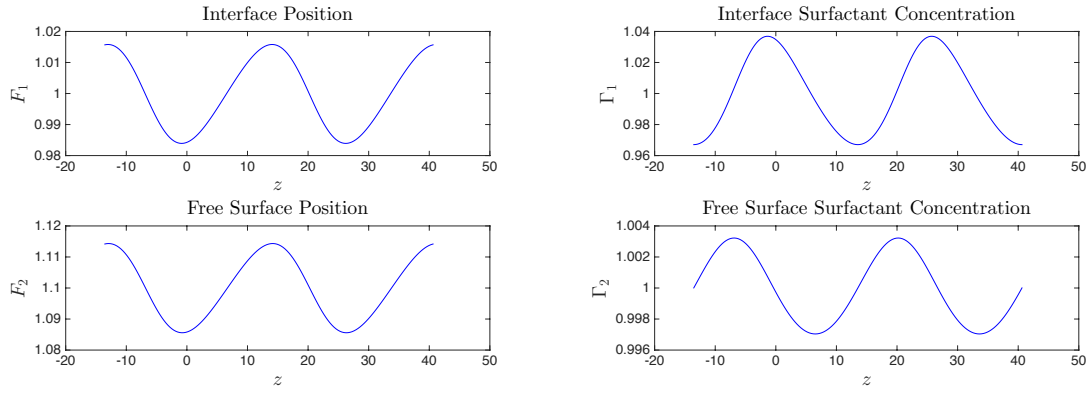

Figure 3.23: Plot of two periods of interface and free surface, position and surfactant concentration for travelling wave solution at $k = 0.232$ with $Ca_1 = Ca_2 = Ro = 1$, $Ma_1 = 0.1$, $Ma_2 = 10.391$, $m = 2$ and $\delta = 0.1$.

In figure 3.23 we can see the positions resemble sine waves with maxima in the same z position. The interface surfactant concentration also resembles a sine wave with relative phase shift to the positions of π while the free surface surfactant concentration has a phase shift of about $\pi/2$ relative to the interface surfactant concentration.

In figure 3.24 the positions resemble a sawtooth waveform. The interface surfactant concentration resembles an inverse sawtooth waveform with the maximums where the minimums are on the interface position. The free surface surfactant concentration more closely resembles a sine wave where the maximums are between the positions of the maximums of the interface position and interface surfactant concentration.

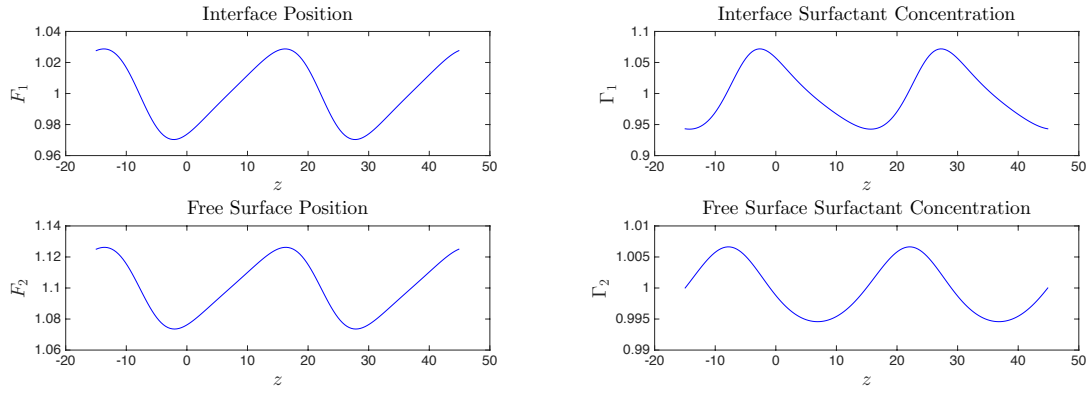

Figure 3.24: Plot of two periods of interface and free surface, position and surfactant concentration for travelling wave solution at $k = 0.21$ with $Ca_1 = Ca_2 = Ro = 1$, $Ma_1 = 0.1$, $Ma_2 = 10.391$, $m = 2$ and $\delta = 0.1$.

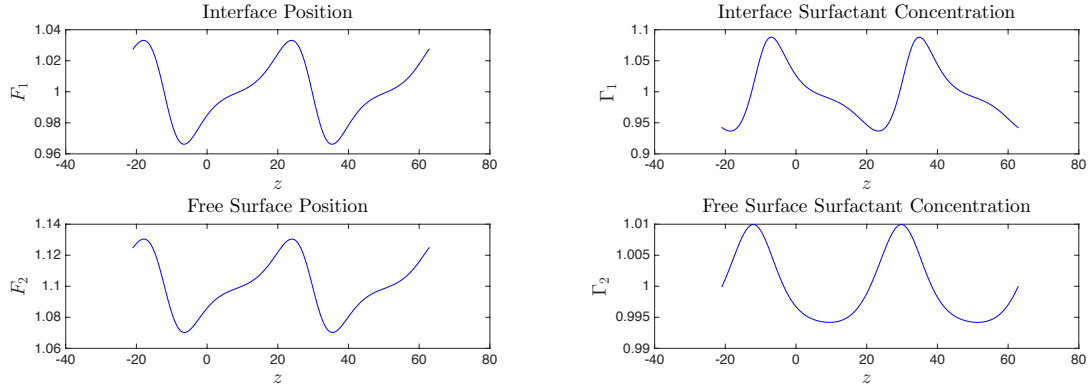

Figure 3.25: Plot of two periods of interface and free surface, position and surfactant concentration for travelling wave solution at $k = 0.15$ with $Ca_1 = Ca_2 = Ro = 1$, $Ma_1 = 0.1$, $Ma_2 = 10.391$, $m = 2$ and $\delta = 0.1$.

In figure 3.25 we can see that a deformation has developed in the middle of the periods in both the position and interface surfactant concentration. The interface surfactant concentration has developed a similar deformation to the left of the period transition. The

free surface surfactant concentration is becoming more pointed at its maximums while the minimums are staying rounded.

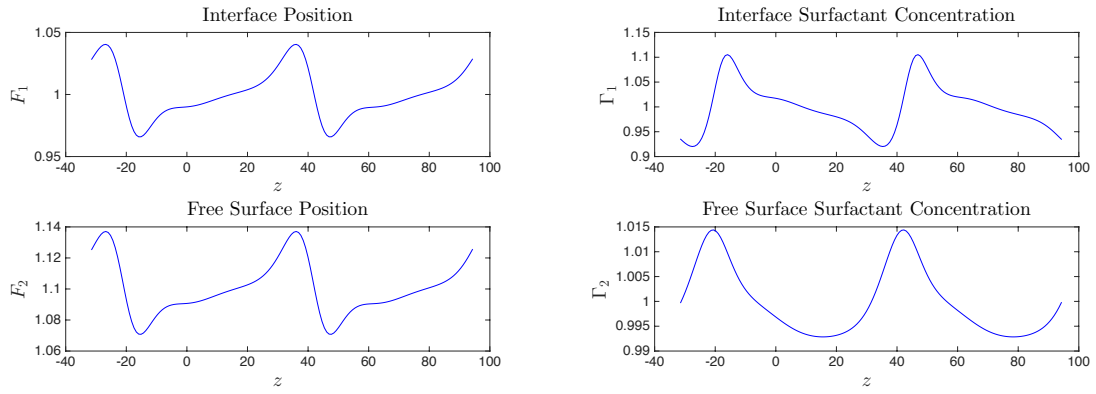

Figure 3.26: Plot of two periods of interface and free surface, position and surfactant concentration for travelling wave solution at $k = 0.1$ with $Ca_1 = Ca_2 = Ro = 1$, $Ma_1 = 0.1$, $Ma_2 = 10.391$, $m = 2$ and $\delta = 0.1$.

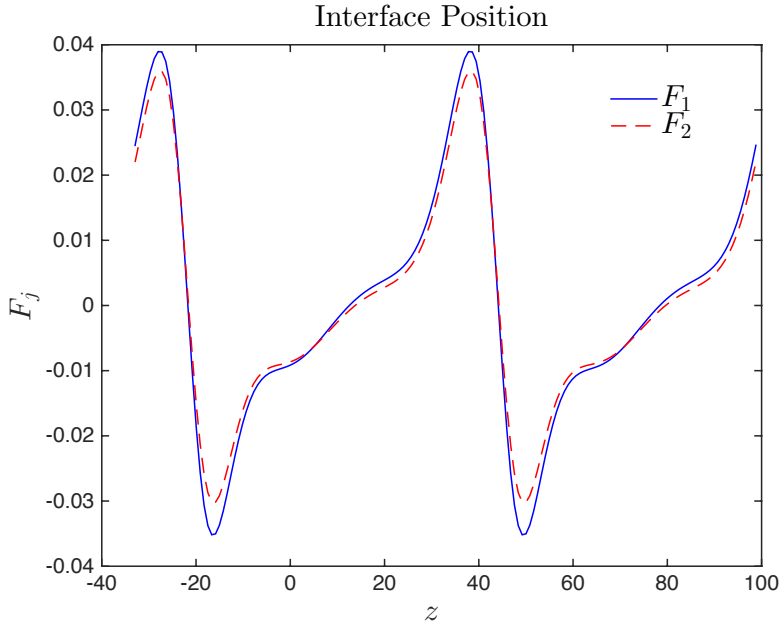

Figure 3.27: Plot of of the comparison between the interface and free surface position for travelling wave solution at $k = 0.1$ with $Ca_1 = Ca_2 = Ro = 1$, $Ma_1 = 0.1$, $Ma_2 = 10.391$, $m = 2$ and $\delta = 0.1$.

Figure 3.26 shows the position of both the interface and the free surface developing into what is starting to look like a Fourier transform of a sawtooth waveform. These profiles are strikingly similar as shown in figure 3.27 where we see the two profiles superimposed over each other. The interface surfactant concentration has a shape resembling an inverse sawtooth waveform. The free surface surfactant concentration is now looking more like a bell curve shape with a small kink on the right hand side of the maximums.

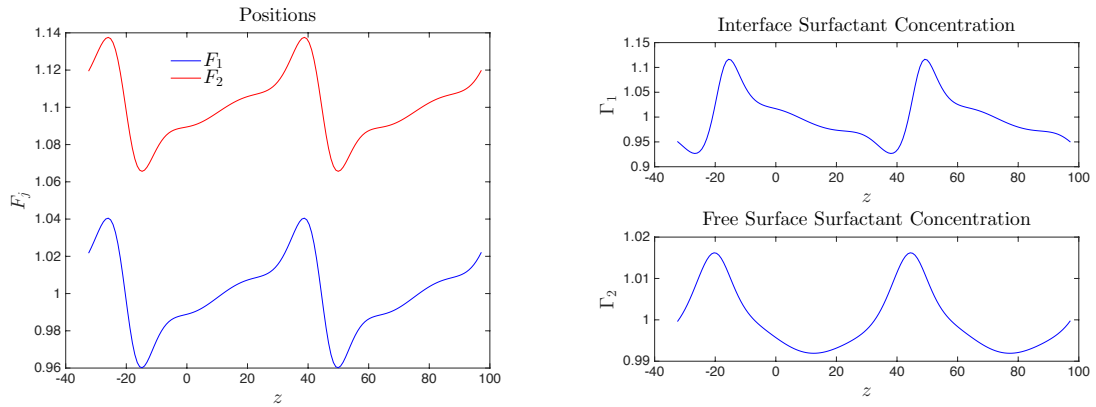

Figure 3.28: Plot of two periods of interface and free surface, position and surfactant concentration for travelling wave solution at $k = 0.09705$ with $Ca_1 = Ca_2 = Ro = 1$, $Ma_1 = 0.1$, $Ma_2 = 10.391$, $m = 2$ and $\delta = 0.1$.

In figure 3.28 we can see more deformations have appeared on the positions and the interface surfactant concentration while the free surface surfactant concentration remains mainly unchanged.

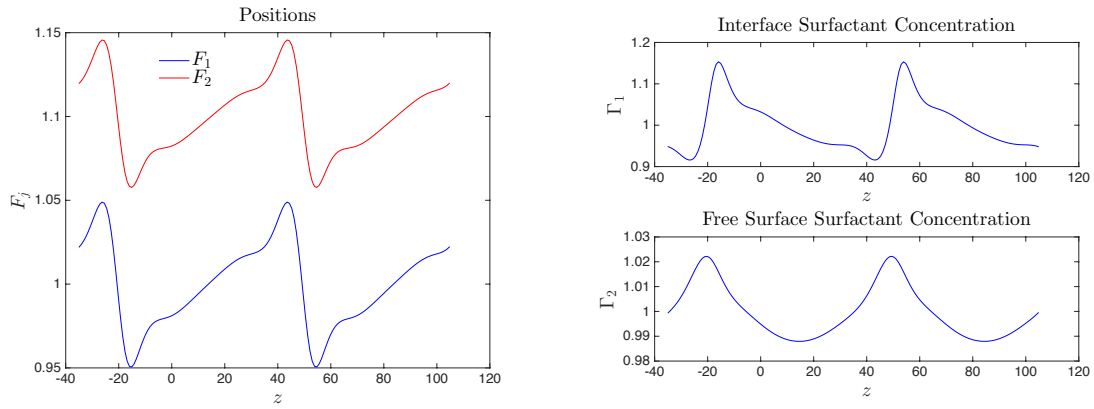

Figure 3.29: Plot of two periods of interface and free surface, position and surfactant concentration for travelling wave solution at $k = 0.09$ with $Ca_1 = Ca_2 = Ro = 1$, $Ma_1 = 0.1$, $Ma_2 = 10.391$, $m = 2$ and $\delta = 0.1$.

In figure 3.29 the interface and free surface are much closer together than in figure 3.28. The interface and free surface surfactant concentrations remain unchanged except for an increase in their amplitudes.

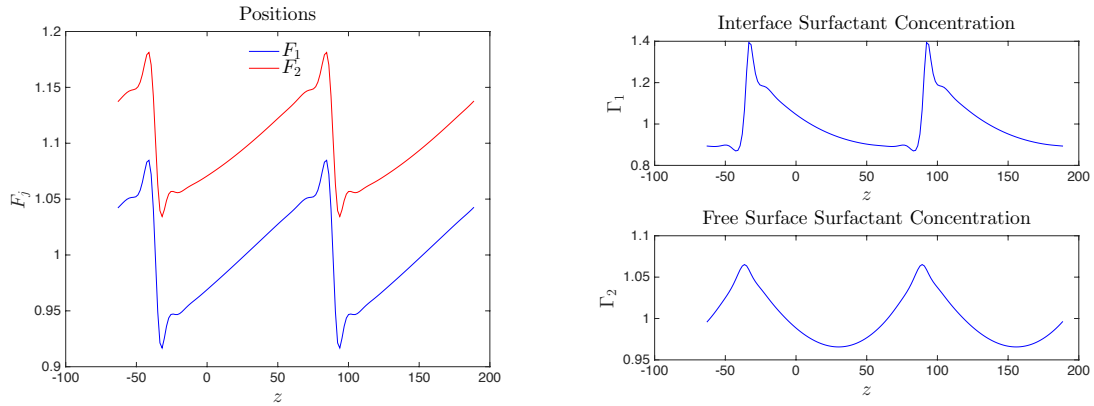

Figure 3.30: Plot of two periods of interface and free surface, position and surfactant concentration for travelling wave solution at $k = 0.05$ with $Ca_1 = Ca_2 = Ro = 1$, $Ma_1 = 0.1$, $Ma_2 = 10.391$, $m = 2$ and $\delta = 0.1$.

in figure 3.30 we can see that the free surface minima are lower than the interface maxima. The maxima on both the positions and the concentrations have become more pointed.

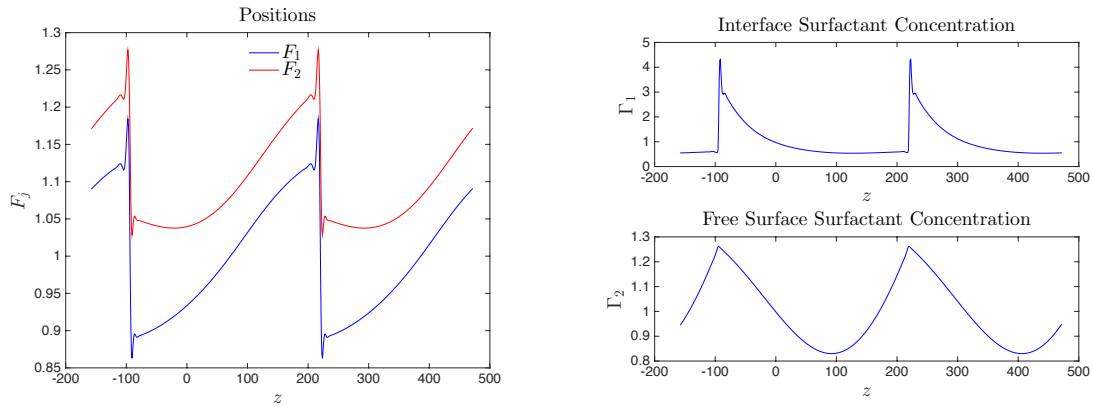

Figure 3.31: Plot of two periods of interface and free surface, position and surfactant concentration for travelling wave solution at $k = 0.02$ with $Ca_1 = Ca_2 = Ro = 1$, $Ma_1 = 0.1$, $Ma_2 = 10.391$, $m = 2$ and $\delta = 0.1$.

In figure 3.31 the positions have developed shock like structures to the left of the period. The interface surfactant concentration also has a shock like structure in the same z position as the positions. The free surface surfactant concentration has developed an apparent discontinuity in the first derivative at the same z position.

Branch 2

In figure 3.32 the interface and free surface positions resemble sine waves with a relative phase shift between the interface and free surface of nearly $\pi/2$. The surfactant concentration on the interface is similar to the interface position while the surfactant concentration on the free surface is similar to a small phase shift of the free surface position.

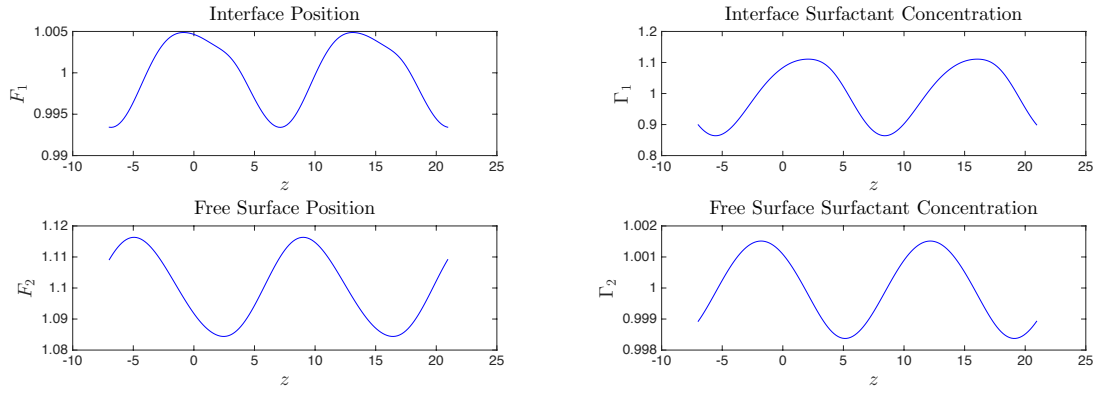

Figure 3.32: Plot of two periods of interface and free surface, position and surfactant concentration for travelling wave solution at $k = 0.452$ with $Ca_1 = Ca_2 = Ro = 1$, $Ma_1 = 0.1$, $Ma_2 = 10.391$, $m = 2$ and $\delta = 0.1$.

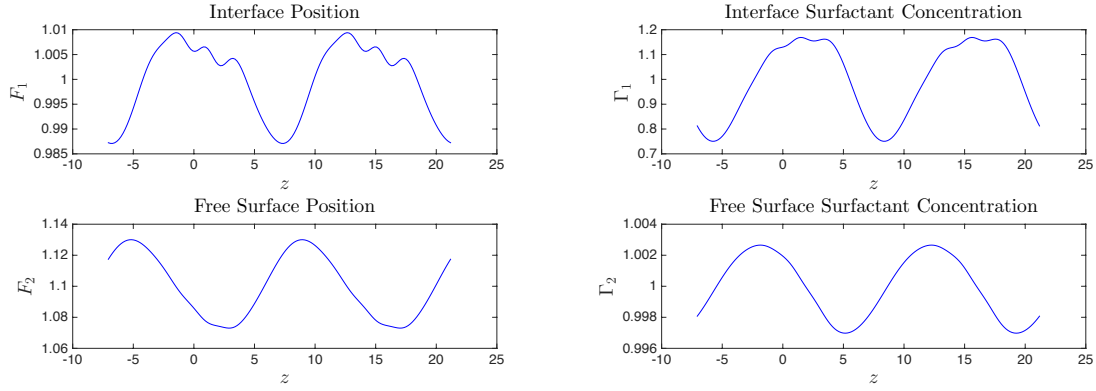

Figure 3.33: Plot of two periods of interface and free surface, position and surfactant concentration for travelling wave solution at $k = 0.445$ with $Ca_1 = Ca_2 = Ro = 1$, $Ma_1 = 0.1$, $Ma_2 = 10.391$, $m = 2$ and $\delta = 0.1$.

In figure 3.33 we can see a deformation in the form of a wave around the middle of the period. The free surface position has a small deformation that mirrors that of the interface but with a much smaller amplitude. The interface surfactant concentration has a small deformation resembling the deformation on the interface position while the free surface

surfactant concentration has a barely noticeable deformation in the same position.

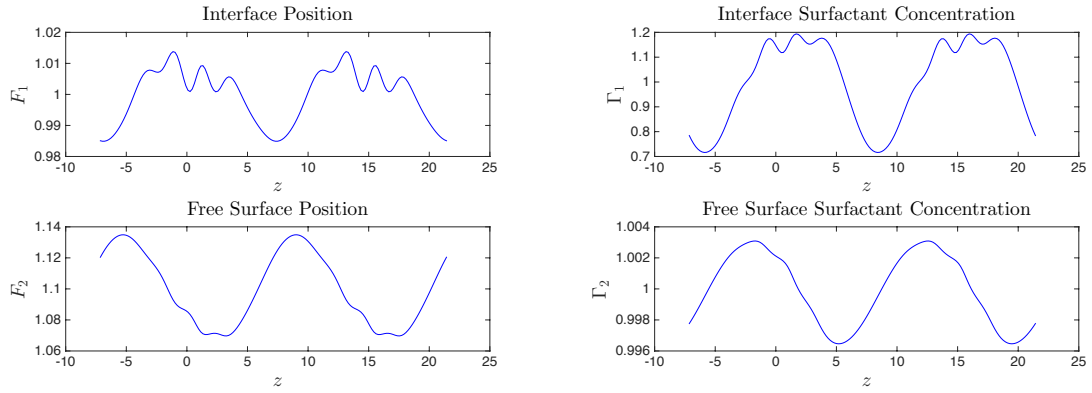

Figure 3.34: Plot of two periods of interface and free surface, position and surfactant concentration for travelling wave solution at $k = 0.44$ with $Ca_1 = Ca_2 = Ro = 1$, $Ma_1 = 0.1$, $Ma_2 = 10.391$, $m = 2$ and $\delta = 0.1$.

In figure 3.34 we can see the deformations on the interface and free surface position and surfactant concentration have increased in amplitude to become more like a wave packet.

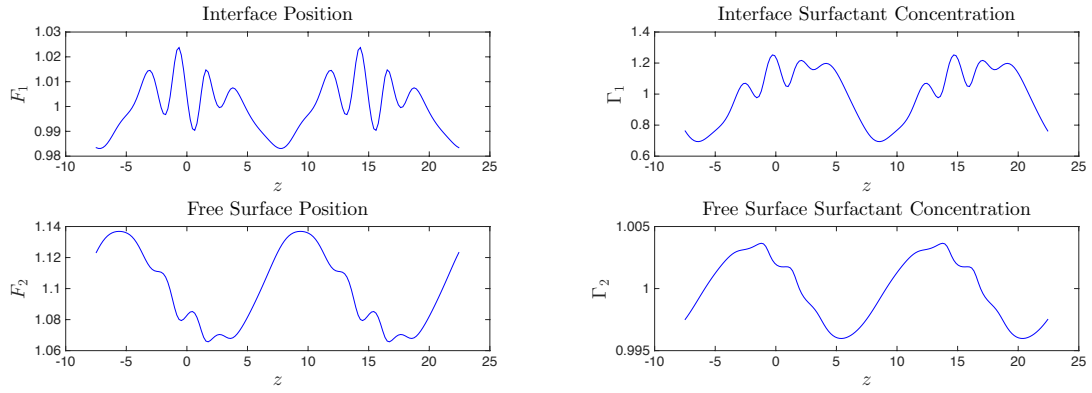

Figure 3.35: Plot of two periods of interface and free surface, position and surfactant concentration for travelling wave solution at $k = 0.42$ with $Ca_1 = Ca_2 = Ro = 1$, $Ma_1 = 0.1$, $Ma_2 = 10.391$, $m = 2$ and $\delta = 0.1$.

Figure 3.35 shows the further increase in amplitude of the deformations. We note here

that the interface position and surfactant concentration has four local maxima in the wave packet per period. The free surface position also has four local maxima. The free surface surfactant concentration wave packet is not defined enough for counting the maxima to be of significant use.

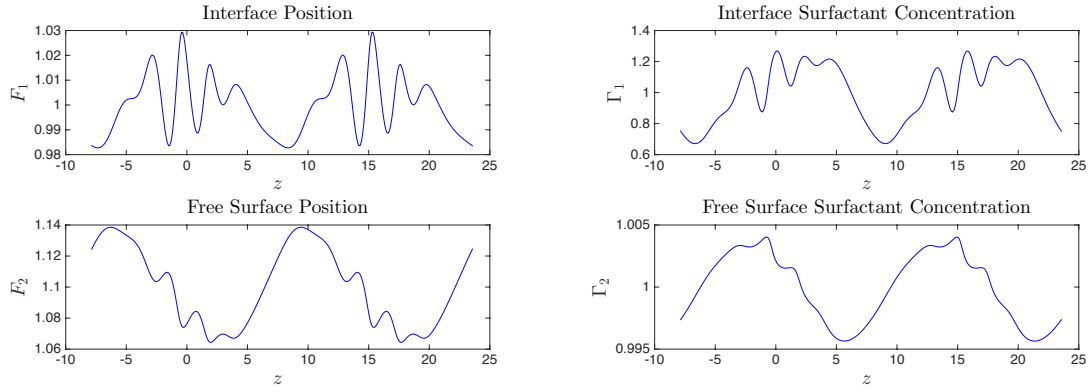

Figure 3.36: Plot of two periods of interface and free surface, position and surfactant concentration for travelling wave solution at $k = 0.4$ with $Ca_1 = Ca_2 = Ro = 1$, $Ma_1 = 0.1$, $Ma_2 = 10.391$, $m = 2$ and $\delta = 0.1$.

In figure 3.36 the interface position wave packet amplitude has become the amplitude of the whole wave. The interface position still has four local maxima but a fifth local maximum is developing to the left of the wave packet. The free surface position wave packet has increased slightly in amplitude as has the interface and free surface surfactant concentration.

In figure 3.37 the interface position wave packet minimum has become much smaller than the minimum outside the wave packet. The interface position now has five local maxima as does the interface surfactant concentration and free surface position. The free surface surfactant concentration still has a small amplitude wave packet.

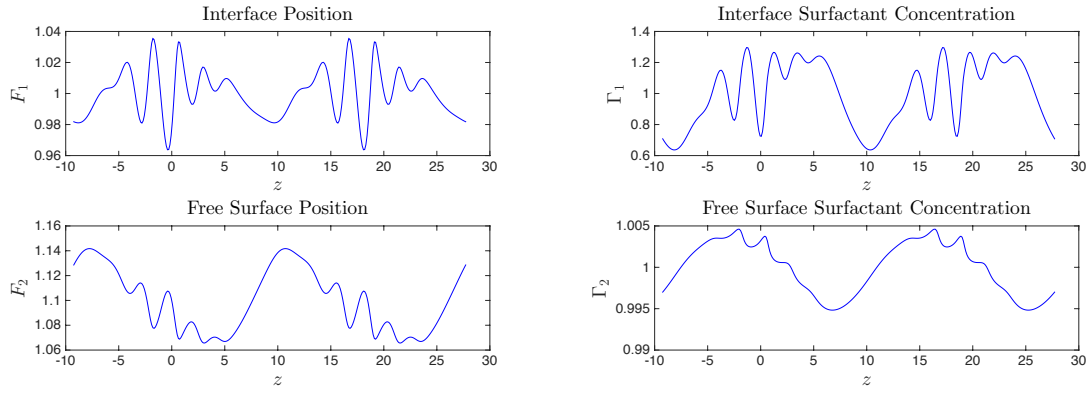

Figure 3.37: Plot of two periods of interface and free surface, position and surfactant concentration for travelling wave solution at $k = 0.34$ with $Ca_1 = Ca_2 = Ro = 1$, $Ma_1 = 0.1$, $Ma_2 = 10.391$, $m = 2$ and $\delta = 0.1$.

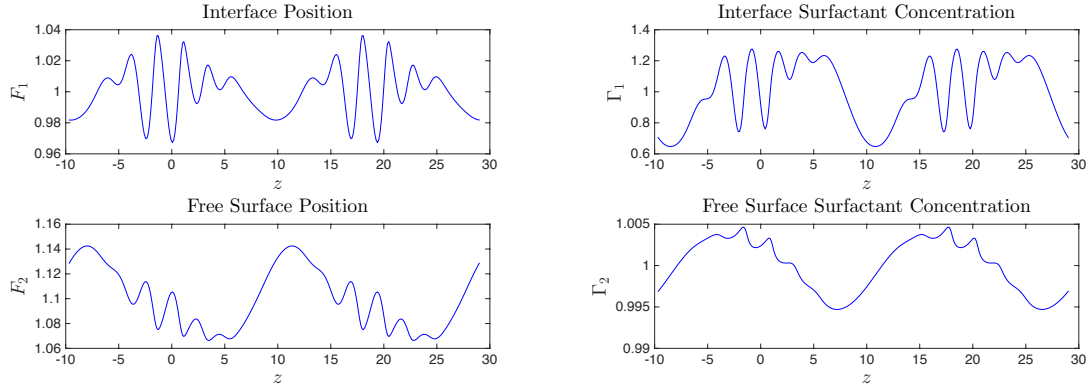

Figure 3.38: Plot of two periods of interface and free surface, position and surfactant concentration for travelling wave solution at $k = 0.325$ with $Ca_1 = Ca_2 = Ro = 1$, $Ma_1 = 0.1$, $Ma_2 = 10.391$, $m = 2$ and $\delta = 0.1$.

In figure 3.38 the wave packet on the interface position has six local maxima and minima. The rest of the profiles have changed little.

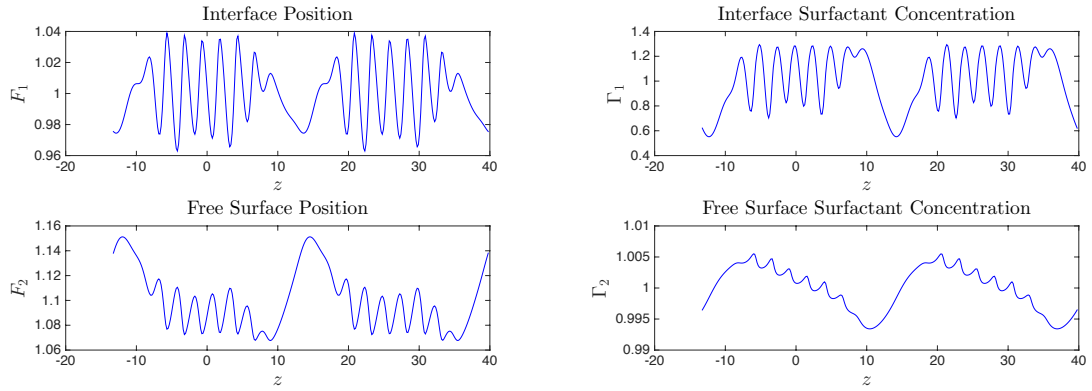

Figure 3.39: Plot of two periods of interface and free surface, position and surfactant concentration for travelling wave solution at $k = 0.237$ with $Ca_1 = Ca_2 = Ro = 1$, $Ma_1 = 0.1$, $Ma_2 = 10.391$, $m = 2$ and $\delta = 0.1$.

In figure 3.39 we observe that the number of oscillations in both interface and free surface position and surfactant concentration increases as k decreases. The new oscillations appear to be forming to the left of the current wave packet as seen when comparing the interface positions in figures 3.37 and 3.38. At $z \approx -5$ in both these figures we can see a small deformation for $k = 0.34$ which becomes a local maximum by $k = 0.325$. The amplitude of the left most oscillation, at $z \approx -4$ to $z \approx -1$, increases between $k = 0.34$ and $k = 0.325$ to become a similar amplitude to the oscillation to the right of $z \approx -1$. The other profiles follow similar patterns.

Branch 3

The profiles in figure 3.40 resemble sine waves with the interface and free surface positions having a phase shift of π. The interface surfactant concentration is a small phase shift of the interface position while the free surface surfactant concentration is a slightly larger phase shift of the free surface position.

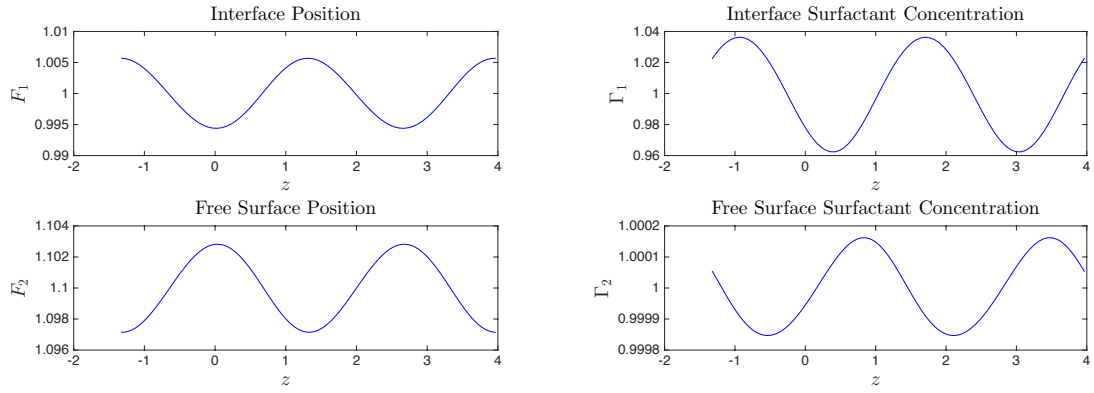

Figure 3.40: Plot of two periods of interface and free surface, position and surfactant concentration for travelling wave solution at $k = 2.3773$ with $Ca_1 = Ca_2 = Ro = 1$, $Ma_1 = 0.1$, $Ma_2 = 10.391$, $m = 2$ and $\delta = 0.1$.

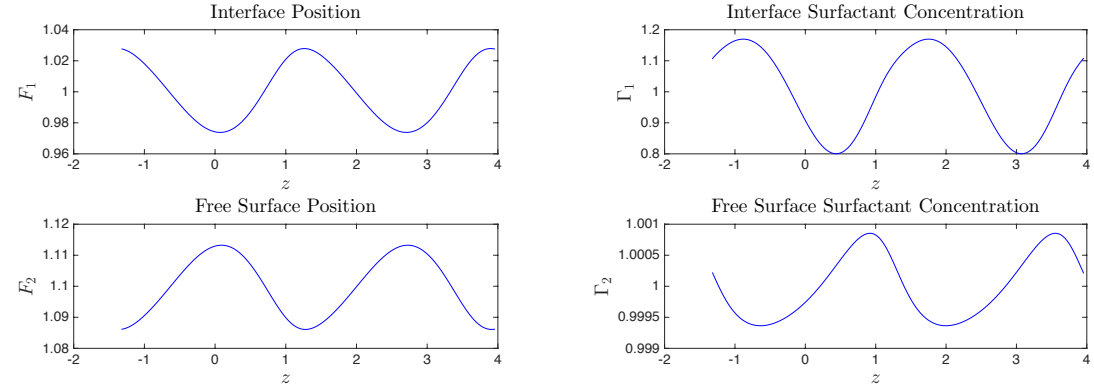

Figure 3.41: Plot of two periods of interface and free surface, position and surfactant concentration for travelling wave solution at $k = 2.3844$ with $Ca_1 = Ca_2 = Ro = 1$, $Ma_1 = 0.1$, $Ma_2 = 10.391$, $m = 2$ and $\delta = 0.1$.

In figure 3.41 we can see the interface position is starting to resemble an inverse sawtooth waveform while the free surface position is starting to resemble a sawtooth waveform keeping the symmetry between the two positions. The maxima of the interface surfactant

concentration have become more rounded and the minima more pointed. The maxima of the free surface surfactant concentration have become more pointed and the minima more rounded while at the same time looking more like a sawtooth waveform.

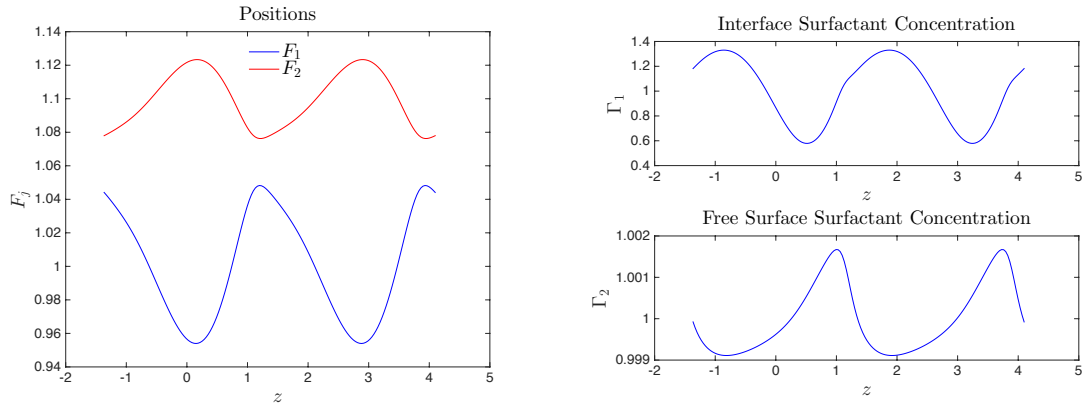

Figure 3.42: Plot of two periods of interface and free surface, position and surfactant concentration for travelling wave solution at $k = 2.3$ with $Ca_1 = Ca_2 = Ro = 1$, $Ma_1 = 0.1$, $Ma_2 = 10.391$, $m = 2$ and $\delta = 0.1$.

In figure 3.42 the interface position is starting to look like an inverse sawtooth waveform whilst the free surface waveform looks like a sawtooth waveform. The interface surfactant concentration is similar to the interface position with more rounded maxima and a deformation at $k \approx 1$. The free surface surfactant concentration has a similar profile to the interface position but with more rounded minima.

In figure 3.43 we can see that the interface and free surface are closer together than in figure 3.42 and between $z \approx 1$ and $z \approx 2$ the positions are becoming more flat. The surfactant concentrations remain unchanged in their shape but have increased in amplitude.

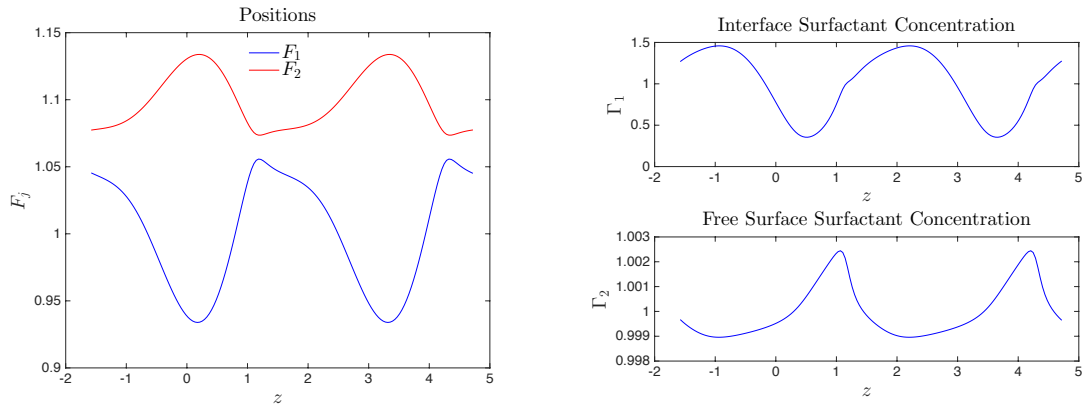

Figure 3.43: Plot of two periods of interface and free surface, position and surfactant concentration for travelling wave solution at $k = 2$ with $Ca_1 = Ca_2 = Ro = 1$, $Ma_1 = 0.1$, $Ma_2 = 10.391$, $m = 2$ and $\delta = 0.1$.

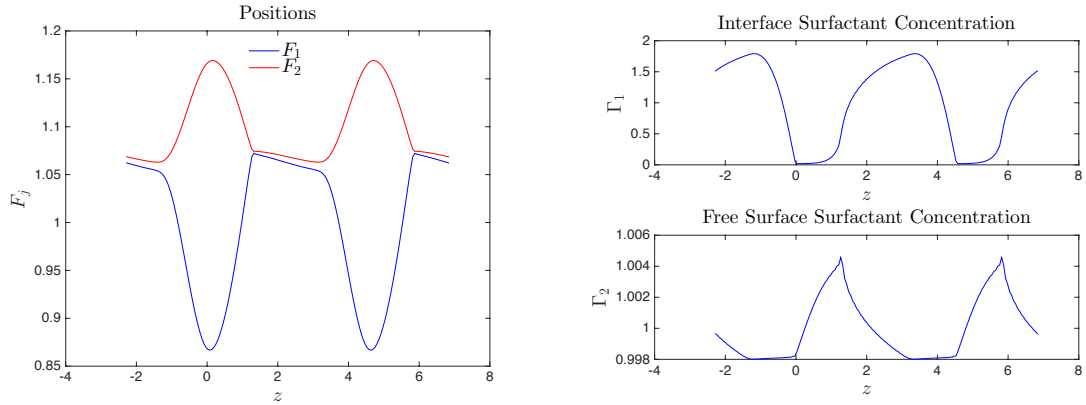

Figure 3.44: Plot of two periods of interface and free surface, position and surfactant concentration for travelling wave solution at $k = 1.38$ with $Ca_1 = Ca_2 = Ro = 1$, $Ma_1 = 0.1$, $Ma_2 = 10.391$, $m = 2$ and $\delta = 0.1$.

In figure 3.44 the interfaces are almost touching with the upper fluid tending to beads connected by a thin layer of fluid. The interface surfactant concentration is close to zero at $z \approx 0$ in the centre of the period. The free surface surfactant concentration deviates

from the base level of 1 only by a small amount in comparison to the interface surfactant concentration.

Branch 4

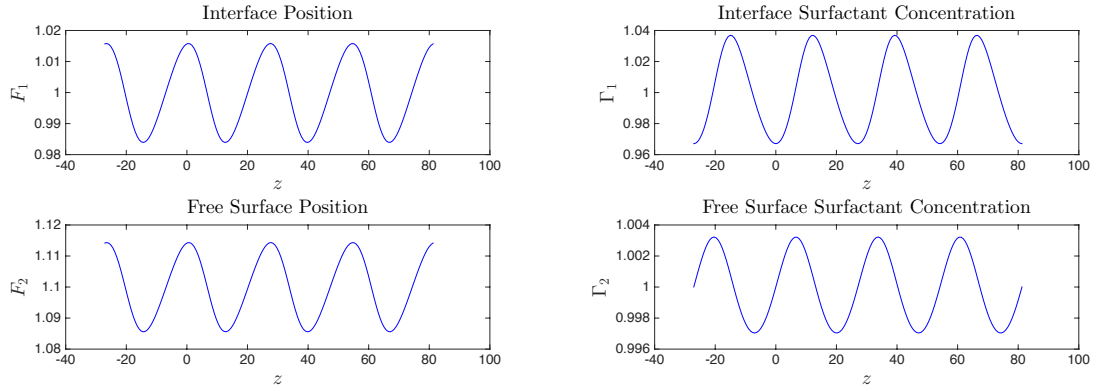

Figure 3.45: Plot of two periods of interface and free surface, position and surfactant concentration for travelling wave solution at $k = 0.116$ with $Ca_1 = Ca_2 = Ro = 1$, $Ma_1 = 0.1$, $Ma_2 = 10.391$, $m = 2$ and $\delta = 0.1$.

Figure 3.45 shows the interface and free surface positions and surfactant concentrations for the pseudo branch near the bifurcations point of the fourth branch denoted by an 'o' on the right of figure 3.21. These profiles are identical to the ones found in figure 3.23.

Figure 3.46 shows the wave profiles just after the bifurcation point where every other local maxima and minima are lower and higher respectively than the global maxima and minima respectively.

In figure 3.47 the interface surfactant concentration, interface and free surface position local maxima and minima from figure 3.46 have become almost equal to each other. The free surface surfactant concentration has reduced to a single maximum per period and a nearly flat profile away from the maxima.

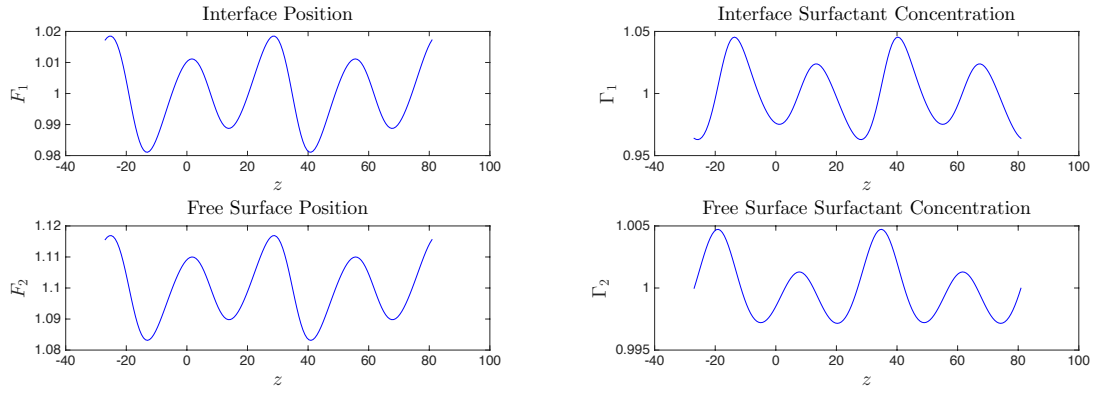

Figure 3.46: Plot of two periods of interface and free surface, position and surfactant concentration for travelling wave solution at $k = 0.1165$ with $Ca_1 = Ca_2 = Ro = 1$, $Ma_1 = 0.1$, $Ma_2 = 10.391$, $m = 2$ and $\delta = 0.1$.

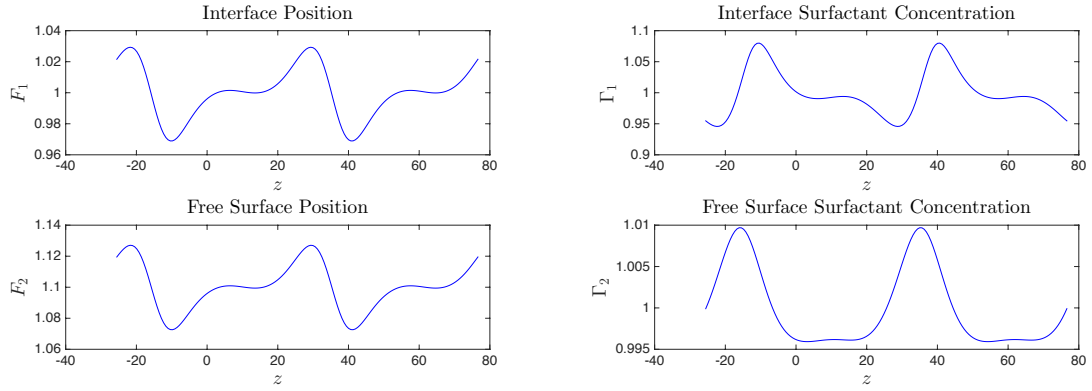

Figure 3.47: Plot of two periods of interface and free surface, position and surfactant concentration for travelling wave solution at $k = 0.123$ with $Ca_1 = Ca_2 = Ro = 1$, $Ma_1 = 0.1$, $Ma_2 = 10.391$, $m = 2$ and $\delta = 0.1$.

The figures presented for the rest of this branch are for wave numbers after the turning point where, following the branch from the bifurcation point, it changes from k increasing to k decreasing.

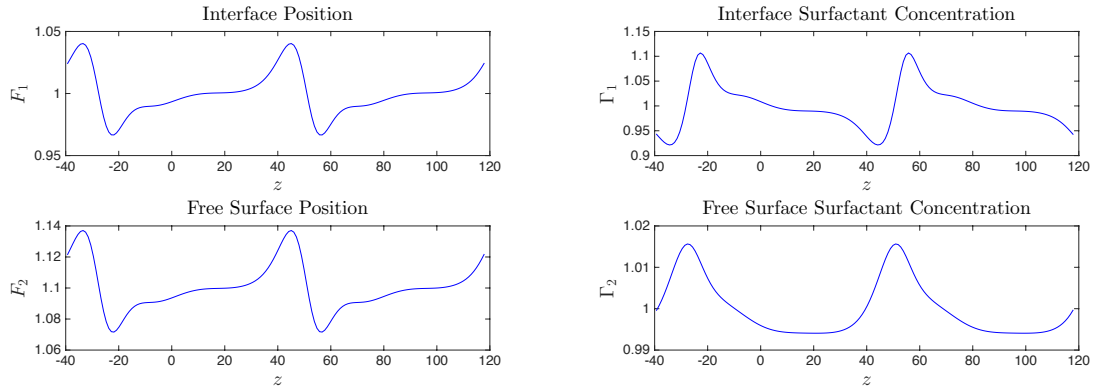

Figure 3.48: Plot of two periods of interface and free surface, position and surfactant concentration for travelling wave solution at $k = 0.08$ with $Ca_1 = Ca_2 = Ro = 1$, $Ma_1 = 0.1$, $Ma_2 = 10.391$, $m = 2$ and $\delta = 0.1$.

In figure 3.48 for the positions we observe that the maximum and minimum within a period stay close together while at the same time migrating further away from the maximum and minimum in the next period. The interface surfactant concentration follows a similar pattern. The free surface surfactant concentration has become more rounded at its minima.

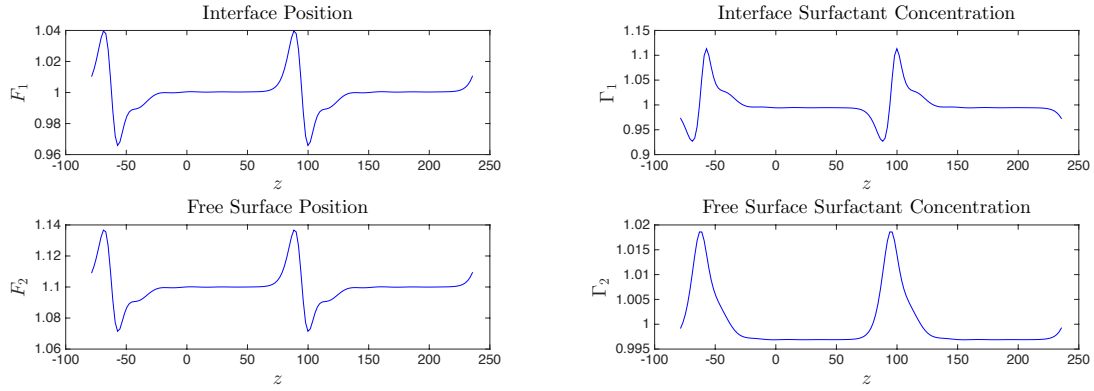

Figure 3.49: Plot of two periods of interface and free surface, position and surfactant concentration for travelling wave solution at $k = 0.04$ with $Ca_1 = Ca_2 = Ro = 1$, $Ma_1 = 0.1$, $Ma_2 = 10.391$, $m = 2$ and $\delta = 0.1$.

In figure 3.49 the positions have become pulses with a flat area in between them. The

interface surfactant concentration has again developed in the same way as the positions. The free surface surfactant concentration has developed into a single wave per period with a flat area between them.

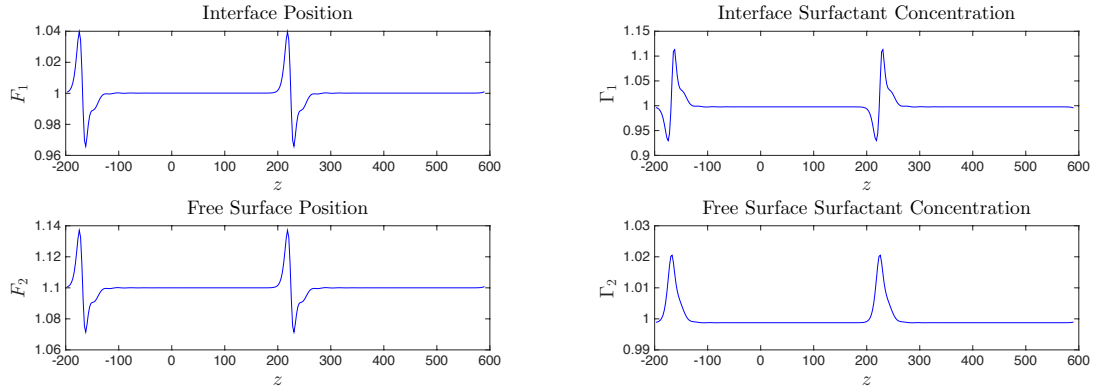

Figure 3.50: Plot of two periods of interface and free surface, position and surfactant concentration for travelling wave solution at $k = 0.016$ with $Ca_1 = Ca_2 = Ro = 1$, $Ma_1 = 0.1$, $Ma_2 = 10.391$, $m = 2$ and $\delta = 0.1$.

In figure 3.50 the profiles remain unchanged in shape but the distance between pulses has increased in the positions and interface surfactant concentration and the distance between the single waves has increased in the free surface surfactant concentration.

3.2.4 Case Study 4 - $Ca_1 = 1.1, Ca_2 = 0.8, Ro = 1, m = 0.2, \delta = 0.35, Ma_1 = 0.1405, Ma_2 = 0.3$

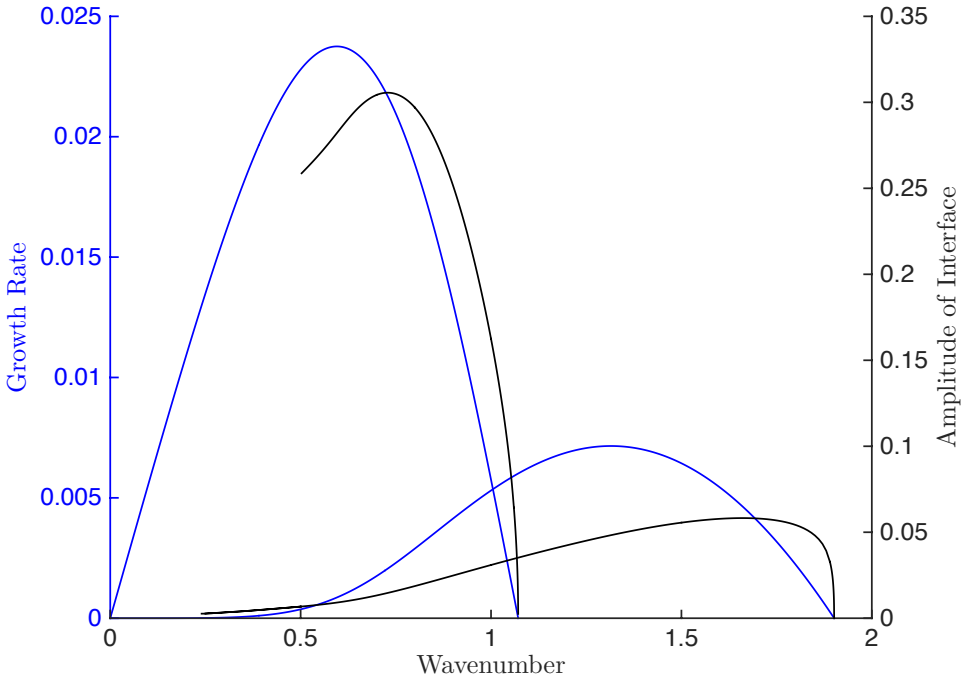

Figure 3.51: Comparison of the growth rate based on the linear stability to the amplitude of the travelling wave solution by wavenumber.

We have found travelling wave branches for a two layer flow where $Ca_1 = 1.1$, $Ca_2 = 0.8$, $Ro = 1$, $Ma_1 = 0.1405$, $Ma_2 = 0.3$, $m = 0.2$ and $\delta = 0.35$ as shown in figure 3.51. Here we have two unstable modes which overlap. We have found two travelling wave branches. The first branch bifurcates from $k = 1.0713$ towards $k = 0$, which becomes difficult to resolve near $k = 0.5$ due to the interface surfactant tending to zero for part of the period, and the second branch bifurcates from $k = 1.9011$ towards $k = 0$.

Branch 1

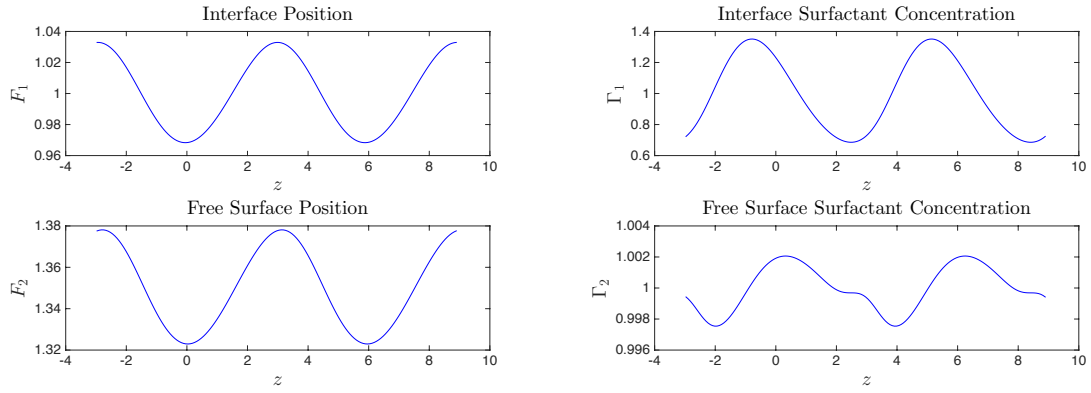

Figure 3.52: Plot of two periods of interface and free surface, position and surfactant concentration for travelling wave solution at $k = 1.06$ with $Ca_1 = 1.1$, $Ca_2 = 0.8$, $Ro = 1$, $Ma_1 = 0.1405$, $Ma_2 = 0.3$, $m = 0.2$ and $\delta = 0.35$.

In figure 3.52 the interface and free surface positions are similar sine waves. The interface surfactant concentration resembles a sine wave with relative phase shift of π to the interface position while the free surface surfactant concentration looks like the interface surfactant concentration with a defamation at $z \approx 3$. It is unusual for the traveling wave solution so close to the bifurcation point to be much of a perturbation from a sine wave.

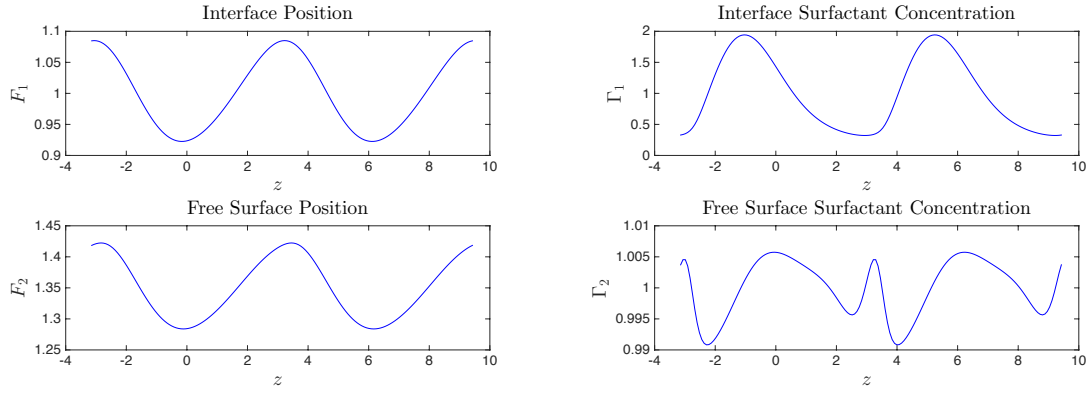

Figure 3.53: Plot of two periods of interface and free surface, position and surfactant concentration for travelling wave solution at $k = 1$ with $Ca_1 = 1.1$, $Ca_2 = 0.8$, $Ro = 1$, $Ma_1 = 0.1405$, $Ma_2 = 0.3$, $m = 0.2$ and $\delta = 0.35$.

In figure 3.53 the interface and free surface position shapes remain unchanged except in amplitude. The interface surfactant concentration has started looking like an inverse sawtooth waveform whilst at the same time increasing the amplitude rapidly compared to the positions and the free surface surfactant concentration. The deformation on the free surface surfactant concentration has become more pronounced producing a local maximum of a similar height to the global maxima.

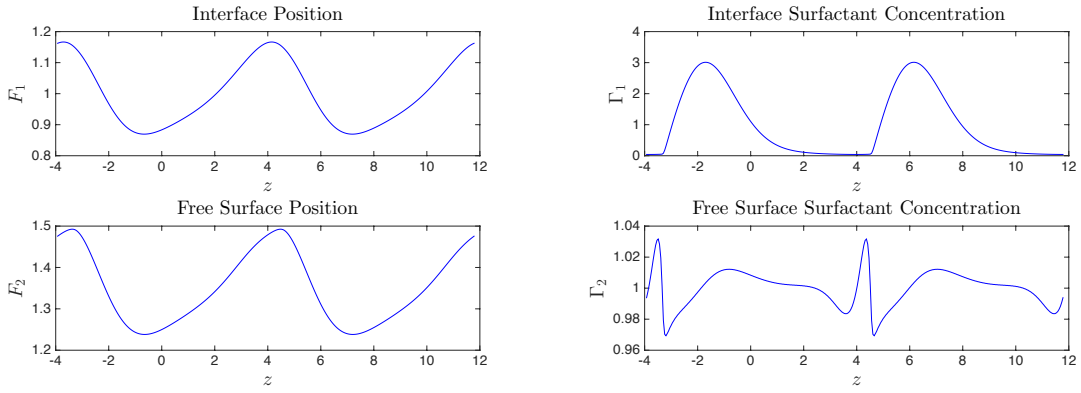

Figure 3.54: Plot of two periods of interface and free surface, position and surfactant concentration for travelling wave solution at $k = 0.8$ with $Ca_1 = 1.1$, $Ca_2 = 0.8$, $Ro = 1$, $Ma_1 = 0.1405$, $Ma_2 = 0.3$, $m = 0.2$ and $\delta = 0.35$.

In figure 3.54 the interface and free surface positions are starting to look like sawtooth waveforms. The interface surfactant concentration has become zero at the transition between periods while the free surface surfactant concentration has developed a pulse in the position of zero surfactant concentration on the interface.

In figure 3.55 the interface and free surface positions have developed a deformation to the left of the maxima in the same position where the interface surfactant concentration becomes zero. The range for which the interface surfactant concentration is zero has increased while keeping its shape. The free surface surfactant concentration is developing

what appears to look like a discontinuity at least in the first derivative.

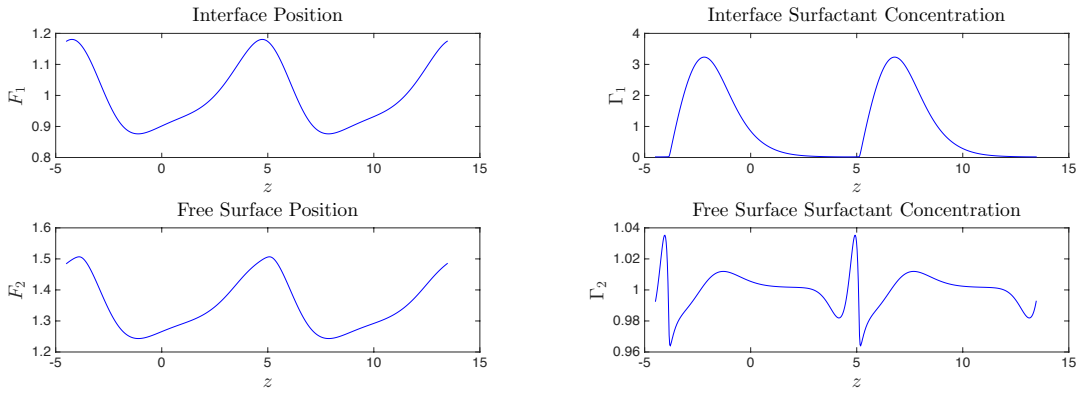

Figure 3.55: Plot of two periods of interface and free surface, position and surfactant concentration for travelling wave solution at $k = 0.7$ with $Ca_1 = 1.1$, $Ca_2 = 0.8$, $Ro = 1$, $Ma_1 = 0.1405$, $Ma_2 = 0.3$, $m = 0.2$ and $\delta = 0.35$.

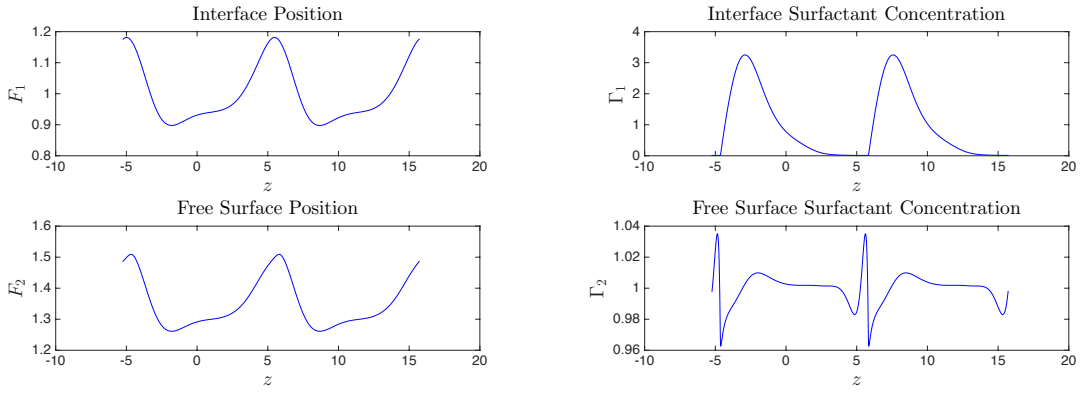

Figure 3.56: Plot of two periods of interface and free surface, position and surfactant concentration for travelling wave solution at $k = 0.6$ with $Ca_1 = 1.1$, $Ca_2 = 0.8$, $Ro = 1$, $Ma_1 = 0.1405$, $Ma_2 = 0.3$, $m = 0.2$ and $\delta = 0.35$.

In figure 3.56 the deformation on the interface and free surface positions has increased so that a pulse has started to form at the transition between periods. The interface surfactant concentration has remained vastly unchanged. The distance between pulses of

the free surface surfactant concentration has increased in line with what we would expect with decreasing the wavenumber, k.

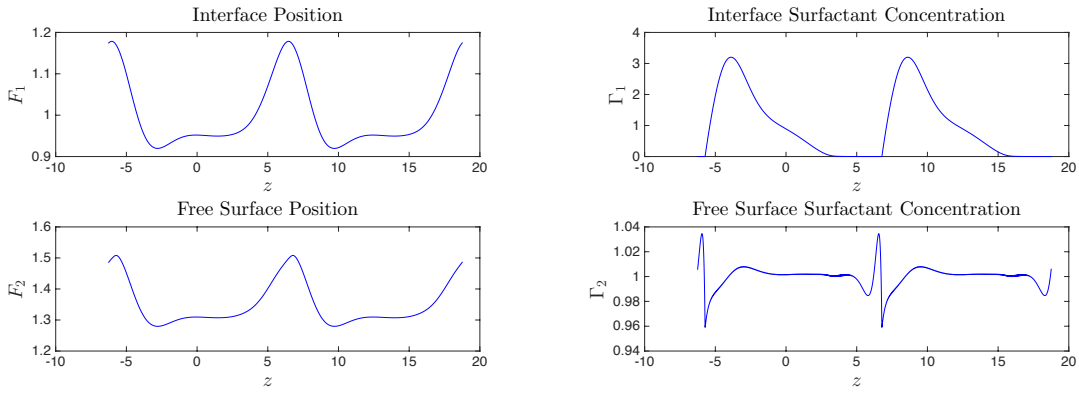

Figure 3.57: Plot of two periods of interface and free surface, position and surfactant concentration for travelling wave solution at $k = 0.5025$ with $Ca_1 = 1.1$, $Ca_2 = 0.8$, $Ro = 1$, $Ma_1 = 0.1405$, $Ma_2 = 0.3$, $m = 0.2$ and $\delta = 0.35$.

In figure 3.57 the interface and free surface position and concentration remain mainly qualitatively unchanged except noting that due to the decrease in the wavenumber, k, the distance between the main features has increased. We should note that the apparent fuzziness in the free surface surfactant concentration is due to a numerical instability most probably caused by the rapid change at the pulse in the free surface surfactant concentration.

Branch 2

In figure 3.58 the interface position resembles a sine wave while the free surface position resembles a reflection of the interface position. The interface surfactant concentration is similar to the interface position while the free surface surfactant concentration is similar to a sine wave with a phase shift of $\pi/2$ relative to the free surface position.

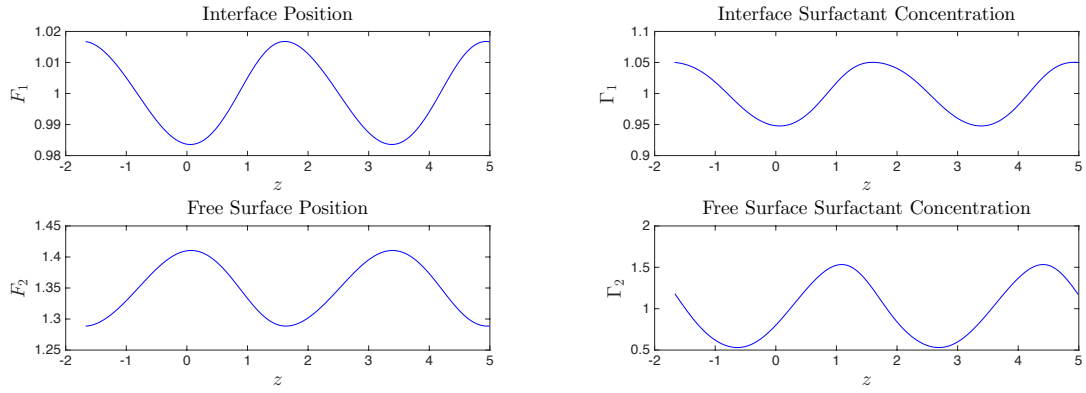

Figure 3.58: Plot of two periods of interface and free surface, position and surfactant concentration for travelling wave solution at $k = 1.89$ with $Ca_1 = 1.1$, $Ca_2 = 0.8$, $Ro = 1$, $Ma_1 = 0.1405$, $Ma_2 = 0.3$, $m = 0.2$ and $\delta = 0.35$.

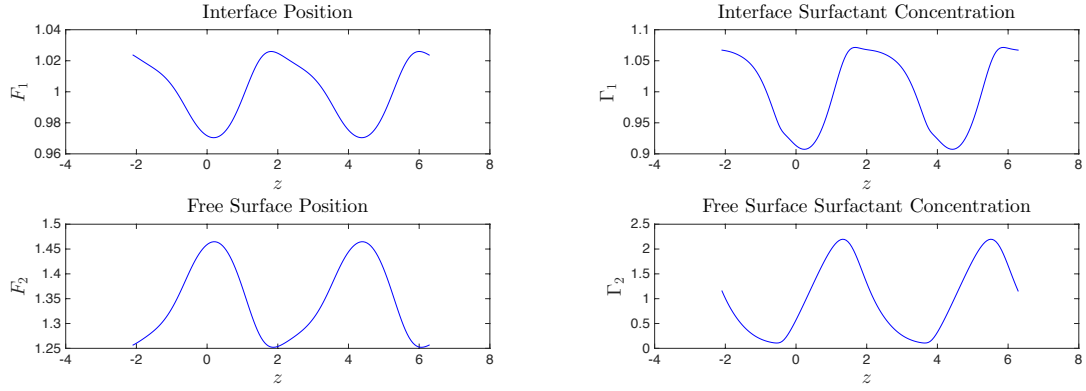

Figure 3.59: Plot of two periods of interface and free surface, position and surfactant concentration for travelling wave solution at $k = 1.5$ with $Ca_1 = 1.1$, $Ca_2 = 0.8$, $Ro = 1$, $Ma_1 = 0.1405$, $Ma_2 = 0.3$, $m = 0.2$ and $\delta = 0.35$.

In figure 3.59 the interface position has developed a deformation to the right of the maximum and the free surface has developed a matching smaller deformation to the right of the minimum. The interface surfactant concentration has developed a deformation in the

same position as on the interface position while the free surface surfactant concentration has developed a deformation in the same position.

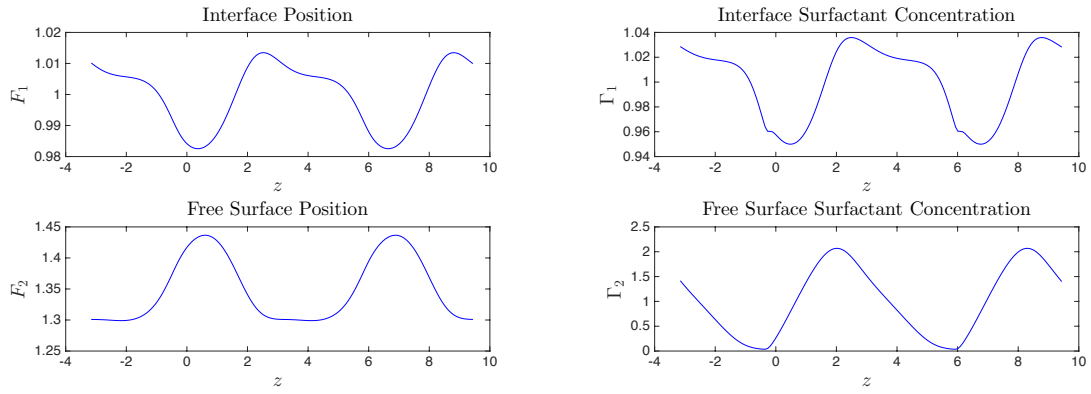

Figure 3.60: Plot of two periods of interface and free surface, position and surfactant concentration for travelling wave solution at $k = 1.0$ with $Ca_1 = 1.1$, $Ca_2 = 0.8$, $Ro = 1$, $Ma_1 = 0.1405$, $Ma_2 = 0.3$, $m = 0.2$ and $\delta = 0.35$.

In figure 3.60 the deformation on the interface position has become comparable to the maxima while the deformation in the free surface position has become almost identical to the minima. The interface surfactant concentration deformation has become comparable to the maxima and the free surface surfactant concentration has almost become zero just to left of the centre of the period.

In figure 3.61 the interface position has developed several oscillations which appears to be a pulse on a sine wave. The interface surfactant concentration has a similar profile to the interface position with a sharp point at the minima. On the free surface position a deformation has appeared at the middle of the period while the minima has become more rounded. The free surface surfactant concentration has become zero at the middle of the period while the amplitude has stayed the same.

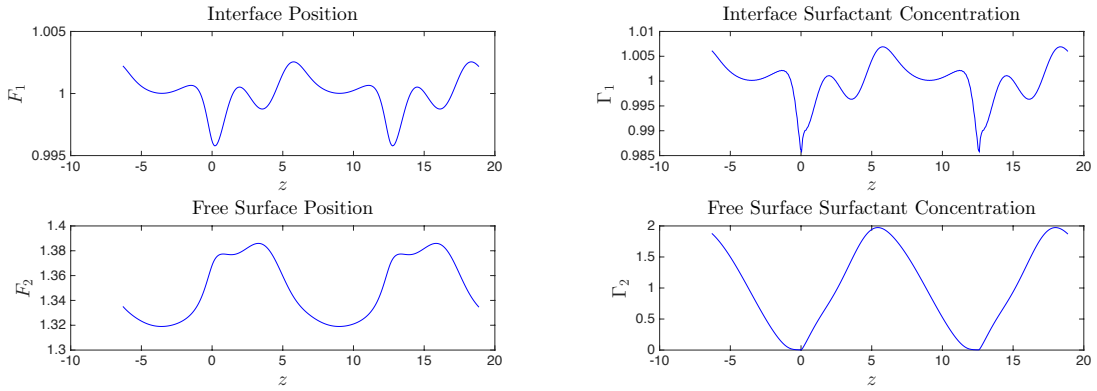

Figure 3.61: Plot of two periods of interface and free surface, position and surfactant concentration for travelling wave solution at $k = 0.5$ with $Ca_1 = 1.1$, $Ca_2 = 0.8$, $Ro = 1$, $Ma_1 = 0.1405$, $Ma_2 = 0.3$, $m = 0.2$ and $\delta = 0.35$.

3.2.5 Case Study 5 - $Ca_1 = Ca_2 = Ro = 1$, $m = 2$, $\delta = 0.1$, $Ma_1 = 0.274237$ and $Ma_2 = 2$

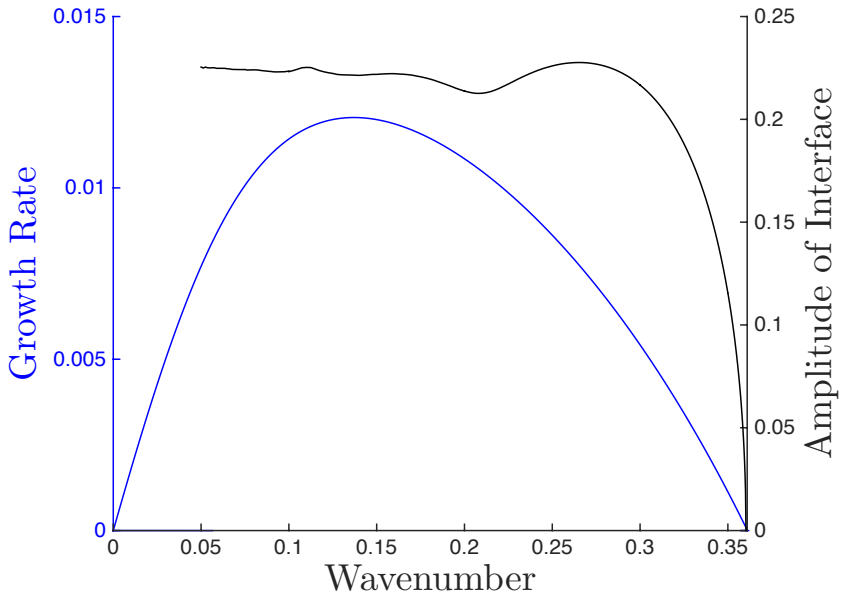

Figure 3.62: Comparison of the growth rate based on the linear stability to the amplitude of the travelling wave solution by wavenumber with $Ca_1 = Ca_2 = Ro = 1$, $Ma_1 = 0.274237$, $Ma_2 = 2$, $m = 2$ and $\delta = 0.1$.

We have found travelling wave branches for a two layer flow where $Ca_1 = Ca_2 = Ro = 1$, $Ma_1 = 0.274237$, $Ma_2 = 2$, $m = 2$ and $\delta = 0.1$ as shown in figure 3.62 and 3.63. Here we have two unstable modes which meet at a point of zero growth. We have found two travelling wave branches. The first branch bifurcates from $k = 0.3603$ towards $k = 0$. At $k = 0.05$ the first branch becomes difficult to resolve further, possibly due to the increase in the wavelength meaning the features of the profiles become more localised and so much more spatial points are needed to resolve. The second branch bifurcates from $k = 1.9479$ towards $k = 0$. As the second branch passes $k = 1$ it becomes much more difficult to resolve which seems to be because of a rapidly decreasing interface amplitude but using a smaller step in k does not seem to let the branch progress further.

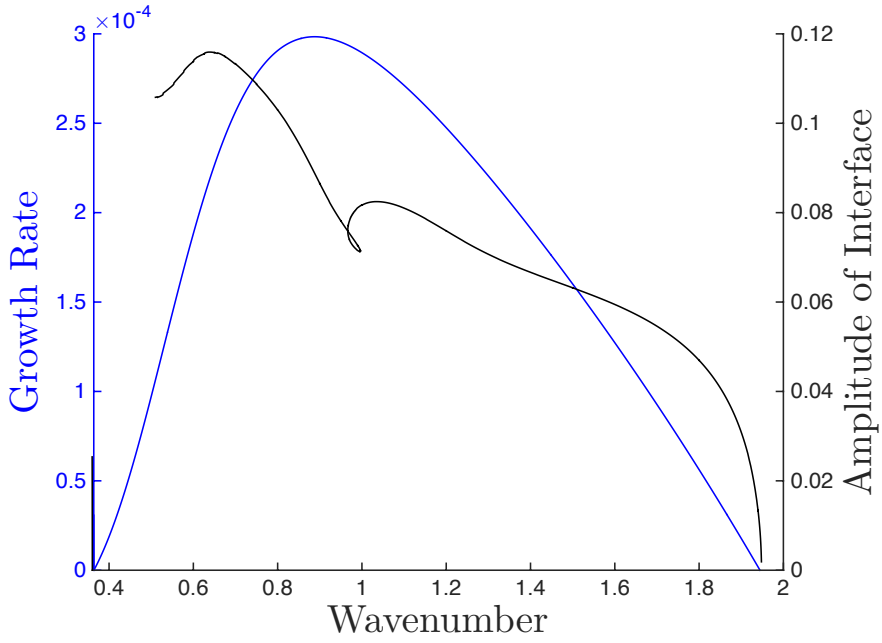

Figure 3.63: Comparison of the growth rate based on the linear stability to the amplitude of the travelling wave solution by wavenumber with $Ca_1 = Ca_2 = Ro = 1$, $Ma_1 = 0.274237$, $Ma_2 = 2$, $m = 2$ and $\delta = 0.1$.

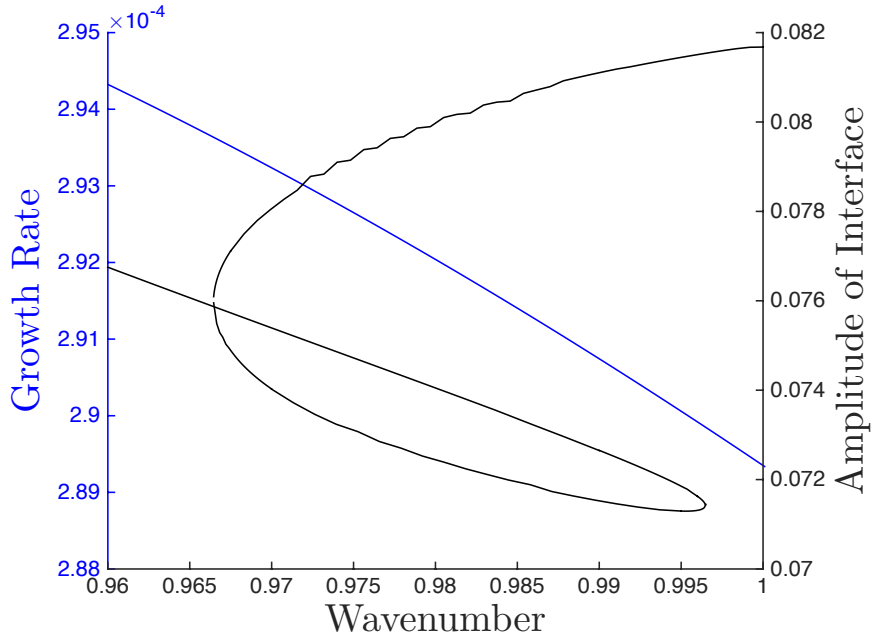

Figure 3.64: Comparison of the growth rate based on the linear stability to the amplitude of the travelling wave solution by wavenumber with $Ca_1 = Ca_2 = Ro = 1$, $Ma_1 = 0.274237$, $Ma_2 = 2$, $m = 2$ and $\delta = 0.1$.

Branch 1

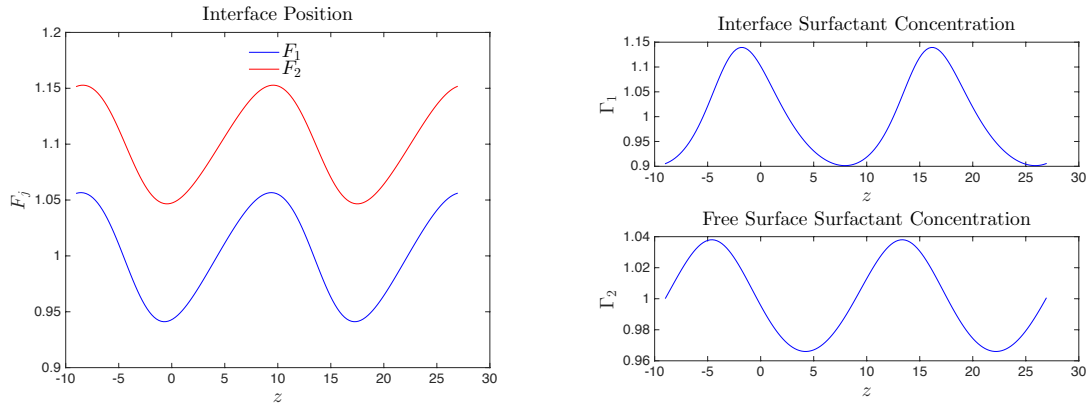

Figure 3.65: Plot of two periods of interface and free surface, position and surfactant concentration for travelling wave solution at $k = 0.35$ with $Ca_1 = Ca_2 = Ro = 1$, $Ma_1 = 0.274237$, $Ma_2 = 2$, $m = 2$ and $\delta = 0.1$.

In figure 3.65 the interface and free surface positions resemble sine waves with the same phase shift. The interface surfactant concentration is a sine wave with a relative phase shift to the interface position of approximately π while the free surface surfactant concentration is a phase shift of approximately $\pi/2$ to the free surface position.

In figure 3.66 the interface and free surface positions have started to transform into a sawtooth waveform. The interface surfactant is starting to look like a bell curve shape while the free surface surfactant concentration remains mainly unchanged.

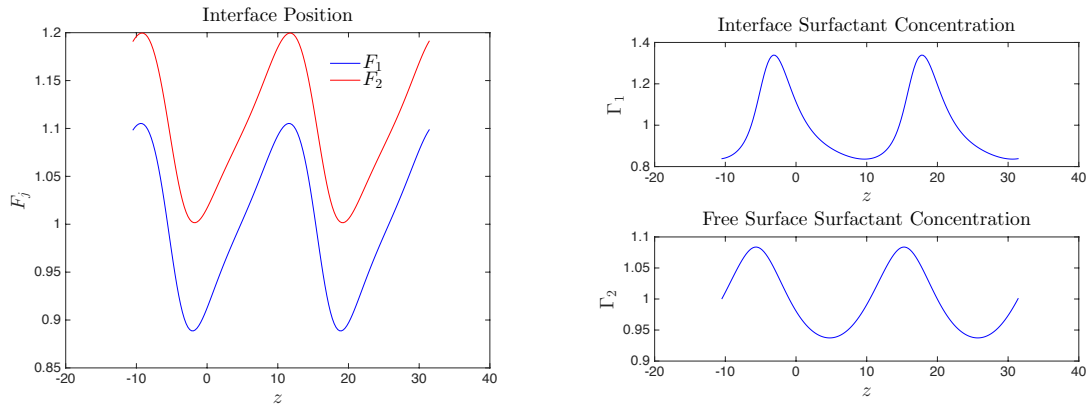

Figure 3.66: Plot of two periods of interface and free surface, position and surfactant concentration for travelling wave solution at $k = 0.3$ with $Ca_1 = Ca_2 = Ro = 1$, $Ma_1 = 0.274237$, $Ma_2 = 2$, $m = 2$ and $\delta = 0.1$.

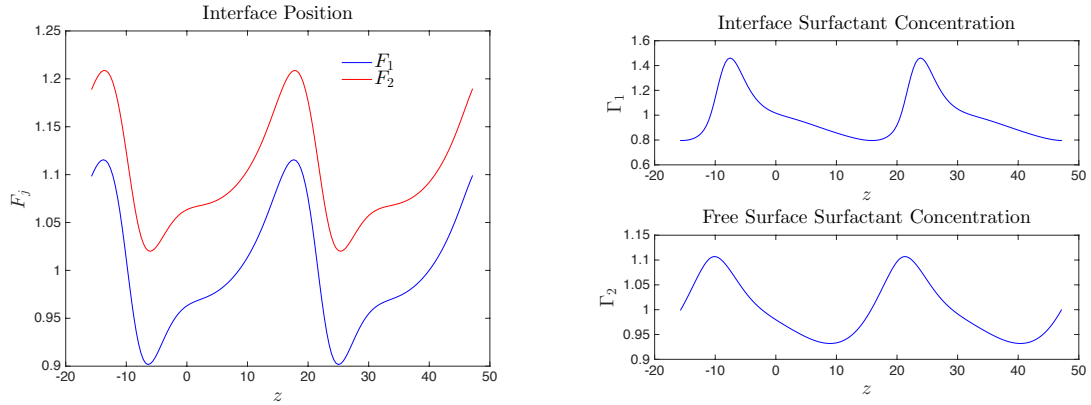

Figure 3.67: Plot of two periods of interface and free surface, position and surfactant concentration for travelling wave solution at $k = 0.2$ with $Ca_1 = Ca_2 = Ro = 1$, $Ma_1 = 0.274237$, $Ma_2 = 2$, $m = 2$ and $\delta = 0.1$.

In figure 3.67 the interface and free surface position has developed a deformation to the left of the maximum. The interface and free surface surfactant concentration are looking more like bell curve shapes.

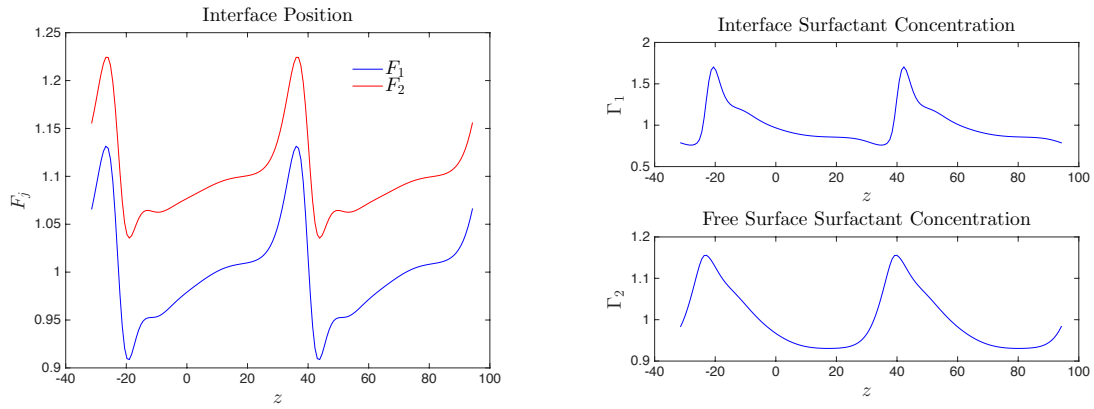

Figure 3.68: Plot of two periods of interface and free surface, position and surfactant concentration for travelling wave solution at $k = 0.1$ with $Ca_1 = Ca_2 = Ro = 1$, $Ma_1 = 0.274237$, $Ma_2 = 2$, $m = 2$ and $\delta = 0.1$.

In figure 3.68 the interface and free surface position have developed a second deformation to the left of the maximum. The interface surfactant concentration has developed into two distinct parts, to the right of the period the profile is close to flat and over the transition between periods it has an inverse sawtooth waveform with a continuous transition between the two. The free surface surfactant concentration has developed a small deformation to the right of the maximum.

In figure 3.69 the interface and free surface position have developed a flat profile at the right side of the periods. The interface surfactant concentrations flat part has increased while the free surface surfactant concentration has developed a flat part to the right of the period.

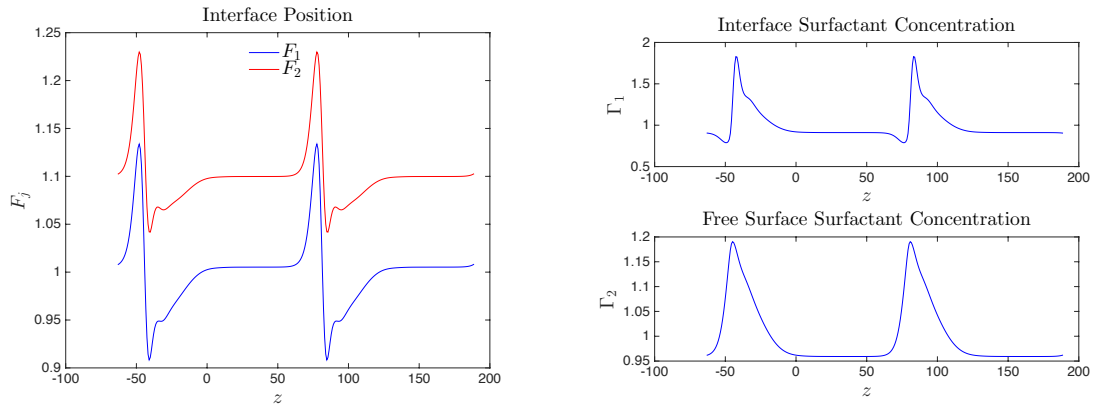

Figure 3.69: Plot of two periods of interface and free surface, position and surfactant concentration for travelling wave solution at $k = 0.05$ with $Ca_1 = Ca_2 = Ro = 1$, $Ma_1 = 0.274237$, $Ma_2 = 2$, $m = 2$ and $\delta = 0.1$.

Branch 2

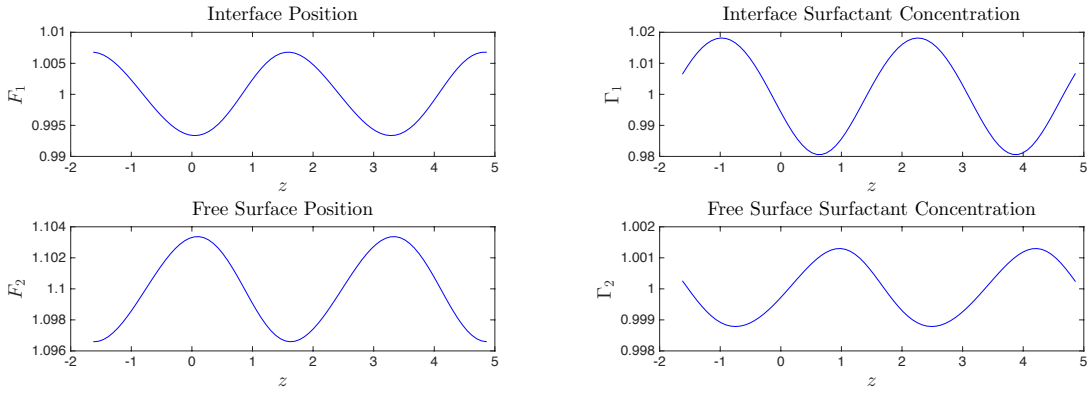

Figure 3.70: Plot of two periods of interface and free surface, position and surfactant concentration for travelling wave solution at $k = 1.94$ with $Ca_1 = Ca_2 = Ro = 1$, $Ma_1 = 0.274237$, $Ma_2 = 2$, $m = 2$ and $\delta = 0.1$.

In figure 3.70 the interface position resembles a sine wave while the free surface position is approximately a refection of the interface position. The interface surfactant surfac-

tant concentration is a shift of approximately $\pi/2$ of the interface position while the free surface surfactant concentration is approximately a reflection of the interface surfactant concentration.

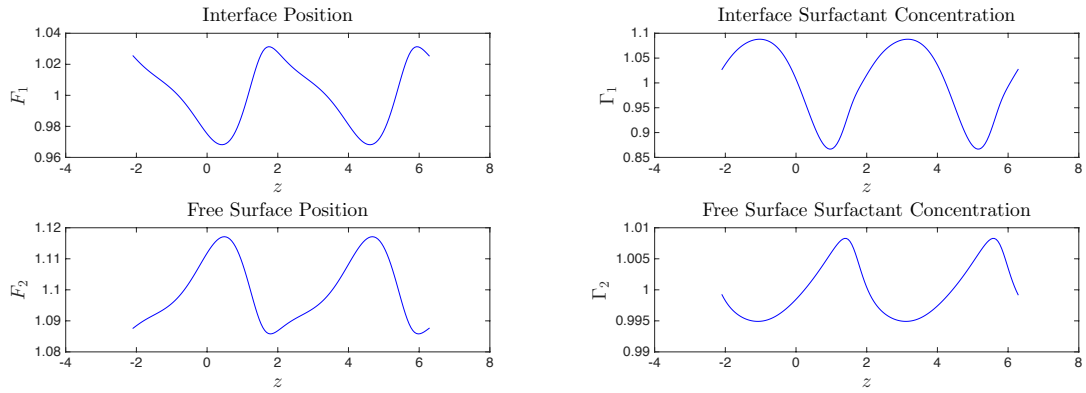

Figure 3.71: Plot of two periods of interface and free surface, position and surfactant concentration for travelling wave solution at $k = 1.5$ with $Ca_1 = Ca_2 = Ro = 1$, $Ma_1 = 0.274237$, $Ma_2 = 2$, $m = 2$ and $\delta = 0.1$.

In figure 3.71 the interface position is starting to look like an inverse sawtooth waveform with a deformation to the right of the maxima while the free surface position is keeping its approximate reflection of the interface position. The interface surfactant concentration looks like a refection of a bell curve shape while the free surface surfactant concentration has kept its approximate reflection of the interface surfactant concentration.

In figure 3.72 the interface and free surface position deformation has increased in size. The interface and free surface surfactant concentration have also developed deformations at the same position as the maxima on the interface position.

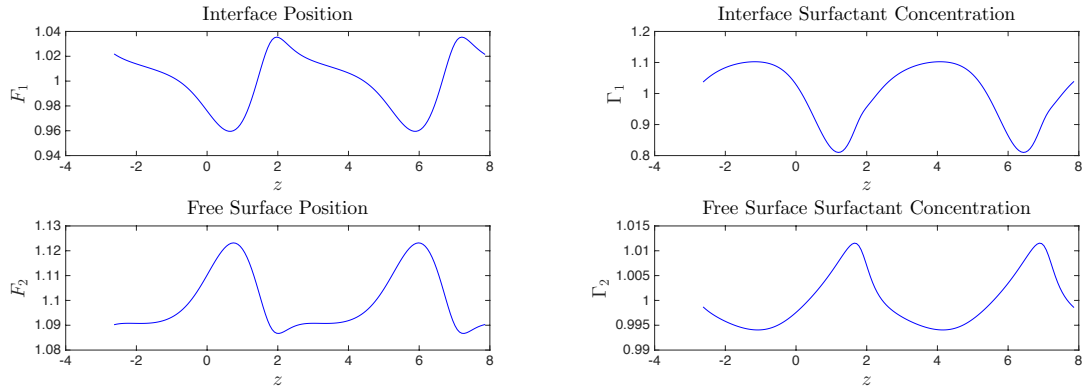

Figure 3.72: Plot of two periods of interface and free surface, position and surfactant concentration for travelling wave solution at $k = 1.2$ with $Ca_1 = Ca_2 = Ro = 1$, $Ma_1 = 0.274237$, $Ma_2 = 2$, $m = 2$ and $\delta = 0.1$.

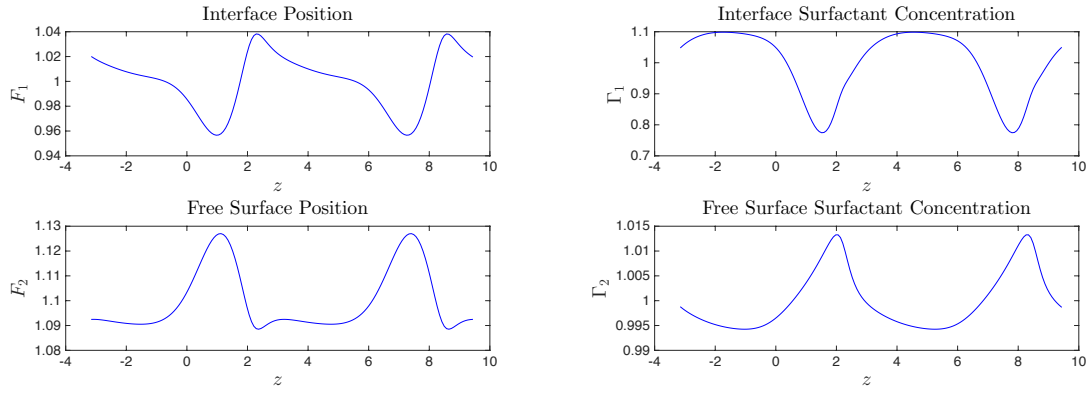

Figure 3.73: Plot of two periods of interface and free surface, position and surfactant concentration for travelling wave solution at $k = 1$ with $Ca_1 = Ca_2 = Ro = 1$, $Ma_1 = 0.274237$, $Ma_2 = 2$, $m = 2$ and $\delta = 0.1$.

In figure 3.73 the interface position deformation has become comparable to the minima whilst the deformation on the free surface position has increased. The interface surfactant concentration deformation has not changed whilst the free surface surfactant concentration

has developed into more of a sawtooth waveform with a curve between the sawtooths.

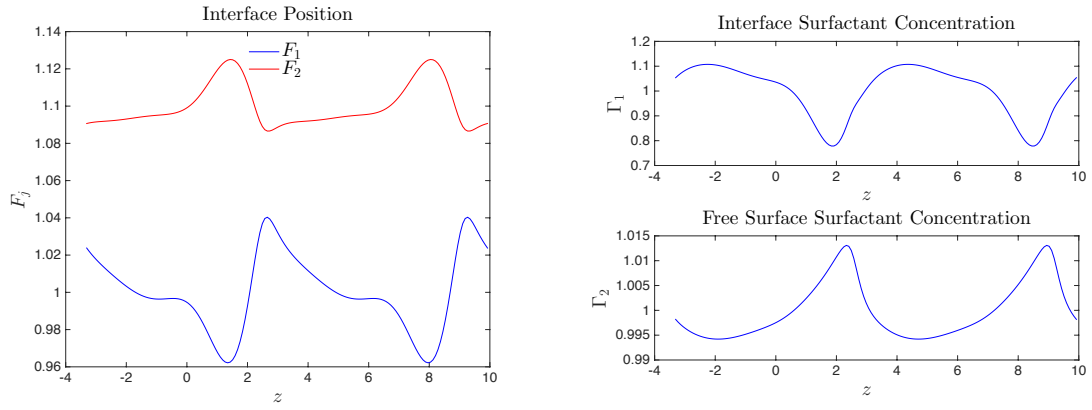

Figure 3.74: Plot of two periods of interface and free surface, position and surfactant concentration for travelling wave solution at $k = 0.95$ with $Ca_1 = Ca_2 = Ro = 1$, $Ma_1 = 0.274237$, $Ma_2 = 2$, $m = 2$ and $\delta = 0.1$.

In figure 3.74 the interface position has developed into a pulse where the maxima and minima are of equal deviation from $F_j = 1$. The free surface position has developed a pulse where the maxima has a much higher deviation from $F_j = 1.095$ than the minima. The interface surfactant concentration has continued its shape but with a straight line developing to the left of the period. The free surface surfactant concentration has remained vastly unchanged.

In figure 3.75 the shapes of the interfaces and surfactant concentrations are very similar to 3.74 but have a sharper point at $z \approx 5$.

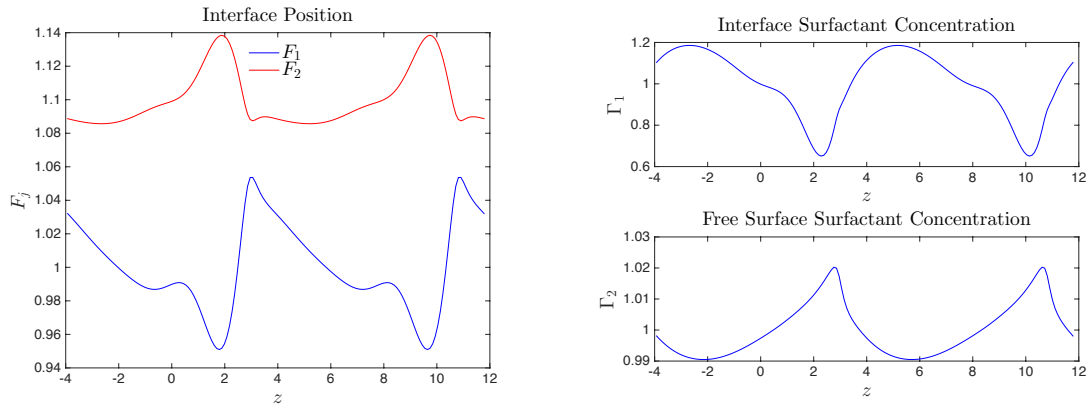

Figure 3.75: Plot of two periods of interface and free surface, position and surfactant concentration for travelling wave solution at $k = 0.8$ with $Ca_1 = Ca_2 = Ro = 1$, $Ma_1 = 0.274237$, $Ma_2 = 2$, $m = 2$ and $\delta = 0.1$.

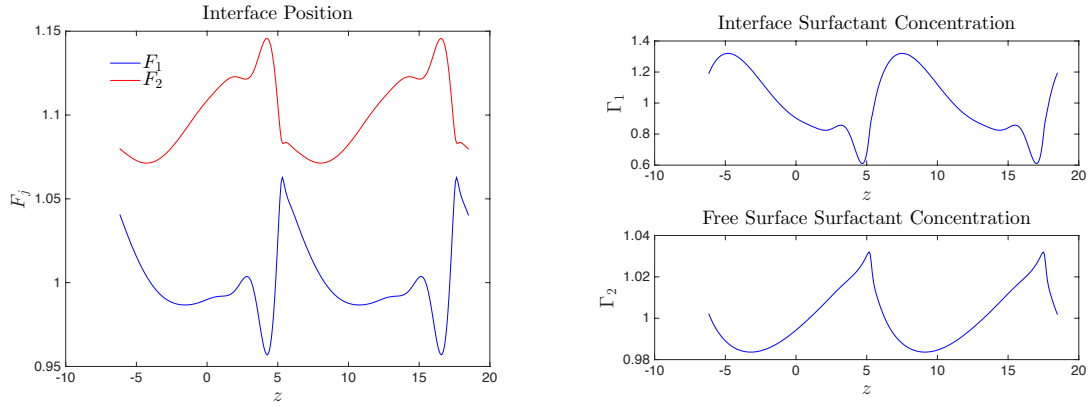

Figure 3.76: Plot of two periods of interface and free surface, position and surfactant concentration for travelling wave solution at $k = 0.51$ with $Ca_1 = Ca_2 = Ro = 1$, $Ma_1 = 0.274237$, $Ma_2 = 2$, $m = 2$ and $\delta = 0.1$.

In figure 3.76 the interfaces and surfactant concentrations continue to become sharper causing a pinching of the upper fluid at $z \approx 6$.

These cases were chosen to represent a cross section of possible parameter values, where we have taken the densities of both layers to be equal for all cases. Case 1 gives traveling wave solutions in the absence of surfactants with a thicker much more viscous upper layer.

Case 2 shows the traveling wave solutions where the viscosities and layer thicknesses are the same, the Marangoni numbers and the Capillary number in the upper layer are equal to 1 and the Capillary number in the lower layer is slightly larger than the upper layer at 1.1. The larger Capillary number in the lower layer is the cause of the instability in the linear growth rate. Case 3 is our first case of multiple unstable modes where we have a more viscous thin upper layer and a much higher surfactant concentration on the free surface of the upper layer. Case 4 is a case where there is a thin less viscous upper layer, the Capillary number of the lower layer is slightly more than the upper layer and there is about twice the surfactant concentration on the upper layer. This leads to the growth rate curves overlapping. In Case 5 there is a thin more viscous upper layer and the Marangoni number on the interface has been tuned to allow the growth rate curves to intersect at a point of neutral stability. This we thought might lead to periodic traveling waves.

Stability of Traveling Wave Solutions

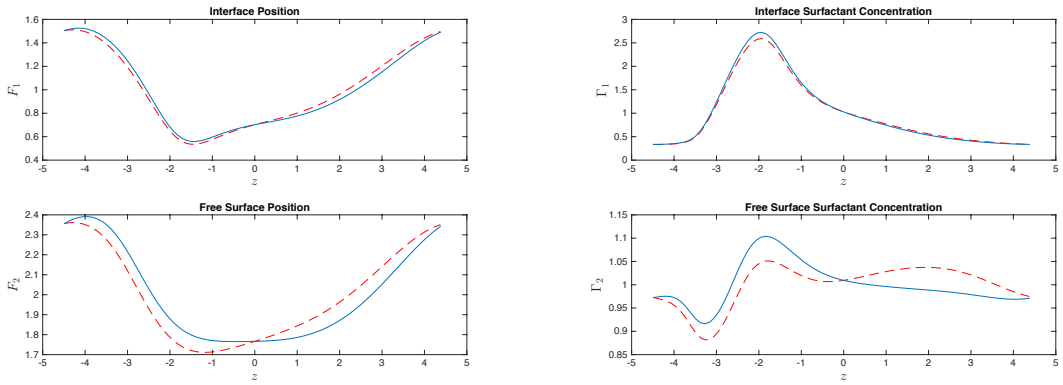

Figure 3.77: Plot of interface and free surface, position and surfactant concentration for travelling wave solution at $k = 0.7$ with $Ca_1 = 1.1$, $Ca_2 = Ro = Ma_1 = Ma_2 = m = 1$ and $\delta = 1.5$ with a perturbation of the surface as a dashed line.

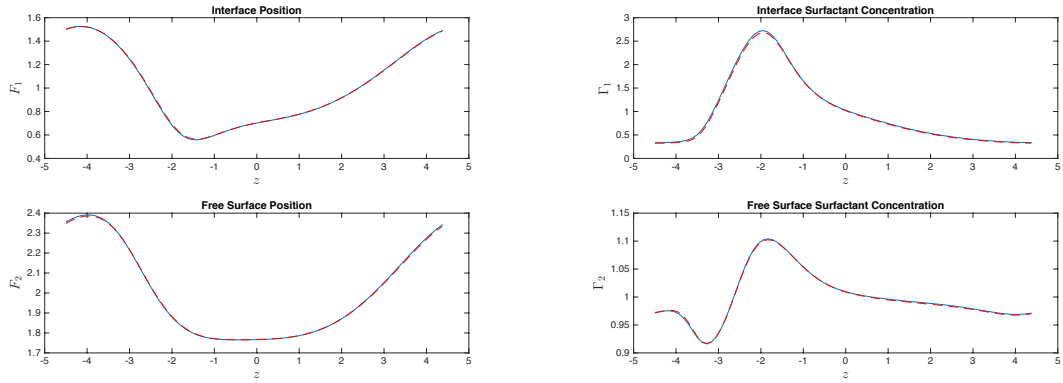

Figure 3.78: Plot of interface and free surface, position and surfactant concentration for travelling wave solution at $k = 0.7$ with $Ca_1 = 1.1$, $Ca_2 = Ro = Ma_1 = Ma_2 = m = 1$ and $\delta = 1.5$ with the long term evolution of the perturbation as a dashed line.

To test the stability of the travelling wave solutions we took a travelling wave solution as computed above and multiplied the solutions by a small perturbation which we took to be $\epsilon \sin(kz)$, where and ran the nonlinear evolution code given in section 2.3 with this as the initial wave profile. Figure 3.77 shows the travelling wave profiles for $k = 0.7$ with $Ca_1 = 1.1$, $Ca_2 = Ro = Ma_1 = Ma_2 = m = 1$ and $\delta = 1.5$ which was computed in section 2.4.2 and the perturbation of the travelling wave profiles where we have chosen $\epsilon = 0.05$. After running the nonlinear evolution code to $\tau = 200$ where the profiles are plotted in figure 3.78. This shows that this particular travelling wave solution is stable for such a perturbation as we have presented.

3.3 Summary

We have shown an extension of Gao & Lu (2007) work by considering an equal layer ratio which can lead to multiple unstable modes not found by Gao and Lu. These solutions with multiple modes can have stable bandwidths sandwiched by unstable bandwidths as

shown for certain values in figure 2.7.

We also extended Gao & Lu (2007) work by considering adding a third layer to their two layer calculations. These also led to solutions with multiple modes where changing the surfactant concentration made one mode change monotonically whilst making the other change non-monotonically. In some cases we found that there can exist a range of stable wavenumbers sandwiched by a region of unstable wavenumbers. This can arise from having the total thickness of the upper layers of fluid equal to the thickness of the lowest layer and surfactant only on the interface between layers 2 and 3. Varying the levels of surfactants in the interfaces and free surface can have interesting effects upon the growth rates of the different modes. One example of this is for a layer thickness as described in the previous sentence with surfactant on the interface between layers 2 and 3. Increasing the concentration of surfactant on the free surface has the effect of monotonically reducing one mode while having a non-monotonic effect upon the other mode. In considering a case which is stable in the absence of surfactant, where upper layers are less viscous than the layers below them, the range or ranges of unstable wavenumbers in the presence of surfactant do not start from zero wavenumber as in the previous cases. After extensive search in the literature this appears to be the first time observing this for multi-layer flow down an inclined plane.

We have derived and solved numerically a set of equations to describe the nonlinear evolution of three layer flow down an inclined plane in the presence of surfactant. Picking an initial wave profile based on the linear stability analysis either the wave stabilises to a flat profile denoting a unidirectional flow or a stable wave profile which we surmised to be a travelling wave profile as given in section 2.3.

We have considered the presence of travelling wave solutions for two layer flow in the presence of surfactants. In the vicinity of the point of zero growth rate, there exists a travelling wave solution of small amplitude. In the travelling wave cases we have considered, at least one of the travelling wave branches tends towards zero wavenumber from the bifurcation point. This suggests that for a set of parameters at least one of the traveling wave branches will tend towards zero wavenumber. In case 1 and 2 the maximum of the amplitudes are close to the maximums of the growth rate for the linear stability.

In case 3 an unexpected branch was found which bifurcates not from a point of zero growth rate as the others found do but from a harmonic of branch 1 in case 3. We expect that there exists other such branches which bifurcate from harmonics of different branches but we make no further effort to find them in this thesis and it is left for further work. The existence of this branch may not depend upon the presence of surfactant since all the branches have harmonics but such a branch has not been found in case 1 where no surfactant is present.

The presence of turning of the branch and the loops created were also unexpected as it suggests multiple traveling wave solutions exist for a single wavenumber. The solution that we expect to observe would depend upon the stability of the different travelling wave solutions and the initial profile taken for an unsteady time dependent calculation as given in section 2.2.

4 Breakup of a Liquid Thread with a Rigid Core

We examine the dynamics of a viscous thread coating a solid core. One example of annular flow with a core in nature is spider silk. Spiders spin silk of two types, one is hard and cylindrical and is the main structure of the web (usually the outwards spokes of the web) and the other which is very elastic and is covered in sticky beads. The sticky beads are initially excreted as an annular thread over an elastic thread. These break up into uniformly spaced beads discussed by Boys (1960).

We conduct a normal mode analysis by assuming a small amplitude perturbation of an annular thread of fluid surrounding a solid core which is initially at rest.

We consider a liquid thread of radius b surrounding a solid core of radius a as in figure 4.1. We take the z-axis to point along the centre of the solid core and the r-axis to point out radially from the centre of the thread, perpendicular to z. We use cylindrical coordinates (r, θ, z) as shown in figure 4.1. We assume the thread has a constant initial velocity along the z-axis which we take to be zero via a simple Galilean transform of the velocity, so that the solid core is moving along with the fluid. We assume there is no θ dependence on the pressure, velocity or the disturbance to the interface, as we do not expect this to affect thread breakup. For a Rayleigh jet the growth rate of the θ mode is always stable giving credence to ignoring the θ mode for our calculations. We are considering small perturbations of the velocity and pressure from the base state described above. We take the Navier-Stokes equations in cylindrical coordinates as given in Acheson (1990), ignoring nonlinear terms since we will be taking small perturbations of the velocity, assuming axis symmetry and ignoring external forces such as gravity we arrive at the equations

$$\frac{\partial u}{\partial t} = -\frac{1}{\rho}\frac{\partial p}{\partial r} + \frac{\mu}{\rho}\left(\frac{\partial^2 u}{\partial r^2} + \frac{1}{r}\frac{\partial u}{\partial r} - \frac{u}{r^2} + \frac{\partial^2 u}{\partial z^2}\right), \tag{4.1a}$$

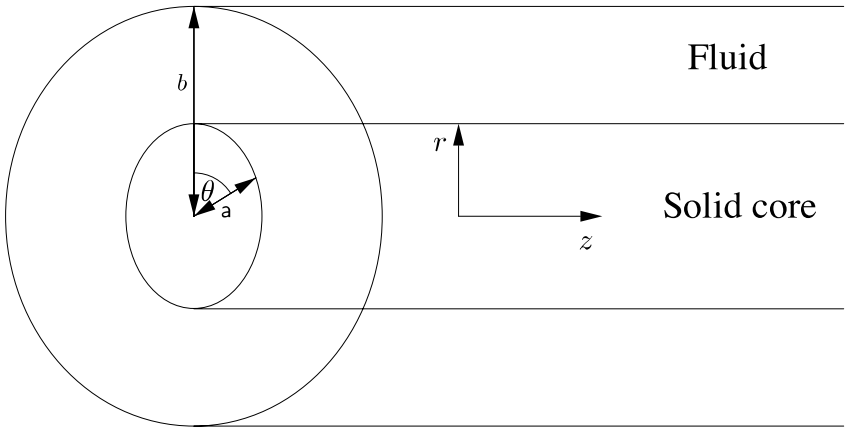

Figure 4.1: Illustration of a layer of fluid coated on the outer surface of a rigid circular rod.

$$\frac{\partial w}{\partial t} = -\frac{1}{\rho}\frac{\partial p}{\partial z} + \frac{\mu}{\rho}\left(\frac{\partial^2 w}{\partial r^2} + \frac{1}{r}\frac{\partial w}{\partial r} + \frac{\partial^2 w}{\partial z^2}\right), \tag{4.1b}$$

$$\frac{\partial u}{\partial r} + \frac{u}{r} + \frac{\partial w}{\partial z} = 0, \tag{4.1c}$$

where μ is the dynamic viscosity, ρ is the density of the fluid, u is the velocity in the r direction, w the velocity in the z direction and p is the pressure. We introduce a streamfunction ψ such that

$$u = \frac{1}{r}\frac{\partial \psi}{\partial z}, \tag{4.2a}$$

$$w = -\frac{1}{r}\frac{\partial \psi}{\partial r}, \tag{4.2b}$$

in which case (4.1c) is automatically satisfied. Taking the partial derivative of (4.1a) with respect to z, the partial derivative of (4.1b) with respect to r and taking the difference of the two equations eliminates the pressure and leaves

$$\frac{\partial}{\partial t}\left(\frac{\partial u}{\partial z} - \frac{\partial w}{\partial r}\right) = \nu\left(\frac{\partial}{\partial z}\left(\nabla^2 u + \frac{u}{r^2}\right) - \frac{\partial}{\partial r}\left(\nabla^2 w\right)\right). \tag{4.3}$$

If we let $D^2 = \frac{\partial^2}{\partial r^2} - \frac{1}{r}\frac{\partial}{\partial r} + \frac{\partial^2}{\partial z^2}$ be a differential operator then (4.3) becomes

$$\frac{\partial (D^2\psi)}{\partial t} = \nu D^4 \psi \tag{4.4}$$

and since D^2 and $\frac{\partial}{\partial t}-\nu D^2$ commute we can show that without loss of generality $\psi = \psi_1+\psi_2$ where

$$D^2\psi_1 = 0, \tag{4.5a}$$

$$\frac{\partial \psi_2}{\partial t} - \nu D^2\psi_2 = 0. \tag{4.5b}$$

We introduce a perturbation which we write as a product of $\exp(int)$ and $\exp(ikz)$. So taking $0 < \epsilon \ll 1$ we write

$$u(r,z,t) = \epsilon U(r)\exp(ikz+int) + C.C., \tag{4.6a}$$

$$w(r,z,t) = \epsilon W(r)\exp(ikz+int) + C.C., \tag{4.6b}$$

$$\psi_1(r,z,t) = \epsilon \Psi_1(r)\exp(ikz+int) + C.C., \tag{4.6c}$$

$$\psi_2(r,z,t) = \epsilon \Psi_2(r)\exp(ikz+int) + C.C., \tag{4.6d}$$

where k is the real wavenumber of the perturbation, where $C.C.$ is the complex conjugate of the first part of the expression and n is the complex growth rate. Substituting (4.6) into (4.5b) gives the differential equation

$$\frac{d^2\Psi_1}{dr^2} - \frac{1}{r}\frac{d\Psi_1}{dr} - k^2\Psi_1 = 0, \tag{4.7}$$

and substituting into (4.5a) gives

$$\frac{d^2\Psi_2}{dr^2} - \frac{1}{r}\frac{d\Psi_2}{dr} - k_1^2\Psi_2 = 0, \tag{4.8}$$

where $k_1^2 = \left(k^2 + \frac{in}{\nu}\right)$. If we let $\Psi_m(r) = r\tilde{\Psi}_m(r)$, for $m = 1, 2$, and substitute into (4.7) and (4.8) and multiply by r then we get the modified Bessel's equation

$$r^2\frac{d^2\tilde{\Psi}_1}{dr^2} + r\frac{d\tilde{\Psi}_1}{dr} - (k^2r^2+1)\tilde{\Psi}_1 = 0, \tag{4.9}$$

for $m = 1$ and similarly for $m = 2$ we get

$$r^2\frac{d^2\tilde{\Psi}_2}{dr^2} + r\frac{d\tilde{\Psi}_2}{dr} - (k_1^2r^2+1)\tilde{\Psi}_2 = 0. \tag{4.10}$$

Solving (4.9) and (4.10) gives

$$\Psi_1 = A_1 r I_1(kr) + B_1 r K_1(kr), \tag{4.11a}$$

$$\Psi_2 = A_2 r I_1(k_1 r) + B_2 r K_1(k_1 r), \tag{4.11b}$$

respectively, where A_1, A_2, B_1 and B_2 are constants to be found and I_1 and K_1 are the modified Bessel functions of the first kind. Substituting back into (4.6) (c and d) we have

$$\psi = r\left\{A_1 I_1(kr) + B_1 K_1(kr) + A_2 I_1(k_1 r) + B_2 K_1(k_1 r)\right\} \exp\left(int + ikz\right), \tag{4.12}$$

which agrees with Tomotika (1935).

The no slip condition and no penetration into the solid core at the surface of the cylinder requires

$$\left[\frac{1}{r}\frac{\partial \psi}{\partial z}\right]_{r=a} = 0, \tag{4.13}$$

$$\left[-\frac{1}{r}\frac{\partial \psi}{\partial r}\right]_{r=a} = 0, \tag{4.14}$$

respectively. We describe the surface of the thread by $r = f(z,t)$ as shown in figure 4.2.

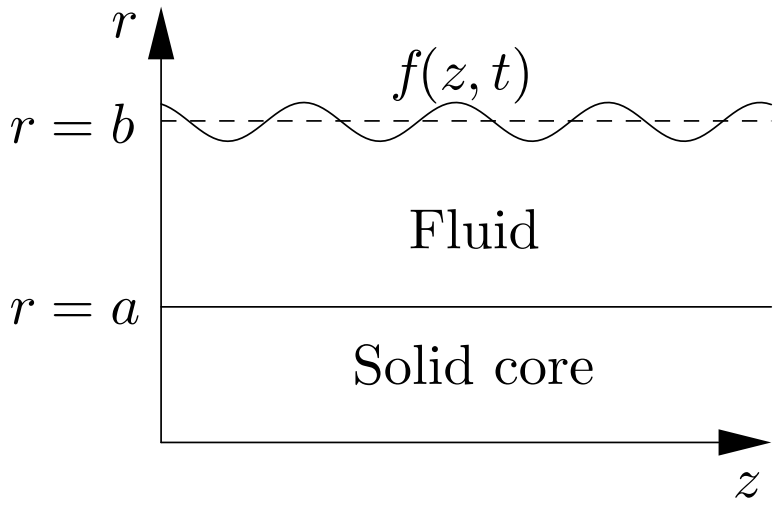

Figure 4.2: Illustration of the surface of a liquid thread over a solid core.

The normal to the surface is given by

$$\mathbf{n} = \frac{\nabla (f - r)}{|\nabla (f - r)|} = \frac{\left(-1, \frac{\partial f}{\partial z}\right)}{\left(1 + \left(\frac{\partial f}{\partial z}\right)^2\right)^{1/2}}. \tag{4.15}$$

We let $f(z,t) = b\left(1 + \epsilon A \exp\left(int + ikz\right)\right)$, where A is unknown, so (4.15) becomes

$$\mathbf{n} = (1/2, -\epsilon bikA \exp\left(int + ikz\right)/2) + \mathcal{O}(\epsilon^2) \tag{4.16}$$

The kinematic condition on the surface of the thread is

$$\frac{D}{Dt}(r - f) = 0, \tag{4.17}$$

which gives after some simplification $A = k\psi/(b^2 n)$.

We know the jump in stress can be expressed by

$$\left[\boldsymbol{\sigma}^{(1)} - \boldsymbol{\sigma}^{(2)}\right] \cdot \mathbf{n} = 2\kappa\gamma\mathbf{n}, \tag{4.18}$$

derived from Acheson (1990), where $\boldsymbol{\sigma}^{(j)}$ is the stress tensor in fluid j, κ is the curvature, γ is the surface tension, $\mathbf{n}$ is the normal vector and the superscripts denote (2) the thread and (1) the surrounding fluid. Left multiplying (4.18) by $\mathbf{n}$ gives

$$\mathbf{n} \cdot \left[\boldsymbol{\sigma}^{(1)} - \boldsymbol{\sigma}^{(2)}\right] \cdot \mathbf{n} = 2\kappa\gamma. \tag{4.19}$$

Since we are considering zero stress induced by fluid (1), or the outer fluid, and we know

$$\boldsymbol{\sigma} = (p_a - p)\mathbf{I} + 2\mu\mathbf{e}, \tag{4.20}$$

where p_a is atmospheric pressure and $\mathbf{e}$ is the rate of strain tensor. Substituting (4.20) into (4.21) gives

$$p_a - p + 2\left[-\mu^{(2)}\mathbf{n} \cdot \mathbf{e}^{(2)} \cdot \mathbf{n}\right] = 2\kappa\gamma. \tag{4.21}$$

Expanding (4.21) and dropping the superscripts gives us

$$p_a - p + 2\mu e_{rr} - 4\mu\frac{\partial f}{\partial z}e_{rz} + 2\mu\left(\frac{\partial f}{\partial z}\right)^2 = 2\kappa\gamma. \tag{4.22}$$

We know that $2\kappa = \nabla \cdot \mathbf{n}$, $e_{rz} = \frac{1}{2}\left(\frac{\partial u}{\partial z} + \frac{\partial w}{\partial r}\right)$ and $e_{rr} = \frac{\partial u}{\partial r}$ (see for example Acheson (1990)). Taking $p = p_0 + \epsilon p_1 \exp(ikz + int))$, at $\mathcal{O}(1)$ we have

$$p_0 = \frac{\gamma}{b} - p_a, \tag{4.23}$$

which represents the pressure balance at the interface with no perturbation. At $\mathcal{O}(\epsilon)$ we have

$$2\mu \left.\frac{dU}{dr}\right|_{r=b} - p_1 = \frac{\gamma A}{b}(1 - k^2 b^2), \tag{4.24}$$

which represents the stress surface tension balance at the interface. We can determine p_1 by substituting ψ into (4.1b) to get

$$\frac{\epsilon p_1}{\rho} = \frac{n}{kr}\frac{\partial \psi}{\partial r} - \frac{\mu}{\rho i k}\left(\left(\frac{2}{r^3} - \frac{1}{r^2} - \frac{k^2}{r}\right)\frac{\partial \psi}{\partial r} - \frac{1}{r^2}\frac{\partial^2 \psi}{\partial r^2} + \frac{1}{r}\frac{\partial^3 \psi}{\partial r^3}\right). \tag{4.25}$$

The tangential stress component is

$$\mathbf{t} \cdot \boldsymbol{\sigma} \cdot \mathbf{n} = 0, \tag{4.26}$$

where $\mathbf{t}$ is the normal tangential vector pointing in the z direction. Substituting in (4.26) for $\mathbf{t}$, $\boldsymbol{\sigma}$ and $\mathbf{n}$ gives

$$-e_{rr}\frac{\partial f}{\partial z} + e_{rz}\left(\frac{\partial f}{\partial z}\right)^2 - e_{rz} + e_{zz}\frac{\partial f}{\partial z} = 0. \tag{4.27}$$

Substituting in for $\mathbf{e}$ gives

$$-\frac{\partial u}{\partial r}\frac{\partial f}{\partial z} + \left(\frac{\partial u}{\partial z} + \frac{\partial w}{\partial r}\right)\left(\frac{\partial f}{\partial z}\right)^2 - \left(\frac{\partial u}{\partial z} + \frac{\partial w}{\partial r}\right) + \frac{\partial w}{\partial z}\frac{\partial f}{\partial z} = 0. \tag{4.28}$$

Since there are no $\mathcal{O}(1)$ terms we look at the $\mathcal{O}(\epsilon)$ terms

$$\frac{\partial u}{\partial z} + \frac{\partial w}{\partial r} = 0. \tag{4.29}$$

Substituting the solution for ψ given in (4.12) into (4.11a), (4.11b), (4.29), (4.24) and (4.25) gives four equations in four variables (A_1, A_2, B_1, B_2) whose solution is non-trivial

if the determinant of the matrix of coefficients is zero,

$$\begin{vmatrix} I_1(ka) & I_1(k_1a) & K_1(ka) & K_1(k_1a) \\ kI_0(ka) & k_1I_0(k_1a) & -kK_0(ka) & -k_1K_0(k_1a) \\ 2k^2I_1(kb) & (k^2+k_1^2)I_1(k_1b) & 2k^2K_1(k_1b) & (k^2+k_1^2)K_1(k_1b) \\ F_1 & F_2 & F_3 & F_4 \end{vmatrix} = 0, \tag{4.30}$$

where

$$\begin{aligned} F_1 = &\left(2\,i\mu\,k^2nb - i\rho\,n^3b^2 - \gamma\,k^4b^2 + \gamma\,k^2\right) I_1(kb) \\ &+ \left(-\rho\,n^2\nu\,bk - 2\,i\mu\,k^3nb^2 + \rho\,n^2\nu\,k\right) I_0(kb), \end{aligned} \tag{4.31a}$$

$$\begin{aligned} F_2 = &\left(-i\rho n^3b^2 - \gamma k^4b^2 + 2i\mu k^2nb + \gamma k^2\right) I_1(k_1b) \\ &+ \left(\rho n^2\nu k_1 - \rho n^2k^2\nu k_1b^2 - 2i\mu k^2k_1nb^2 + \rho n^2\nu k_1^3b^2 - \rho n^2\nu k_1b\right) I_0(k_1b), \end{aligned} \tag{4.31b}$$

$$\begin{aligned} F_3 = &\left(-\gamma k^4b^2 - i\rho n^3b^2 + 2i\mu k^2nb + \gamma k^2\right) K_1(kb) \\ &+ \left(-\rho n^2\nu k + 2\,i\mu k^3nb^2 + \rho n^2\nu bk\right) K_0(kb), \end{aligned} \tag{4.31c}$$

$$\begin{aligned} F_4 = &\left(-i\rho n^3b^2 - \gamma k^4b^2 + 2i\mu k^2nb + \gamma k^2\right) K_1(k_1b) \\ &+ \left(-\rho n^2\nu k_1 + 2i\mu k^2k_1nb^2 + \rho n^2k^2\nu k_1b^2 - \rho n^2\nu {k_1}^3b^2 + \rho n^2\nu k_1b\right) K_0(k_1b). \end{aligned} \tag{4.31d}$$

We can nondimensionalize by letting $L = b/a$ (using a as the length scale), $\Lambda = 2\pi b/\lambda = bk$ (scaling the wavenumber by a period), $S = \gamma\rho b/\mu^2$ and $N = nib^2\rho/\mu$ to give

$$\begin{vmatrix} I_1(\Lambda L) & I_1(\hat{\Lambda} L) & K_1(\Lambda L) & K_1(\hat{\Lambda} L) \\ \Lambda I_0(\Lambda L) & \hat{\Lambda} I_0(\hat{\Lambda}/L) & -\Lambda K_0(\Lambda/L) & -\hat{\Lambda} K_0(\hat{\Lambda}/L) \\ 2\Lambda^2 I_1(\Lambda) & (2\Lambda^2+N) I_1(\hat{\Lambda}) & 2\Lambda^2 K_1(\Lambda) & (2\Lambda^2+N) K_1(\hat{\Lambda}) \\ \hat{F}_1 & \hat{F}_2 & \hat{F}_3 & \hat{F}_4 \end{vmatrix} = 0, \tag{4.32}$$

where

$$\hat{F}_1 = \Lambda^2\left(2 - S + S\Lambda^2\right) I_1(\Lambda) - \left(2\Lambda^3 + N^2\right) I_0(\Lambda), \tag{4.33a}$$

$$\hat{F}_2 = \Lambda^2\left(2N - S + S\Lambda^2\hat{\Lambda}\right) I_1(\hat{\Lambda}) - \hat{\Lambda}\left(2\Lambda^2N + 2N^2\right) I_0(\hat{\Lambda}), \tag{4.33b}$$

$$\hat{F}_3 = \Lambda^2 \left(2N - S + S\Lambda^2\right) K_1(\Lambda) + \Lambda \left(2\Lambda^2 N + N^2\right) K_0(\Lambda), \tag{4.33c}$$

$$\hat{F}_4 = \Lambda^2 \left(2N - S + S\Lambda^2\right) K_1(\hat{\Lambda}) + \hat{\Lambda} \left(2\Lambda^2 N + 2N^2\right) K_0(\hat{\Lambda}), \tag{4.33d}$$

and $\hat{\Lambda} = \sqrt{\Lambda^2 + N}$.

We are only interested in the real part on N for the purposes of determining stability and as such we let N denote the real part of N from here. We cannot get an explicit solution for N in terms of Λ as N appears in the argument of the Bessel functions but we can plot it implicitly by initially fixing Λ at a small value and using Newton's method to solve for N. We then increase Λ by a sufficiently small step size and solve for N and continue in this manner. The numerical method starts to break down near $N = 0$ as setting $N = 0$ in (4.32) makes columns 1 and 2, and 3 and 4 equal so that the left hand side of (4.32) is zero and it is satisfied. So we estimate the solution path as a growth rate curve crosses the N axis by estimating the solution path by assuming that locally the solution is linear and using Newton's method to continue the solution below the axis.

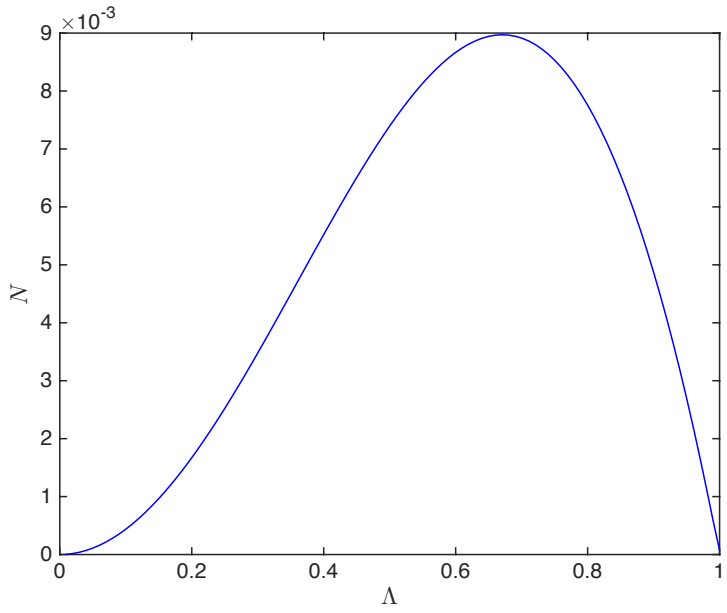

Figure 4.3: Plot of growth rate N against the wavenumber Λ for $S = 1$ and $L = 1/2$.

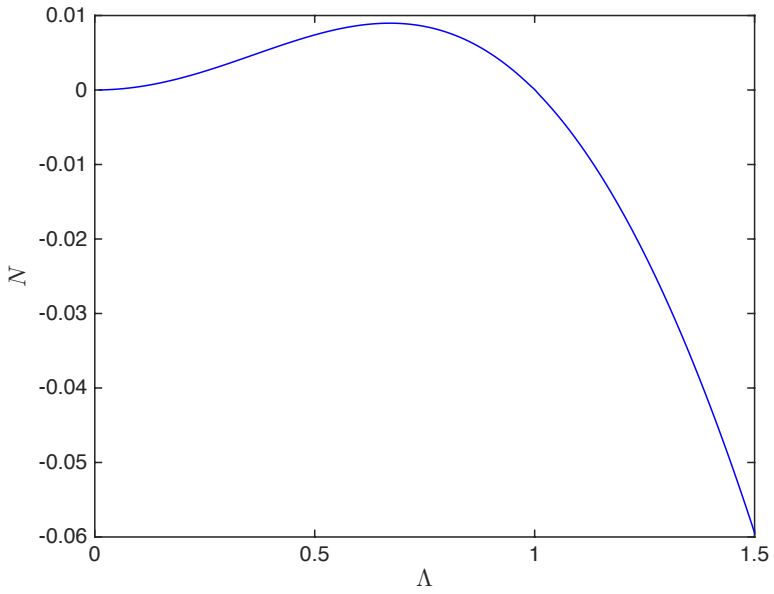

Figure 4.4: Plot of growth rate N against the wavenumber Λ for $S = 1$ and $L = 1/2$.

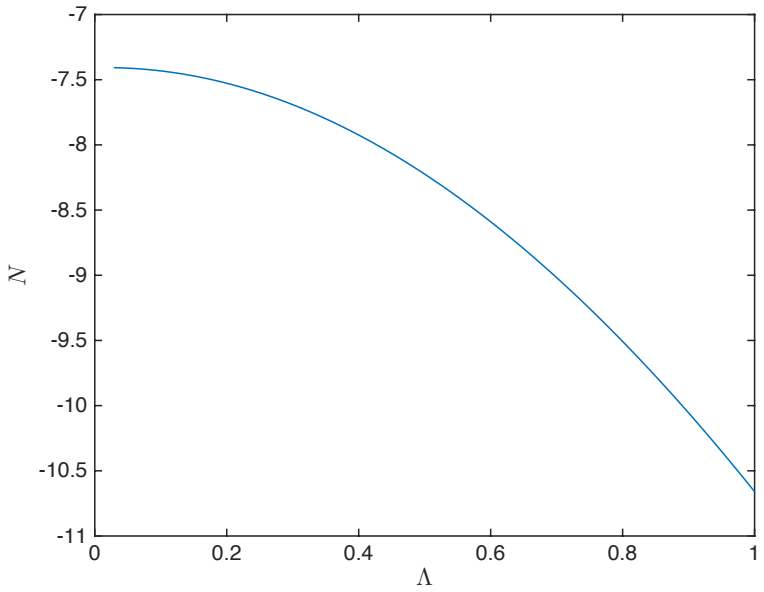

Figure 4.5: Plot of growth rate N against the wavenumber Λ for $S = 1$ and $L = 1/2$.

Plotting for $S = 1$ and $L = 1/2$ and starting at small positive Λ gives us figure 4.3 and 4.4. We have also computed the first completely stable mode as shown in figure 4.5. These are typical plots for the parameters S and L. The cutoff wavenumber is always at $\Lambda = 1$ as a consequence of the scaling given. For the parameter ranges that we have tested

there is always precisely one unstable mode, that we attribute to capillary forces causing a pinching of the fluid jet similar to Rayleigh (1879).

We can compare figure 4.3 directly with Goren (1962) figure 1 where Goren (1962) computed a Taylor expansion of (4.32) around $N = 0$ we have allowed for any N. The maximum in figure 4.3 appears to be identical to that found in Goren (1962) figure 1 but the behaviour for small Λ differs from that of Goren (1962). Near $\Lambda = 0$ in figure 4.3 the behaviour appears to be quadratic in Λ while it appears to be linear in Goren (1962) figure 1.

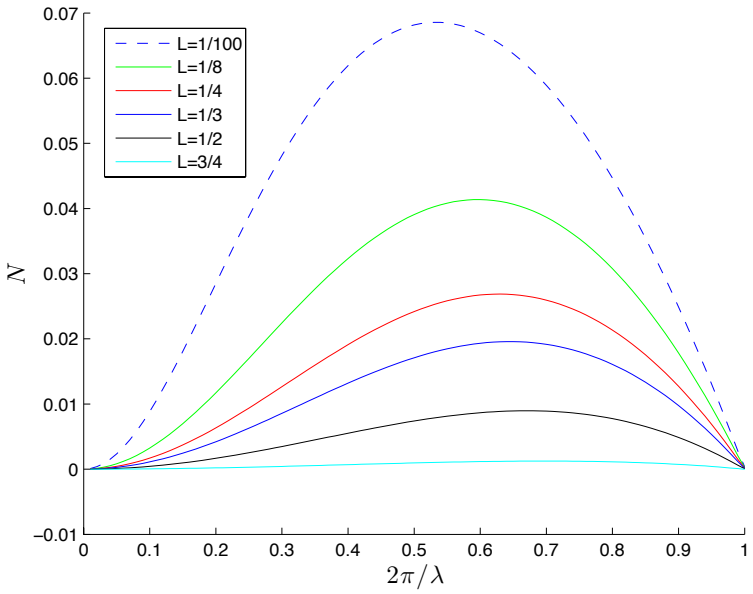

Figure 4.6: Plot of growth rate N against the wavenumber Λ for $S = 1$ and varying L.

The unstable growth rate only changes quantitatively and not qualitatively with S, keeping its shape, destabilising for S increasing and stabilising for S decreasing. Increasing L has a stabilising effect as shown in figure 4.6 as we expect. Since increasing L is equivalent to thinning the fluid layer relative to the solid core. Increasing L also shifts the maximum in the direction of Λ increasing as shown in figure 4.7 where we have normalised the growth

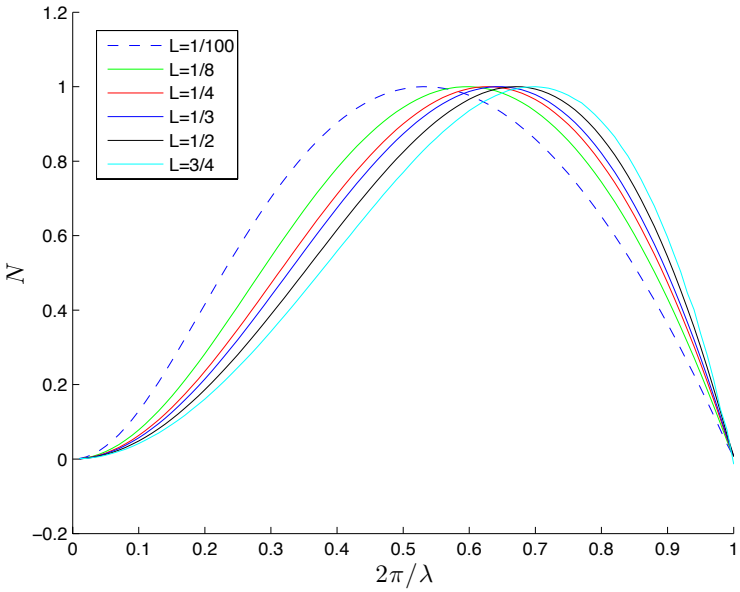

Figure 4.7: Plot of growth rate N against the wavenumber Λ for $S = 1$ and varying L with curves normalised such that their maximum is 1.

rates such that the maximum of each growth rate is $N = 1$.

4.1 Summary

In this section we have considered the stability of an annular thread of fluid with a solid core. As we expect from previous work, we have found that a single unstable mode exists for a given set of parameters. We have verified our work against that of Goren. We have found that varying the parameter S has the effect of scaling the growth rate without changing the Λ coordinate of the maximum growth rate. Changing the parameter L has the effect of scaling the growth rate and changing the Λ coordinate. Increasing L has a stabilising effect upon the growth rate while shifting the maximum in the positive Λ direction.

Conclusion

In section 1, we have given an overview of the experiments we performed on curtain coating stability. We have shown that in general for multiple layers of fluid reducing the flow rate in layer 1 has the effect of reducing the total breakup flow rate and stabilising the curtain.

In section 2.1, for a two layer unidirectional flow given a set of flow rates, for each fluid, we have shown that there exists precisely one set of fluid thicknesses which satisfy the given conditions. We have also postulated that for a three layer unidirectional flow the same holds on the grounds that only one solution been observed experimentally.

In section 2.2, we have extended Gao & Lu (2007) two layer stability analysis with surfactant to consider two layers of fluid with differing thicknesses and extended this to three layers. In Gao & Lu (2007) only two layers of equal thickness were considered. This leads to at most one unstable mode which after extensive testing with the parameters we agree with. We have considered a thinner upper layer where we have shown that not only do we have multiple unstable modes but also a stable bandwidth occurring between two unstable bandwidths.

We also extended Gao & Lu (2007) work by considering adding a third layer to their two layer calculations. These also led to solutions with multiple modes where changing the surfactant concentration made one mode change monotonically whilst making the other change non-monotonically. In some cases we found that there can exist a range of stable wavenumbers sandwiched by a region of unstable wavenumbers. This can arise from having the total thickness of the upper layers of fluid equal to the thickness of the lowest layer and surfactant only on the interface between layers 2 and 3. Varying the levels of surfactants in the interfaces and free surface can have interesting effects upon the growth

rates of the different modes. One example of this is for a layer thickness as described in the previous sentence with surfactant on the interface between layers 2 and 3. Increasing the concentration of surfactant on the free surface has the effect of monotonically reducing one mode while having a non-monotonic effect upon the other mode. In considering a case which is stable in the absence of surfactant, where upper layers are less viscous than the layers below them, the range or ranges of unstable wavenumbers in the presence of surfactant do not start from $k = 0$ as in the previous cases. After extensive search in the literature this appears to be the first time observing this for multi-layer flow down an inclined plane.

In section 3.1, we have derived and solved numerically a set of equations to describe the nonlinear evolution of three layer flow down an inclined plane in the presence of surfactant. Picking an initial wave profile based on the linear stability analysis either the wave stabilises to a flat profile denoting a unidirectional flow or a stable wave profile which we surmised to be a travelling wave profile as given in section 3.2.

In section 3.2, we have considered the presence of travelling wave solutions for three layer flow in the presence of surfactants. In the vicinity of the point of zero growth rate, there exists a travelling wave solution of small amplitude. In the travelling wave cases we have considered, at least one of the travelling wave branches tends towards $k = 0$ from the bifurcation point. This suggests that for a set of parameters at least one of the traveling wave branches will tend towards $k = 0$. In case 1 and 2 the maximum of the amplitudes are near to the maximums of the growth rate for the linear stability.

In case 3 an unexpected branch was found which bifurcates not from a point of zero growth rate as the others found do but from a harmonic of branch 1 in case 3. We expect

that there exists other such branches which bifurcate from harmonics of different branches but we make no further effort to find them in this thesis and it is left for further work. The existence of this branch may not depend upon the presence of surfactant since all the branches have harmonics but such a branch has not been found in case 1 where no surfactant is present.

The presence of turning of the branch and the loops created were also unexpected as it suggests multiple traveling wave solutions exist for a single k. The solution that we expect to observe would depend upon the stability of the different travelling wave solutions and the initial profile taken for an unsteady time dependent calculation as given in section 3.1.

In section 4, we have considered the stability of an annular thread of fluid with a solid core. As we expect from previous work, we have found that a single unstable mode exists for a given set of parameters. We have verified our work against that of Goren (1962). We have found that varying the parameter S has the effect of scaling the growth rate without changing the Λ coordinate of the maximum growth rate. Changing the parameter L has the effect of scaling the growth rate and changing the Λ coordinate. Increasing L has a stabilising effect upon the growth rate while shifting the maximum in the positive Λ direction.

Further Work

The experiments conducted in section 1 describe a starting point both for comparison with theoretical results and for further experimentation extending the limits of the work presented here. With equipment able to produce more consistent low flow rates one would be able to better investigate the effect of lowering the flow rate of layer 1 on the stability of the curtain creating a lubrication layer. Specifically with a lower flow rate one can investigate breakup of three and four layers. These investigations could consider a thin middle layer or thin upper and lower layers to fully consider the effect of 'lubricating' layers. Ambravaneswaran *et al.* (2004) considers steady capillary jets and the transition between a stable thread and the formation of droplets. The transition from a stable jet to droplet formation has a lower flow rate than the transition from droplet formation to a stable jet describing a hysteresis window. This hysteresis window could have a link to the hysteresis window observed in the curtain coating experiments considered here and this link could be further investigated.

From section 2.1 the analysis required to determine if a unique solution exists for a three layer unidirectional flow given a set of flow rates, for each fluid, is not trivial but with some substantial analysis headway may be made via complex analysis using winding numbers. One can use winding numbers to calculate the number of roots within a closed contour on the complex plane.

In section 2.2 and 2.3 we have considered the linear stability of multi layer flows for a range of parameters which show interesting behaviour but this does not cover all parameter ranges. The effect of adding surfactant to the layers for a thin layer compared to the other layers is one avenue of investigation as is considering a thicker upper layer and

varying surfactant concentrations. Indeed the possible configurations even with these five parameters are many. Calculation of neutral stability curves could be considered for the three layer flows considered in this thesis.

The nonlinear evolution equations given in section 3.1 make several simplifications of the flow in order to arrive at equations that we can easily solve numerically. These include a long wave approximation and a constraint on the angle of inclination of the plane. These simplifications could be relaxed to arrive at an equation which describes the flow in the presence of inertia and allows for any angle of the inclined plane. Such as system could be solved using boundary integral computations for steady traveling waves for Stokes flow. This method could also incorporate inertia. For a Navier-Stokes flow we could utilize a finite-element method or a level set method. Another avenue of interest could be traveling waves in three layer layer flows where further work is in preparation in Thompson & Blyth (2016).

This thesis has considered many cases where travelling wave solutions exist but we cannot say that for each case we have found all the travelling wave solutions that exist there. This is shown in the travelling wave branch found in section 3.2.3 case study 3 where a branch was found that did not emerge from a point of zero stability. Methods may exist that find all possible travelling wave solutions for a particular wavenumber but these are not considered in this thesis. Further analysis is needed into the existence of the harmonic branches that are presented in section 3.2.3 case study 3.

The stability of an annular thread of fluid with a solid core presented here, in section 4, is a small extension of well known results. The direction that this research could take is considering a viscoelastic fluid in place of the viscous fluid discussed here to better model

spider silk or to change the solid core for spheres evenly spaced along the centerline of the thread. The second extension here is motivated by the pharmaceutical industry. When manufacturing certain drugs it is desirable to coat the active ingredient in a shell, either to extend the time between the drug being ingested and when the pill is broken down. This encapsulation can be achieved by seeding a fluid thread with particles of the active ingredient periodically along the centre of the fluid. The hope is that the fluid breaks up into equally sized droplets each with a single particle of the active ingredient while also reducing the emergence of satellite droplets.

A Experimental results

Fluid 1

A.1 Single Layer Experiment 1

Experiment number	Q_{ST}	Q_{BR}	Threads
1	28.4	16.9	N/A
2	28	14.35	9 threads
3	28	13.2	8 threads

Experiment number	Q_{ST}	Q_{BR}	Threads
1	28	12.5	8 threads
2	28	10.2	7 threads and 1 oscillating
3	28	9.2	6 threads and 1 oscillating
4	28	7.7	6 threads and 1 oscillating
5	21.6	10.7	N/A
6	21.0	10.5	6 threads and 1 oscillating

A.2 Single Layer Experiment 2

Experiment number	Q_{ST}	Q_{BR}	Threads
1	21	12.7	N/A
2	21	12.9	N/A
3	21.0	10.7	N/A

A.3 Single Layer Experiment 3

Experiment number	Q_{ST}	Q_{BR}	Threads
1	23.2	12.4	N/A
2	23.2	10.0	N/A
3	23.2	9.4	N/A

A.4 Two Layer Experiment 1

Experiment number	Q_1	$Q_{2,ST}$	$Q_{2,BR}$
1	10.5	9.3	6.6
2	10.5	7.2	0 (still stable)
3	8	11.7	3.9
4	7	13.0	4.8
5	9	11.1	0 (still stable)
6	6	13.9	5.9
7	5	15.1	6.4

A.5 Two Layer Experiment 2

Experiment number	Q_1	$Q_{2,ST}$	$Q_{2,BR}$
1	4	17.3	9.8
2	4	17.0	10.3
3	8	13.5	4.5
4	7	13.6	8.7
5	7	13.6	8.5
6	7	13.6	10
7	8	13.5	5.9
8	8	13.5	3.8
9	7	14	6.9
10	7	14	5.1
11	7	14	5.1

A.6 Two Layer Experiment 3

Experiment number	Q_1	$Q_{2,ST}$	$Q_{2,BR}$
1	8	11.5	6.0
2	8	11.5	8.1
3	8	11.5	3.6
4	8	11.5	7.4
5	7	13.2	7.9
6	7	12.8	9.1
7	7	12.8	8.0
8	7	12.8	4.1
9	6	14.2	10.4
10	6	14.2	9.1
11	6	14.2	7.5
12	6	14.2	7.6

A.7 Three Layer Experiment 1

Experiment number	Q_1	Q_2	$Q_{3,ST}$	$Q_{3,BR}$
1	4	4	12.3	8.1
2	4	4	12.3	8.7
3	4	4	12.3	6.0
4	4	4	12.3	2.3
5	4	4	14.0	8.2
6	4	4	12.3	10.3
7	4	4	12.3	6.2
8	4	4	12.3	4.0
9	4	4	12.3	8.0
10	4	4	12.3	7.7

A.8 Three Layer Experiment 2

Experiment number	Q_1	Q_2	$Q_{3,ST}$	$Q_{3,BR}$
1	4	3	13.5	9.8
2	4	3	13.5	5.6
3	4	3	13.5	9.2
4	4	3	13.5	10.6
5	4	3	13.5	9.0
6	4	3	13.5	8.8
7	4	3	13.5	8.9
8	4	3	13.5	5.9
9	3	4	13.5	9.9
10	3	4	13.5	4.4
11	3	4	13.5	10.4
12	3	4	13.5	9.9

A.9 Three Layer Experiment 3

Experiment number	Q_1	Q_3	$Q_{2,ST}$	$Q_{2,BR}$
1	4	4	14.0	9.0
2	4	4	14.0	8.2
3	4	4	14.0	10.5
4	4	4	14.0	9.0
5	4	3	14.1	8.8
6	4	3	14.1	7.6
7	4	3	14.1	9.8
8	4	3	14.1	10.2
9	3	4	14.1	10.0
10	3	4	14.1	4.5
11	3	4	14.1	6.7
12	3	4	14.1	9.8

A.10 One layer experiment

Experiment number	Q_{ST}	Q_{BR}
1	21.0	13.0
2	21.0	14.6
3	21.0	15.4
4	21.0	14.5

A.11 Two layer experiment

Experiment number	Q_1	$Q_{2,ST}$	$Q_{2,BR}$
1	7.0	14.0	11.0
2	7.0	14.0	11.0
3	7.0	14.0	11.0
4	8.5	14.0	8.0

Fluid 2

A.12 One layer experiment

Experiment number	Q_{ST}	Q_{BR}
1	16.9	9.9
2	16.9	7.2
3	16.9	4.5
4	16.9	10.9
5	16.9	7.8
6	16.9	5.5
7	16.9	5.7
8	16.9	7.3

Experiment number	Q_{ST}	Q_{BR}
1	17.2	3.2
2	17.2	4.1
3	17.2	11.2
4	17.2	6.8
5	17.2	4.8
6	17.2	6.0
7	17.2	4.8
8	17.2	5.0

A.13 Two layer experiment

Experiment number	Q_1	$Q_{2,ST}$	$Q_{2,BR}$
1	4.0	13.5	4.5
2	4.0	13.5	3.2
3	4.0	13.5	9.4
4	4.0	13.5	7.1
5	4.0	13.5	6.2
6	4.0	13.5	4.2
7	4.0	13.5	3.2
8	4.0	13.5	3.3

Experiment number	Q_1	$Q_{2,ST}$	$Q_{2,BR}$
1	3.0	14.8	4.3
2	3.0	14.8	11.1
3	3.0	14.8	0
4	3.0	14.8	1.7
5	3.0	14.8	1.7
6	3.0	14.8	1.3
7	3.0	14.8	0
8	3.0	14.8	2.8

A.14 Three layer experiment

Experiment number	Q_1	Q_3	$Q_{2,ST}$	$Q_{2,BR}$
1	3	3	10.7	0
2	3	3	10.7	0 (stable)

Fluid 3

A.15 One layer experiment

Experiment number	Q_{ST}	Q_{BR}
1	22.7	21.0
2	22.7	8.4
3	22.7	7.3
4	22.7	12.8
5	22.7	8.1
6	22.7	17.3
7	22.7	8.3
8	22.7	14.5

A.16 Two layer experiment

Q_1 = fluid 3, Q_2 = fluid 2

Experiment number	Q_1	$Q_{2,ST}$	$Q_{2,BR}$
1	6.0	N/A	4.7
2	6.0	N/A	9.7
3	6.0	N/A	3.5
4	6.0	N/A	7.8

Experiment number	Q_1	$Q_{2,ST}$	$Q_{2,BR}$
1	5.0	17.5	4.5
2	5.0	17.5	7.9
3	5.0	17.5	8.5

Q_1 = fluid 2, Q_2 = 3

Experiment number	Q_1	$Q_{2,ST}$	$Q_{2,BR}$
1	6.0	25	12
2	6.0	26.9	9.5
3	6.0	27	8.2

Experiment number	Q_1	$Q_{2,ST}$	$Q_{2,BR}$
1	5.0	28.3	8.0
2	5.0	28.3	7.8
3	5.0	16.2	5.0
4	5.0	16.2	9.2
5	5.0	16.2	7.4

Fluid 4: 80% glycerol and 0.21% SDS.

A.17 One layer experiment

Experiment number	Q_{ST}	Q_{BR}
1	16.1	9.7
2	16.1	5.6
3	15.7	7.5
4	15.7	9.1
5	15.7	8.0
6	15.7	8.2
7	15.7	8.8
8	15.7	7.7

A.18 Two layer experiment

Q_1 = fluid 4, Q_2 = fluid 3

Experiment number	Q_1	$Q_{2,ST}$	$Q_{2,BR}$
1	4.0	12.1	2.2
2	4.0	12.1	7.3
3	4.0	12.1	5.5
4	4.0	12.1	6.0
5	4.0	12.1	5.1
6	4.0	12.1	2.4
7	4.0	12.1	5.1
8	4.0	12.1	0*

*Period of stability then breakup.

Experiment number	Q_1	$Q_{2,ST}$	$Q_{2,BR}$
1	3.0	12.8	4.7
2	3.0	12.8	4.9
3	3.0	12.8	5.2
4	3.0	12.8	5.4
5	3.0	12.8	5.4
6	3.0	12.8	2.4
7	3.0	12.8	3.7
8	3.0	12.8	3.6

Q_1 = fluid 3, Q_2 = fluid 4

Experiment number	Q_1	$Q_{2,ST}$	$Q_{2,BR}$
1	4.0	11.3	6.3
2	4.0	11.3	10.0
3	4.0	11.3	6.8
4	4.0	11.3	5.0
5	4.0	11.3	7.0
6	4.0	11.3	3.3
7	4.0	11.3	5.5
8	4.0	11.3	1.8

Experiment number	Q_1	$Q_{2,ST}$	$Q_{2,BR}$
1	3.0	11.9	1.3 on meter
2	3.0	11.9	3.0
3	3.0	11.9	1.3 on meter
4	3.0	11.9	3.9
5	3.0	11.9	3.4
6	3.0	11.9	2.5
7	3.0	11.9	3.8
8	3.0	11.9	4.3

Fluid 5

A.19 One layer experiment

Experiment number	Q_{ST}	Q_{BR}
1	12.3	10.7
2	12.3	8.8
3	12.3	9.0
4	12.3	8.0
5	12.3	8.1
6	12.3	11.4
7	12.3	9.9
8	12.3	9.4

Fluid 6

A.20 One layer experiment

Experiment number	Q_{ST}	Q_{BR}
1	14.4	12.9
2	12.9	9.4
3	13.0	7.8
4	12.3	6.8
5	11.6	10.0
6	11.1	10.5
7	11.1	6.6
8	11.1	6.3

A.21 Two layer experiment

Q_1 = fluid 5, Q_2 = fluid 2

Experiment number	Q_1	$Q_{2,ST}$	$Q_{2,BR}$
1	4.0	10.0	2.7
2	4.0	10.0	4.2
3	4.0	10.0	6.3
4	4.0	10.0	6.4
5	4.0	10.0	2.3
6	4.0	10.0	6.2
7	4.0	10.0	3.9
8	4.0	10.0	2.0

Experiment number	Q_1	$Q_{2,ST}$	$Q_{2,BR}$
1	3.0	10.7	7.0
2	3.0	10.7	4.9
3	3.0	10.7	7.1
4	3.0	10.7	3.9
5	3.0	10.7	9.8
6	3.0	10.7	4.5
7	3.0	10.7	9.8
8	3.0	10.7	3.4

Q_1 = fluid 2, Q_2 = fluid 6

Experiment number	Q_1	$Q_{2,ST}$	$Q_{2,BR}$
1	4.0	8.2	5.1
2	4.0	8.2	4.6
3	4.0	8.2	1.8
4	4.0	8.2	5.2
5	4.0	8.2	5.0
6	4.0	8.2	6.0
7	4.0	8.2	4.6
8	4.0	8.2	5.8

Experiment number	Q_1	$Q_{2,ST}$	$Q_{2,BR}$
1	3.0	8.2	3.8
2	3.0	8.2	2.5
3	3.0	8.2	3.0
4	3.0	8.2	4.1
5	3.0	8.2	3.7
6	3.0	8.2	3.1
7	3.0	8.2	2.6
8	3.0	8.2	3.7

Fluid 7

Experiment number	Q_{ST}	Q_{BR}
1	14.8	0
2	14.8	3.8
3	14.8	6

References

Acheson, D. J. 1990 *Elementary Fluid Dynamics*. Oxford University Press.

Ambravaneswaran, Bala, Subramani, Hariprasad J., Phillips, Scott D. & Basaran, Osman A. 2004 Dripping-jetting transitions in a dripping faucet. *Phys. Rev. Lett.* **9**3, 034501.

Baumeister, P. W. 2004 *Optical coating technology*. SPIE Press.

Benjamin, T. B. 1957 Wave formation in laminar flow down an inclined plane. *J. Fluid Mech.* **2**, 554–574.

Blyth, M. 2008 Effect of an electric field on the stability of contaminated film flow down an inclined plane. *J. Fluid Mech.* **595**, 221–237.

Blyth, M. G. & Pozrikidis, C. 2004 Effect of surfactant on the stability of film flow down an inclined plane. *J. Fluid Mech.* **521**, 241–250.

Boatto, S., Kadanoff, L. P. & Olla, P. 1993 Traveling-wave solutions to thin-film equations. *Physical Review E* **48 6**, 4423–4431.

Boys, C. V. 1960 *Soap Bubbles and the Forces Which Mould Them*. Heinemenn.

Brown, D. R. 1961 A study of the behaviour of a thin sheet of moving liquid. *Journal of Fluid Mechanics* **10**, 279–305.

Chen, K-P. 1993 Wave formation in the gravity-driven low-reynolds number flow of two liquid films down an inclined plane. *Phys. Fluids* **5** (12), 3038–3048.

Dyson, R. J., Branner, J., Breward, C. W. J. & Howell, P. D. 2009 Long-wavelength stability of an unsupported multilayer liquid film falling under gravity. *Journal of Engineering Mathematics* **64**, 237–250.

Gao, P. & Lu, X-Y. 2007 Effect of surfactants on the inertialess instability of a two-layer film flow. *J. Fluid Mech.* **591**, 495–507.

Gao, P. & Lu, X-Y. 2008 Mechanism of the long-wave inertialess instability of a two-layer film flow. *J. Fluid Mech.* **608**, 379–391.

Goren, S. L. 1962 The instability of an annular thread of fluid. *Journal of Fluid Mechanics* **12**, 309–319.

Halpern, D. & Frenkel, A. L 2003 Destabilization of a creeping flow by interfacial surfactant: linear theory extended to all wavenumbers. *J. Fluid Mech.* **485**, 191–220.

Hesla, T. I., pranckh, F. R. & Preziosi, L. 1986 Squire's theorem for two stratified fluids. *Physics of Fluids* **29**, 2808–2811.

Jiang, W. Y., Helenbrook, B. & Lin, S. P. 2004 Inertialess instability of a two-layer liquid film flow. *Phys. Fluids* **16** (3), 652–663.

Jiang, W. Y., Helenbrook, B. T., Lin, S. P. & Weinstein, S. J. 2005 Low-reynolds-number instabilities in three-layer flow down an inclined wall. *J. Fluid Mech.* **539**, 387–416.

Jiang, W. Y. & Lin, S. P. 2005 Enhancement or suppression of instability in a two-layered liquid film flow. *Phys. Fluids* **17** (5), 054105.

Kao, T. W. 1968 Role of viscosity stratification in the stability of two-layer flow down an incline. *J. Fluid Mech.* **33** (03), 561–572.

Krebs, F. C. 2009 Fabrication and processing of polymer solar cells: A review of printing and coating techniques. *Solar Energy Materials and Solar Cells* **93**, 394–412.

LaPorte, R. J. 1997 *Hydrophilic polymer coatings for medical devices*. CRC Press.

Lin, S. P. 1970 Stabilizing effects of surface-active agents on a film flow. *AIChE Journal* **16** (3), 375–379.

Lin, S. P. 1981 Stability of a viscous liquid curtain. *J. Fluid Mech.* **104**, 111–118.

Liu, J., Paul, J. D. & Gollub, J. P. 1993 Measurements of the primary instabilities of film flows. *J. Fluid Mech.* **250**, 69–101.

Loewenherz, D. S. & Lawrence, C. J. 1989 The effect of viscosity stratification on the stability of a free surface flow at low reynolds number. *Phys. Fluids* **1** (10), 1686–1693.

Pozrikidis, C. 1998 Gravity-driven creeping flow of two adjacent layers through a channel and down a plane wall. *J. Fluid Mech.* **371**, 345–376.

Pozrikidis, C. 2003 Effect of surfactants on film flow down a periodic wall. *J. Fluid Mech.* **496**, 105–127.

Rayleigh, Lord 1879 On the instability of jets. *Proceedings of the London Mathematical Society* **10**, 4–13.

Rosen, M. J. & Kunjappu, J. T. 2012 *Surfactants and Interfacial Phenomena*. John Wiley & Sons, Inc.

Samanta, A. 2014 Effect of surfactants on the instability of a two-layer film flow down an inclined plane. *Phys. Fluids* **26**, 094105.

Squire, H. B. 1933 On the stability for three-dimensional disturbances of viscous fluid flow between parallel walls. *Proceedings of the Royal Society of London. Series A, Containing Papers of a Mathematical and Physical Character* **1**42 (847), pp. 621–628.

Taylor, G. I. 1959 The dynamics of thin sheets of fluid. iii. disintegration of fluid sheets. *Proceedings of the Royal Society of London* **253**, 313–321.

Thompson, J. & Blyth, M. 2016 Effect of surfactant on multi-layer film flow down an inclined plane. *In Preparation* .

Tomotika, S. 1935 On the instability of a cylindrical thread of a viscous liquid surrounded by another viscous fluid. *Proceedings of the Royal Society* **150**, 322–337.

Tseluiko, D., Blyth, M. G., Papageorgiou, D. T. & Vanden-Broeck, J. M. 2008 Electrified viscous thin film flow over topography. *J. Fluid Mech.* **597**, 449.

Wang, C. K., Seaborg, J. J. & Lin, S. P. 1978 Instability of multi-layered liquid films. *Phys. Fluids* **21** (10), 1669–1673.

Weinstein, S. J. & Chen, K. P. 1999 Large growth rate instabilities in three-layer flow down an incline in the limit of zero reynolds number. *Phys. Fluids* **11** (11), 3270–3282.

Weinstein, S. J. & Kurz, M. R. 1991 Long-wavelength instabilities in three-layer flow down an incline. *Phys. Fluids* **3** (11), 2680–2687.

Whitaker, S. & Jones, L. O. 1966 Stability of falling liquid films. effect of interface and interfacial mass transport. *AIChE Journal* **12** (3), 421–431.

Yih, C.-S. 1963 Stability of liquid flow down an inclined plane. *Phys. Fluids* **6**, 321–334.